USING IN-SITU AND REMOTELY-SENSED OBSERVATIONS TO ESTIMATE THE INFLUENCE OF AMAZON RIVER CHEMISTRY AND DISCHARGE ON ATMOSPHERIC CARBON DIOXIDE UPTAKE IN THE WESTERN TROPICAL NORTH ATLANTIC OCEAN

by

LINQUAN MU

(Under the Direction of Patricia L. Yager)

ABSTRACT

The Amazon River is the world's largest river by discharge. Its massive delivery of freshwater, carbon, and nutrients to the ocean significantly impacts the ecosystem and air–sea fluxes of carbon dioxide (CO_2) in the western tropical North Atlantic Ocean (WTNA). Spatial and temporal dynamics of the carbonate system in the Amazon River-ocean continuum remain poorly understood, however, due to under-sampling of the river plume and limited historical data from the river mouth. This study aims to explore these CO_2 dynamics in the plume-influenced WTNA, their sensitivity to seasonal discharge and river chemistry, and their contribution to the global carbon cycle.

We conducted six river cruises in the lower reach of the Amazon River and three oceanic cruises in the WTNA during multiple seasons between 2010–2012. At the river mouth,

dissolved inorganic carbon (DIC) and alkalinity (ALK) end members from the Amazon were determined and are now reported for the first time. DIC and ALK were ~230–300 μmol L^{-1} lower than those measured ~1000 km upriver from the mouth, historically used to represent the Amazon's contribution to the ocean. Our measured DIC end member was ~100 μmol L^{-1} higher than that of a previous estimate, causing a ~25% increase in the net community production calculated for the mesohaline region of the plume. Inorganic nutrients at the mouth were also measured and compared with previous literature, showing differences in concentrations and seasonal variability that may indicate long term changes in river chemistry and human impact.

During the oceanic expeditions, we estimated the seasonal air–sea CO_2 fluxes using *in situ* and remotely-sensed observations, and analyzed the deviation of the pCO_2-salinity relationships from conservative mixing calculated by our newly-determined river end members. The plume was a major sink for atmospheric CO_2 in June, and a weak source/sink in July and September. Differences in monthly CO_2 fluxes were primarily due to seasonal discharge and salinity distributions of the plume. An eighteen-year (2003–2020) satellite-derived time series of CO_2 fluxes revealed June-2010 as somewhat of an anomaly, although a strong June CO_2 sink was consistently observed over the past two decades. Further exploration of other months and years will be necessary to confirm any significant climate-driven trends.

INDEX WORDS: carbon dioxide, pCO_2, Amazon River, river plume, air–sea CO_2 flux, ocean carbon sequestration, dissolved inorganic carbon, satellite imagery, ocean color, discharge, inorganic nutrient, western tropical North Atlantic Ocean

USING IN-SITU AND REMOTELY-SENSED OBSERVATIONS TO ESTIMATE THE INFLUENCE OF AMAZON RIVER CHEMISTRY AND DISCHARGE ON ATMOSPHERIC CARBON DIOXIDE UPTAKE IN THE WESTERN TROPICAL NORTH ATLANTIC OCEAN

by

LINQUAN MU

B.S., East China Normal University, China, 2011

M.S., University of Georgia, 2014

A Dissertation Submitted to the Graduate Faculty of The University of Georgia in Partial Fulfillment of the Requirements for the Degree

DOCTOR OF PHILOSOPHY

ATHENS, GEORGIA

2021

USING IN-SITU AND REMOTELY-SENSED OBSERVATIONS TO ESTIMATE THE INFLUENCE OF AMAZON RIVER CHEMISTRY AND DISCHARGE ON ATMOSPHERIC CARBON DIOXIDE UPTAKE IN THE WESTERN TROPICAL NORTH ATLANTIC OCEAN

by

LINQUAN MU

Major Professor: Patricia L. Yager

Committee: Adrian B. Burd
Brian M. Hopkinson
Charles S. Hopkinson
Patricia M. Medeiros
Helga do Rosario Gomes

Electronic Version Approved:

Ron Walcott
Vice Provost for Graduate Education and Dean of the Graduate School
The University of Georgia
August 2021

ACKNOWLEDGEMENTS

This study was supported by the National Science Foundation (ANACONDAS, OCE-0934095 and OCE-1133277), and the Gordon & Betty Moore Foundation (ROCA, GBMF-MMI-2293 and 2928). I want to thank the ANACONDAS and ROCA science teams, and the captains and crew of the RV *Knorr*, RV *Melville*, RV *Atlantis* for their support of the scientific goals of the ANACONDAS project. I thank the Brazilian National Council for Scientific and Technological Development (CNPq, Portuguese: Conselho Nacional de Desenvolvimento Científico e Tecnológico) for permission to sample in the lower reaches of the river, and the Brazilian Navy for the permission to sample in the Brazil EEZ in 2012. I want to thank my adviser, Tish Yager, for teaching me how to be an independent researcher and always being there for me. I thank the Department of Marine Sciences at the University of Georgia for providing me financial support through Teaching Assistantships, Research Assistantships, and Departmental Fellowships, and the UGA Graduate School for a COVID-19 Summer Assistantship.

TABLE OF CONTENTS

Page

LIST OF TABLES

Page

LIST OF FIGURES

Page

CHAPTER 1

INTRODUCTION

As the world's largest river by discharge, the Amazon River contributes ~20% of the global riverine discharge to the ocean. Its massive delivery of freshwater to the ocean produces an extensive layer of fresher seawater, called the "plume", floating on the surface of the western tropical North Atlantic Ocean (WTNA). This plume significantly impacts the dynamics of carbon dioxide (CO_2) in the region. This study aims to explore the spatial and temporal dynamics of the air–sea CO_2 flux in the plume-influenced WTNA, its sensitivity to seasonal discharge and river chemistry, and its contribution to the global carbon cycle.

Air–Sea CO_2 Exchange on Continental Shelves

Continental shelf waters, extending from the coastline to a depth of about 200 m towards the open ocean, act as a highly dynamic transition zone where rivers, estuaries, land, ocean, and atmosphere converge and interact (Chen and Borges, 2009; Bianchi et al., 2013; Laruelle et al., 2018). Unlike the open oceans, where copious observations of air-sea CO_2 fluxes have been conducted by large international research programs since the 1980s (Fasham et al., 2001; Pfeil et al., 2012; etc.), coastal oceans have been poorly sampled and frequently neglected in past studies of air-sea carbon fluxes. Such a knowledge gap may be due primarily to the complex nature of carbon system dynamics in these shelf waters (Borges 2005; Muller-Karger et al., 2005; Chen and Borges, 2009; Liu et al., 2010).

Oceanographers have debated whether the coastal waters as a whole are a net source or sink for atmospheric CO_2, despite their success in assessing the air-sea CO_2 exchange of the open ocean (Chen et al., 2013). Many early researchers believed that estuaries and coastal waters function as a CO_2 source (Smith and Mackenzie, 1987; Kempe, 1995; Smith and Hollibaugh, 1993; Cai et al., 1999; Dai et al., 2008; etc.), but few data existed for other continental margins until recent years (Chen et al., 2013). Many continental shelves absorb CO_2 from the atmosphere during the summer season (Borges et al., 2005; Chen and Borges, 2009; etc.). A number of shelf regions that were originally thought to be sources of CO_2, are now considered sinks because of a large CO_2 drawdown observed in multiple winter data sets (Thomas et al., 2004; Cai et al., 2006; Jiang et al., 2008). Thus, oceanographers agreed that the coastal waters as a whole was a net sink for atmospheric CO_2, contributing ~20% of the global ocean carbon sink despite the area being only 7% of the surface ocean (Chen et al., 2013).

Historical controversies on the CO_2 flux direction in the shelf waters originated from the complex nature of the coastal carbon systems. For example, coastal waters receive a considerable amount of both inorganic and organic carbon from the terrestrial ecosystem, in addition to exchanges with the atmosphere, sediments and open ocean (Frankignoulle and Borges, 2001; Chen and Borges, 2009). The interactions of carbon from multiple sources results in greater seasonal and spatial variability, making representative carbon flux measurements in the coastal system substantially more challenging than in the open ocean. In fact, the large uncertainty involved in estimating the coastal air-sea CO_2 flux has become a major obstacle for a precise calculation of the global carbon budget (Tsunogai et al., 1999;

Muller-Karger et al., 2005; Cai et al., 2013). Improving the accuracy of flux estimates in the coastal system is therefore required for a meaningful carbon budget assessment on the global scale.

CO_2 Fluxes in the Amazon River Plume

A river plume refers to a thin layer of fresher water on the surface of the ocean, outside the bounds of an estuary or river channel (Figure 1.1). Because of high discharge, large tropical rivers can greatly impact coastal carbon systems (Tsunogai et al., 1999; Chen et al., 2012; Bauer et al., 2013) and even impact offshore ocean conditions (Subramaniam et al., 2008). Fueled by organic matter transported from the terrestrial system, and low total carbonate, rivers are highly supersaturated with respect to dissolved CO_2 gas as respiration exceeds autochthonous gross primary production (Smith and Mackenzie, 1987; Richey et al., 2002). Upon reaching the ocean and mixing with seawater, riverine waters become increasingly less saturated, and eventually undersaturated in CO_2 due to two primary factors: 1) a significant shift in carbonate chemistry equilibria as a result of mixing with ocean waters, and 2) a typically strong phytoplankton bloom fueled by riverine nutrients, once the waters clarify and stratification provides enhanced light availability (Edmond et al., 1981; Smith and Demaster, 1996; Ternon et al., 2000; Kortzinger, 2003).

Large river plumes are critical constituents of coastal systems and have prominent impacts on the CO_2 dynamics and carbon fluxes in the plume-affected oceans. As the world's largest river, the Amazon River flows into the WTNA at a rate of nearly 0.2 Sverdrup (1 Sv = 1 million cubic meters per second), creating a low salinity Amazon River plume (ARP) that covers an area as large as ~2 million km^2 and covering 20% of the WTNA (Coles et al., 2013;

Kortzinger, 2003; Subramaniam et al., 2008). The Amazon-impacted continental shelf is defined from the southern limit of the plume (west of 47°W) northward to French Guiana (~6°N) and seaward to the shelf break, which starts at the 100 m isobath (Smoak, 2010; summarized in Lefevre et al., 2017). The plume heads offshore into deeper waters from French Guiana to as far north as the Caribbean (~15°N), or as far east as ~40°W. The ARP carries a significant load of terrestrially-derived nutrients and organic matter, contributing tremendously to the carbon budget of this marginal system. Assessing the surface water CO_2 distribution and air-sea fluxes with higher accuracy in the ARP will help determine the source versus sink status of this region.

Several studies have provided an estimate of the CO_2 exchange in the ARP by estimating the overall sink in the plume from an extrapolation based on a relatively stable relationship between the pCO_2 and salinity (Ternon et al. 2000; Kortzinger 2003; Cooley et al. 2007; Lefevre et al. 2010; Ibánhez et al., 2015; Lefèvre et al., 2017). Körtzinger (2003) combined a pCO_2 versus sea surface salinity (SSS) relationship ($15 < SSS < 34.9$) from a single November cruise with the monthly climatological SSS means of the Word Ocean Atlas 2001 to integrate an air-sea CO_2 flux. This approach resulted in an overall CO_2 sink of 14 Tg C yr^{-1} for the plume area of 2.4×10^6 km^2 (defined as $S < 34.9$), corresponding to an average air-sea CO_2 flux density of –1.37 mol m^{-2} d^{-1}. Cooley et al. (2007) estimated seasonal fluxes based on multiple cruises from different seasons and different years, and reported an annual sink of 15 ± 6 Tg C yr^{-1}. Lefèvre et al. (2010) estimated a CO_2 flux of –0.35 mol m^{-2} yr^{-1} and a smaller plume surface area of 1.1×10^6 km^2 (also defined as $S < 34.9$), giving an integrated CO_2 sink of 5 Tg C yr^{-1} for the Amazon River plume. These fluxes are all extremely low

compared with the CO_2 emission from the Amazon River itself (500 Tg C yr^{-1}, Richey et al., 2002), but they are large enough to offset a proportion of typical tropical North Atlantic Ocean outgassing (30 Tg C yr^{-1}, Mikaloff- Fletcher et al. 2007; Subramaniam et al 2008).

Cruise Information and Chapters Layout

A better understanding of the CO_2 flux in the ARP is fundamental before it can be placed in a global context, particularly in light of global change. In this dissertation, I look at data from three oceanic surveys in the ARP during 2010–2012, including a transect to the Amazon River mouth, along with six sampling expeditions within the lower reaches of the river itself. It is worth pointing out that there has only been once before this study (Lefèvre et al., 2017) when the carbon fluxes were reported for the inner plume of the Amazon River, due to its inaccessibility, and the lower reaches have never before been sampled this extensively. The oceanic expeditions in 2010 and 2011 mainly sampled the mid- and outer plume for approximately a month, whereas the 2012 was able to get to the river mouth for the first time hitherto. This data set allowed us to gain valuable knowledge on the carbon flux of the inner Amazon River and the different CO_2-regulating mechanisms close to river mouth compared with plume farther offshore. The oceanic cruises also provided high resolution pCO_2 and DO data sets, supported by a large number of other field measurements (e.g., Yeung et al. 2012; Coles et al. 2013; Goes et al. 2014; Chong et al. 2014; Satinsky et al. 2014; Medeiros et al. 2015; Seidel et al. 2015; Conroy et al. 2016; Zielinski et al. 2016; Conroy et al. 2017; Weber et al. 2017; Satinsky et al. 2017; Stenegren et al. 2017; Doherty et al. 2017; de O. Silva et al 2017; Gomes et al. 2018), to examine the seasonality of the air–sea CO_2 fluxes in this highly dynamic region in terms of both physical and biogeochemical processes. The riverine

measurements provide a key baseline, or "river endmember" for calculations of the biogeochemical impact of physical and biological processes in the plume.

In Chapter 2, I present data from six expeditions to the lower reach of the Amazon River during multiple seasons between 2010–2012 (Figure 1.2). During these river cruises, dissolved inorganic carbon (DIC) and alkalinity (ALK) end members from the Amazon were determined at the mouth and reported for the first time. Inorganic nutrients were also measured and compared with previous literature. These new measurements significantly change our estimates of the global impact of the ARP.

In Chapter 3, I report and analyze data from three oceanic cruises in the Amazon River plume. During these expeditions (Figure 1.3), we estimated the seasonal air–sea CO_2 fluxes using *in situ* and remotely-sensed observations, and analyzed the deviation of the pCO_2-salinity relationships from conservative mixing calculated by our newly-determined river end members. We find that the plume is a strong carbon sink during June, but that outgassing from the outer edges of the plume can offset uptake by the mid-salinity regions during July and September.

In the Addendum to Chapter 3, an eighteen-year (2003–2020) satellite-derived time series during the highest river discharge month of June is reported to explore the interannual variability and trends of the plume size and CO_2 flux. This analysis revealed June-2010 as somewhat of an anomaly, although a strong June CO_2 sink was consistently observed over the past two decades. Further exploration of other months and years will be necessary to confirm any significant climate-driven trends.

References

Bauer, J. E., Cai, W. J., Raymond, P. A., Bianchi, T. S., Hopkinson, C. S., & Regnier, P. A. (2013). The changing carbon cycle of the coastal ocean. *Nature*, *504*(7478), 61-70.

Bianchi, T., Allison, M., & Cai, W. (2014). An introduction to the biogeochemistry of river-coastal systems. In *Biogeochemical Dynamics at Major River-Coastal Interfaces Linkages with Global Change* (pp. 3-18): Cambridge University Press.

Borges, A. V., Delille, B., & Frankignoulle, M. (2005). Budgeting sinks and sources of CO2 in the coastal ocean: Diversity of ecosystems counts. *Geophysical Research Letters*, *32*(14).

Cai, W. J., Pomeroy, L. R., Moran, M. A., & Wang, Y. (1999). Oxygen and carbon dioxide mass balance for the estuarine-intertidal marsh complex of five rivers in the southeastern US. *Limnology and Oceanography*, *44*(3), 639-649.

Cai, W. J., Dai, M., & Wang, Y. (2006). Air-sea exchange of carbon dioxide in ocean margins: A province-based synthesis. *Geophysical Research Letters*, *33*(12).

Cai, W. J., Chen, C. A., & Borges, A. (2013). Carbon dioxide dynamics and fluxes in coastal waters influenced by river plumes. *Biogeochemical Dynamics at Major River-Coastal Interfaces, edited by: Bianchi, TS, Allison MA, and Cai, W.-J., Cambridge University Press, Cambridge*, 155-173.

Chen, C. T. A., & Borges, A. V. (2009). Reconciling opposing views on carbon cycling in the coastal ocean: Continental shelves as sinks and near-shore ecosystems as sources of atmospheric CO2. *Deep Sea Research Part II: Topical Studies in Oceanography*, *56*(8-10), 578-590.

Chen, C. T. A., Huang, T. H., Fu, Y. H., Bai, Y., & He, X. (2012). Strong sources of CO2 in upper estuaries become sinks of CO2 in large river plumes. *Current Opinion in Environmental Sustainability*, *4*(2), 179-185.

Chen, C. T. A., Huang, T. H., Chen, Y. C., Bai, Y., He, X., & Kang, Y. (2013). Air–sea exchanges of CO2 in the world's coastal seas. *Biogeosciences*, *10*(10), 6509-6544.

Chong, L. S., Berelson, W. M., McManus, J., Hammond, D. E., Rollins, N. E., & Yager, P. L. (2014). Carbon and biogenic silica export influenced by the Amazon River Plume: Patterns of remineralization in deep-sea sediments. *Deep Sea Research Part I: Oceanographic Research Papers*, *85*, 124-137.

Coles, V. J., Brooks, M. T., Hopkins, J., Stukel, M. R., Yager, P. L., & Hood, R. R. (2013). The pathways and properties of the Amazon River Plume in the tropical North Atlantic Ocean. *Journal of Geophysical Research: Oceans*, *118*(12), 6894-6913.

Conroy, B. J., Steinberg, D. K., Stukel, M. R., Goes, J. I., & Coles, V. J. (2016). Meso-and microzooplankton grazing in the Amazon River plume and western tropical North Atlantic. *Limnology and Oceanography*, *61*(3), 825-840.

Conroy, B. J., Steinberg, D. K., Song, B., Kalmbach, A., Carpenter, E. J., & Foster, R. A. (2017). Mesozooplankton graze on cyanobacteria in the amazon river plume and western tropical north Atlantic. *Frontiers in microbiology*, *8*, 1436.

Cooley, S. R., Coles, V. J., Subramaniam, A., & Yager, P. L. (2007). Seasonal variations in Amazon plume-related atmospheric carbon sink. *Global Biogeochemical Cycles*, *21*(3).

Dai, M., Zhai, W., Cai, W. J., Callahan, J., Huang, B., Shang, S., et al. (2008). Effects of an estuarine plume-associated bloom on the carbonate system in the lower reaches of the

Pearl River estuary and the coastal zone of the northern South China Sea. *Continental Shelf Research*, *28*(12), 1416-1423.

Doherty, M., Yager, P. L., Moran, M. A., Coles, V. J., Fortunato, C. S., Krusche, A. V., et al. (2017). Bacterial biogeography across the Amazon River-ocean continuum. *Frontiers in Microbiology*, *8*, 882.

Edmond, J. M., Boyle, E. A., Grant, B., & Stallard, R. F. (1981). The chemical mass balance in the Amazon plume I: the nutrients. *Deep Sea Research Part A. Oceanographic Research Papers*, *28*(11), 1339-1374.

Fasham, M. J., Balino, B. M., Bowles, M. C., Anderson, R., Archer, D., Bathmann, U., et al. (2001). A new vision of ocean biogeochemistry after a decade of the Joint Global Ocean Flux Study (JGOFS). *AMBIO: A Journal of the Human Environment*, *2001*(Sp. No. 10), 4-31.

Frankignoulle, M., & Borges, A. V. (2001). European continental shelf as a significant sink for atmospheric carbon dioxide. *Global biogeochemical cycles*, *15*(3), 569-576.

Goes, J. I., H. R. Gomes, A. M. Chekalyuk, E. J. Carpenter, J. P. Montoya, V. J. Coles, P. L. Yager, et al. (2014). Influence of the Amazon River discharge on the biogeography of phytoplankton communities in the western tropical North Atlantic. *Progress in Oceanography 120*: 29–40.

Gomes, H. D. R., Xu, Q., Ishizaka, J., Carpenter, E. J., Yager, P. L., & Goes, J. I. (2018). The influence of riverine nutrients in niche partitioning of phytoplankton communities–a contrast between the Amazon River Plume and the ChangJiang (Yangtze) River diluted water of the East China Sea. *Frontiers in Marine Science*, *5*, 343.

Ibánhez, J. S. P., Diverrès, D., Araujo, M., & Lefèvre, N. (2015). Seasonal and interannual variability of sea-air CO2 fluxes in the tropical Atlantic affected by the Amazon River plume. *Global Biogeochemical Cycles*, *29*(10), 1640-1655.

Jiang, L. Q., Cai, W. J., Wanninkhof, R., Wang, Y., & Lüger, H. (2008). Air-sea CO2 fluxes on the US South Atlantic Bight: Spatial and seasonal variability. *Journal of Geophysical Research: Oceans*, *113*(C7).

Kempe, S. (1995). Coastal seas: a net source or sink of atmospheric carbon dioxide? *LOICZ Report and Studies*, *1*, 27.

Körtzinger, A. (2003). A significant CO2 sink in the tropical Atlantic Ocean associated with the Amazon River plume. *Geophysical Research Letters*, *30*(24).

Laruelle, G. G., Cai, W. J., Hu, X., Gruber, N., Mackenzie, F. T., & Regnier, P. (2018). Continental shelves as a variable but increasing global sink for atmospheric carbon dioxide. *Nature Communications*, *9*(1), 1-11.

Lefèvre, N., Diverrès, D., & Gallois, F. (2010). Origin of CO2 undersaturation in the western tropical Atlantic. *Tellus B: Chemical and Physical Meteorology*, *62*(5), 595-607.

Lefèvre, N., Flores Montes, M., Gaspar, F. L., Rocha, C., Jiang, S., De Araújo, M. C., & Ibánhez, J. (2017). Net heterotrophy in the Amazon continental shelf changes rapidly to a sink of CO2 in the outer Amazon plume. *Frontiers in Marine Science*, *4*, 278.

Liu, K. K., Atkinson, L., Quiñones, R., & Talaue-McManus, L. (Eds.). (2010). *Carbon and nutrient fluxes in continental margins: a global synthesis*. Springer Science & Business Media.

Medeiros, P. M., Seidel, M., Ward, N. D., Carpenter, E. J., Gomes, H. R., Niggemann, J., et al. (2015). Fate of the Amazon River dissolved organic matter in the tropical Atlantic Ocean. *Global Biogeochemical Cycles*, *29*(5), 677-690.

Mikaloff Fletcher, S. E., Gruber, N., Jacobson, A. R., Gloor, M., Doney, S. C., Dutkiewicz, S., et al. (2007). Inverse estimates of the oceanic sources and sinks of natural CO2 and the implied oceanic carbon transport. *Global Biogeochemical Cycles*, *21*(1).

Muller-Karger, F. E., Varela, R., Thunell, R., Luerssen, R., Hu, C., & Walsh, J. J. (2005). The importance of continental margins in the global carbon cycle. *Geophysical Research Letters*, *32*(1).

Pfeil, B., Olsen, A., Bakker, D. C., Hankin, S., Koyuk, H., Kozyr, A., et al. (2013). A uniform, quality controlled Surface Ocean CO2 Atlas (SOCAT). *Earth System Science Data*, *5*(1), 125-143.

Richey, J. E., Melack, J. M., Aufdenkampe, A. K., Ballester, V. M., & Hess, L. L. (2002). Outgassing from Amazonian rivers and wetlands as a large tropical source of atmospheric CO2. *Nature*, *416*(6881), 617-620.

Satinsky, B. M., Crump, B. C., Smith, C. B., Sharma, S., Zielinski, B. L., Doherty, M., et al. (2014). Microspatial gene expression patterns in the Amazon River Plume. *Proceedings of the National Academy of Sciences*, *111*(30), 11085-11090.

Satinsky, B. M., Smith, C. B., Sharma, S., Landa, M., Medeiros, P. M., Coles, V. J., et al. (2017). Expression patterns of elemental cycling genes in the Amazon River Plume. *The ISME journal*, *11*(8), 1852-1864.

Seidel, M., Yager, P. L., Ward, N. D., Carpenter, E. J., Gomes, H. R., Krusche, A. V., et al. (2015). Molecular-level changes of dissolved organic matter along the Amazon River-to-ocean continuum. *Marine Chemistry*, *177*, 218-231.

Silva, B. S. O., Coutinho, F. H., Gregoracci, G. B., Leomil, L., De Oliveira, L. S., Froes, A., et al. Virioplankton assemblage structure in the lower river and ocean continuum of the Amazon. *MSphere*, 2017, 2 (5), e00366-e17.

Smith, S. V., & Mackenzie, F. T. (1987). The ocean as a net heterotrophic system: implications from the carbon biogeochemical cycle. *Global Biogeochemical Cycles*, *1*(3), 187-198.

Smith, S. V., & Hollibaugh, J. T. (1993). Coastal metabolism and the oceanic organic carbon balance. *Reviews of Geophysics*, *31*(1), 75-89.

Smith Jr, W. O., & Demaster, D. J. (1996). Phytoplankton biomass and productivity in the Amazon River plume: correlation with seasonal river discharge. *Continental Shelf Research*, *16*(3), 291-319.

Smoak, J. M. (2010). The Amazon shelf. *Carbon and Nutrient Fluxes in Continental Margins: a Global Synthesis, eds KK Liu, L. Atkinson, R. Qui-ones, and LT McManus (New York, NY: Springer)*, 443-449.

Stenegren, M., Berg, C., Padilla, C. C., David, S. S., Montoya, J. P., Yager, P. L., & Foster, R. A. (2017). Piecewise structural equation model (SEM) disentangles the environmental conditions favoring diatom diazotroph associations (DDAs) in the western tropical north Atlantic (WTNA). *Frontiers in Microbiology*, *8*, 810.

Subramaniam, A., Yager, P. L., Carpenter, E. J., Mahaffey, C., Björkman, K., Cooley, S., et al. (2008). Amazon River enhances diazotrophy and carbon sequestration in the tropical North Atlantic Ocean. *Proceedings of the National Academy of Sciences*, *105*(30), 10460-10465.

Ternon, J. F., Oudot, C., Dessier, A., & Diverres, D. (2000). A seasonal tropical sink for atmospheric CO2 in the Atlantic Ocean: the role of the Amazon River discharge. *Marine Chemistry*, *68*(3), 183-201.

Thomas, H., Bozec, Y., Elkalay, K., & De Baar, H. J. (2004). Enhanced open ocean storage of CO2 from shelf sea pumping. *Science*, *304*(5673), 1005-1008.

Tsunogai, S., Watanabe, S., & Sato, T. (1999). Is there a "continental shelf pump" for the absorption of atmospheric CO2? *Tellus B: Chemical and Physical Meteorology*, *51*(3), 701-712.

Weber, S. C., Carpenter, E. J., Coles, V. J., Yager, P. L., Goes, J., & Montoya, J. P. (2017). Amazon River influence on nitrogen fixation and export production in the western tropical North Atlantic. *Limnology and Oceanography*, *62*(2), 618-631.

Yeung, L. Y., Berelson, W. M., Young, E. D., Prokopenko, M. G., Rollins, N., Coles, V. J., et al. (2012). Impact of diatom-diazotroph associations on carbon export in the Amazon River plume. *Geophysical Research Letters*, *39*(18).

Zielinski, B. L., Allen, A. E., Carpenter, E. J., Coles, V. J., Crump, B. C., Doherty, M., et al. (2016). Patterns of transcript abundance of eukaryotic biogeochemically-relevant genes in the Amazon River Plume. *PLoS One*, *11*(9), e0160929.

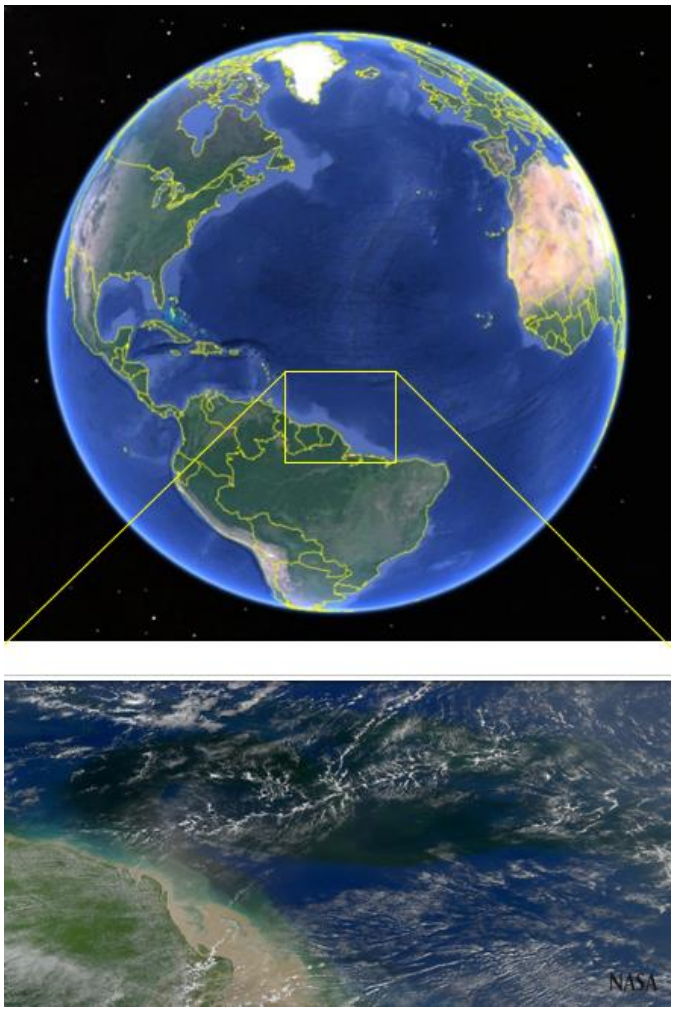

Figure 1.1. Location of the Amazon River plume. Top image from Google earth. Bottom image courtesy of Norman Kuring (Ocean Biology Processing Group, National Aeronautics and Space Administration / Goddard Space Flight Center, Greenbelt, MD).

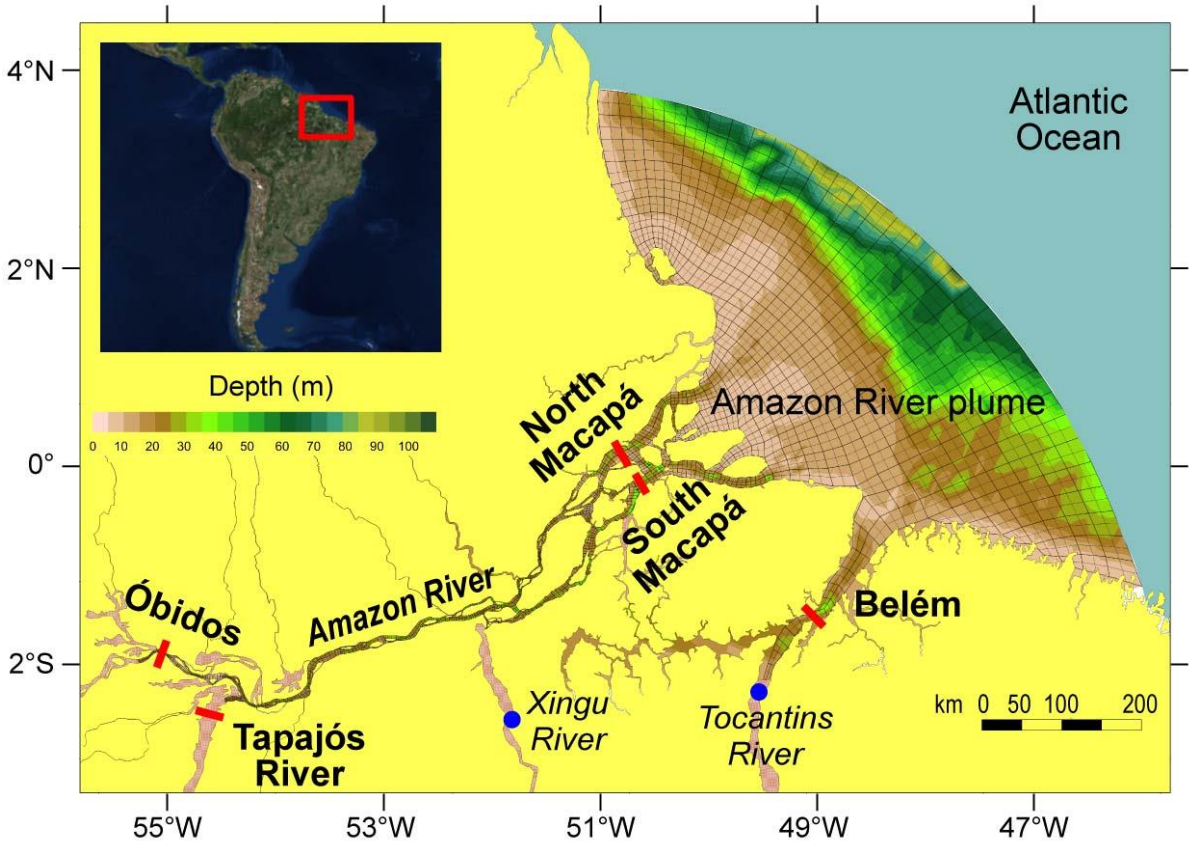

Figure 1.2. Geochemical surveys were taken at two inner gateways (Óbidos and Tapajós) and three outer gateways (North Macapá, South Macapá, and Belém) along the lower Amazon River during 2010–2012 (modified from Ward et al. 2015).

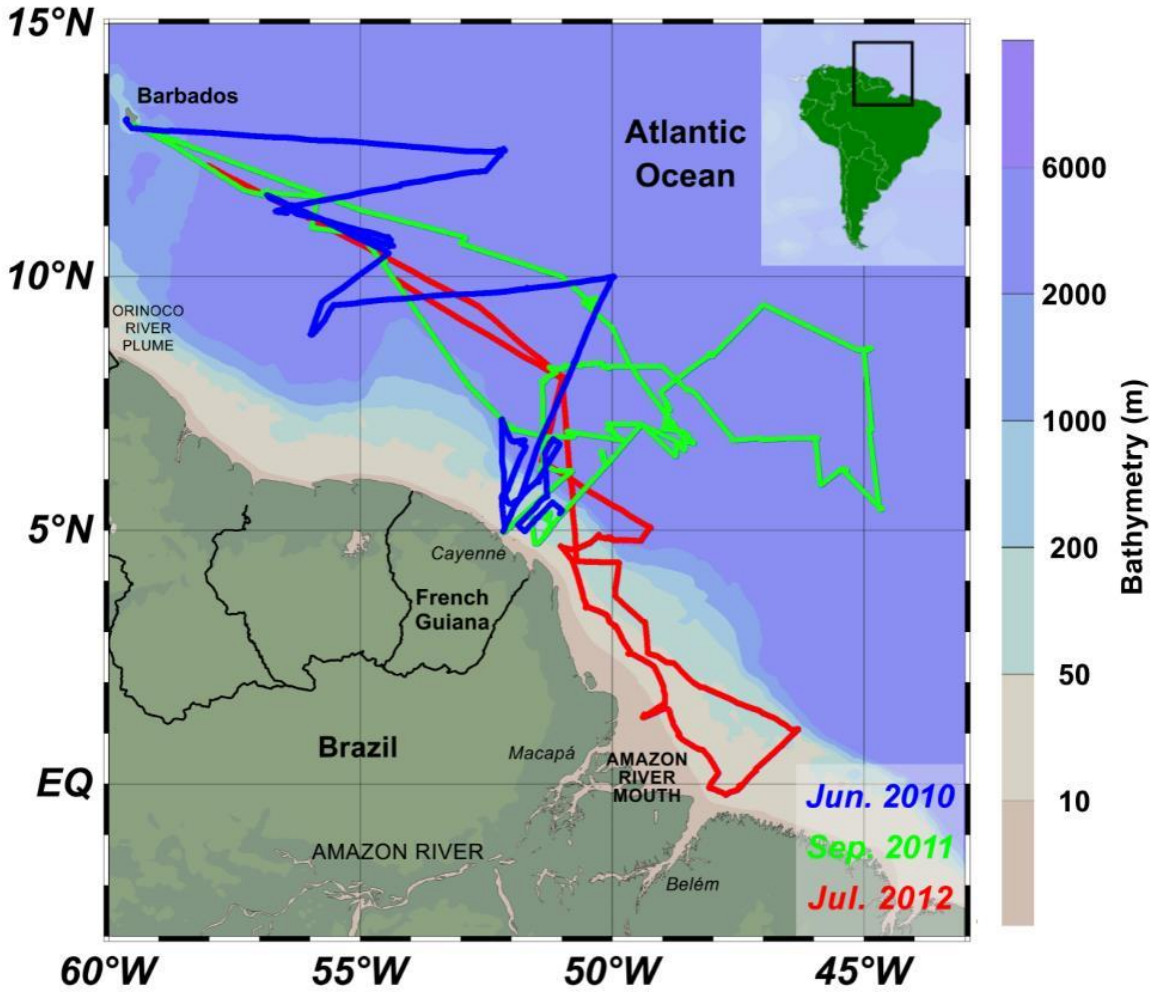

Figure 1.3. Site map and three oceanic cruise tracks 2010–2012.

CHAPTER 2

CARBONATE AND NUTRIENT CONTRIBUTIONS FROM THE AMAZON RIVER TO THE WESTERN TROPICAL NORTH ATLANTIC OCEAN[1]

[1]Linquan Mu, Benjamin Page, Nicholas Ward, Alex Krusche, Alexandra Montebelo, Carlos Eduardo de Rezende, Jeffrey Richey, and Patricia L. Yager. To be submitted to *Geophysical Research Letters*.

Abstract

The Amazon River contributes considerable freshwater and dissolved constituents to the global ocean, and its offshore plume significantly impacts biogeochemical cycling in the western tropical North Atlantic Ocean. Here we report findings from a multi-season field effort in the lower reach of the Amazon River to determine the concentrations and variability of the full carbonate system along with dissolved inorganic nitrogen, phosphorus, and silica. At the mouth, seasonally averaged dissolved inorganic carbon (DIC) and total alkalinity (ALK) were 457 ± 60 and 370 ± 82 μmol L^{-1}, respectively. Nutrients were similar to historical reports, but suggest some human impact. When combined with discharge, this outflow contributes ~3200 and 2600 Gmol y^{-1} of DIC and ALK, respectively, to the Atlantic Ocean. Results confirm that the carbonate system at the river mouth differs significantly from measurements made upriver at Manaus and Óbidos, historically used to represent the Amazon's contribution to the ocean.

1. Introduction

The Amazon River supplies ~20% of terrestrial freshwater discharge to the global ocean, the largest single contribution by far of any river. It generates a highly seasonal offshore plume that covers ~2 million km^2 of the western tropical North Atlantic Ocean (WTNA) with a thin (5–25 m) layer of lower-salinity water (Lentz & Limeburner, 1995; Salisbury et al., 2011), having a major impact on the marine ecosystem and biogeochemical cycling. In contrast to the rest of the tropical ocean, which outgasses carbon dioxide (CO_2) to the atmosphere (Mikaloff Fletcher et al., 2007; Takahashi et al., 2009; 2017), the plume provides a globally significant atmospheric CO_2 sink (Cooley et al., 2007; Subramaniam et al., 2008; Mu et al., 2021).

Considered "dilute" with respect to many dissolved ions, Ryther et al. (1967) suggested that the Amazon River depressed regional productivity. Early satellite images revealed, however, that the WTNA exhibits ocean color enhancement (Muller-Karger et al., 1989), although the origin of the color was debated (Longhurst, 1993; Muller-Karger et al., 1995; Longhurst et al., 1995). Key to the debate was the source of nutrients (Smith & DeMaster, 1996; DeMaster & Pope, 1996); productivity based on riverine nitrate or ammonium constitutes a biologically mediated transfer of carbon from the atmosphere to the ocean (Eppley & Peterson, 1979) or "carbon sequestration," whereas upwelled or eddy-pumped marine nitrate does not lead to sequestration since nutrients from depth are also accompanied by high CO_2.

Advancements in satellite technology combined with field measurements to confirm the Amazon River as the major source of the enhanced color in the WTNA (Del Vecchio & Subramaniam, 2004; Hu et al., 2004). Particulate organic carbon (POC) in the outer Amazon plume is 20x higher than nearby open ocean stations, and primarily marine in origin (Druffel et al., 2005). Thus, the color enhancement is not just riverine organic matter advected

offshore, but autochthonous marine primary production enhanced by the presence of the plume. Yet, riverine nitrate is used up almost entirely on the shelf (DeMaster & Pope, 1996) and undetectable in much of the outer plume (Subramaniam et al., 2008; Weber et al. 2017). Productivity must instead be supported by substantial contributions from nitrogen-fixing cyanobacteria (Carpenter et al., 1999; Carpenter et al., 2004; Capone et al., 2005; Weber et al., 2017). Total carbon sequestration by the plume (Subramaniam et al., 2008) is therefore the sum of that supported by new nitrogen from the river (~7 Tg C yr^{-1}) and that supported by nitrogen fixation (~20 Tg C yr^{-1}). With these estimates, the Amazon plume alone could offset most of the 30 Tg C yr^{-1} outgassed by the rest of the tropical North Atlantic Ocean (Mikaloff-Fletcher et al., 2007).

The outer plume is only one component of the Amazon River continuum, however. Significant outgassing occurs in the central basin (0.5 Pg C yr^{-1}; Richey et al., 2002), the tidally-influenced lower reaches (>20 Tg C y^{-1}; Sawakuchi et al., 2017) and the inner plume on the Brazil shelf ($0 < S < 15$; ~1 Tg C $month^{-1}$; Mu et al., 2021; Valerio et al. 2021). CO_2 emissions from the basin's surface waters are an order of magnitude higher than the fluvial export of organic and inorganic carbon to the ocean, and are thought to be driven by a combination of microbial respiration (Ward et al., 2013; 2018) and wetland CO_2 input along the mainstem (Abril et al., 2014). In contrast, clear-water várzeas along the lower reaches may enhance net community production and reduce CO_2 outgassing.

Accurately assessing the net carbon impact of the Amazon plume requires knowledge of river endmembers (Ternon et al., 2000; Körtzinger, 2003; Cooley & Yager, 2006; Cooley et al., 2007). Until now, no systematic measurements of the full carbonate system have ever been made at the Amazon mouth, and there is only spotty coverage for nutrients (Williams, 1968; Gibbs, 1972; Stallard & Edmond, 1983; Gaillardet et al., 1997). Zero-salinity intercepts from regressions of shelf or plume data (Edmond et al., 1981; DeMaster & Pope, 1996;

Cooley & Yager, 2006) are typically made in campaign mode, with little known about seasonal variability. Mixing models and mass-balance efforts (e.g., DeMaster & Aller, 2001; Ternon et al., 2000; Körtzinger, 2003; Cooley & Yager, 2006; Cooley et al., 2007) incorporate measurements from Óbidos, but these estimates are criticized (Körtzinger, 2003) since they ignore several major tributaries entering the mainstem further downstream (Richey et al., 1990; Devol et al., 1995) as well as riverine exchange with floodplain lakes and macrotidal mangrove creeks (e.g., Araujo et al., 2018; Call et al., 2019). The optimal approach is direct measurements at the river-ocean interface at the mouth.

As part of a multi-disciplinary international field program, the *River Ocean Continuum of the Amazon* (ROCA), our river field team surveyed six times over three years (2010–2012) for the full carbonate system and inorganic nutrients at five main stations (or "gateways") of the Amazon River outflow to the ocean (Table 2.1), sampling surface and subsurface waters (or "channels") in the center and near the banks of each gateway. Here we summarize the critical endmember concentrations observed over the seasons, estimate their transport rates as well as their variability at the mouth, and then calculate the river's overall annual impact on the tropical ocean.

2. Methods

2.1. Sampling and *in situ* measurement

Our expeditions extended the basic measurement program of CAMREX (Richey et al., 1990; Devol et al., 1995) to these lower reach sites, with particular attention to determining the distribution of carbonate system species and nutrients. As with CAMREX, most samples were processed in Brazilian laboratories. We sampled six times (Sep-2010, Dec-2010, May-2011, Sep-2011, Apr-2012, and Jul-2012) over three years, across two inner gateways (Tapajós and Óbidos) and three outer gateways (North Macapá, South Macapá, and Belém) of the Amazon outflow to the ocean (Figure 2.1 and Table 2.1). During about the same time

periods (May-2010, Sep-2011, and Jul-2012), an oceanographic field team, *ANACONDAS*, was sampling offshore in the Amazon River plume (Mu et al., 2021).

In situ samples were collected from surface and subsurface (50% river depth) waters at three positions across each gateway (left, center, right channel), with the exception of Tapajós, where only the center channel was sampled. Subsurface depth was ~25–35 m at Tapajós and Óbidos, and ~15–20 m at the three outer gateways. Measured properties included pH, dissolved inorganic carbon (DIC), total alkalinity (ALK), and partial pressure of CO_2 (pCO_2), along with dissolved nitrate + nitrite (NO_x), nitrite (NO_2^-), ammonium (NH_4^+), phosphate (PO_4^{3-}), and silica (Si). Most samples were analyzed at Centro de Energia Nuclear na Agricultura (CENA), USP, Brazil. A subset of DIC and ALK were processed at UGA, Athens, Georgia, USA.

2.2. Carbonate system

pH was analyzed in an overflowing graduated cylinder with an Orion 250A plus meter (with Orion probe model 9107BN) standardized by three Orion buffers at pHs of 4.01, 5.00, and 7.00, respectively.

The full set of DIC samples was measured at CENA using a Shimadzu TOCV-CPH instrument (Neu et al., 2016) and quantified with a Non-Dispersive Infrared (NDIR) detector. Samples were injected into an acidified vessel within the instrument, where all DIC was converted into CO_2 and carried to the detector through N_2 gas. A subset (N=24) of DIC was collected according to standard ocean protocols (Dickson et al., 2007) and then analyzed at UGA using a SOMMA/coulometer (Johnson et al., 1993; Cooley & Yager, 2006) with a Sea-Bird conductivity cell to improve mass determinations. UGA DIC measurements were calibrated for accuracy with Certified Reference Material (CRM; Dickson et al., 2003) and gave precision <1 μmol kg^{-1}, even on turbid river water (which was allowed to settle before processing). UGA DIC samples produced consistently higher concentrations than duplicates

measured at CENA and the deviation between duplicate pairs grew larger with increasing DIC (Figure 2.2a). Lower CENA DIC results may be due to unaccounted-for outgassing, since the CENA samples were pre-filtered. The full set of CENA DIC data were thus corrected to UGA data with a standard linear regression of the 24 duplicate pairs ($R^2 = 0.90$) as if it were a standard curve.

A subset of ALK samples (N=14) were collected according to standard ocean protocols (Dickson et al., 2007) and then analyzed at UGA using an open-cell automated potentiometric titrator (precision ~2 µmol/kg; Dickson et al., 2003; Cooley & Yager, 2006) routinely calibrated with CRMs. Alkalinity for the full set of river samples was calculated from pH and corrected CENA DIC using CO2SYS (Pierrot et al., 2006; K1 & K2 from Millero 1979). These calculated alkalinities showed good correlation with the ALK measurements ($R = 0.91$; Figure 2.2b), with a linear regression slope not significantly different from 1 and a y-intercept not significantly different from 0. Thus, we report the calculated ALK throughout this paper. In some instances, a lower ALK measured at UGA was likely due to the presence of riverine organic acids, impacting the titration.

Surface water pCO_2 was measured on the river whenever possible (N=24; all stations sampled at least once, except at Tapajos during the May-2011 and Apr-2012 expeditions). pCO_2 was determined by headspace equilibration following the methods of Cole et al. (1994). We filled 1-L bottles by overflowing with bubble-free water twice and capped the bottle securely and immediately. We introduced 60 mL of ambient air (or N_2) and equilibrated the sample by vigorous shaking for 60 seconds before the headspace was removed by syringe. Samples were collected in triplicate, along with ambient air samples, and stored in glass vials until the time of analysis with an infrared gas analyzer (Li-Cor LI-820).

These *in situ* pCO_2 measurements can be used to validate our other carbonate system parameters. Calculated pCO_2 from shipboard pH and UGA DIC using CO2SYS (Pierrot et

al., 2006; K1 & K2 from Millero 1979) showed good correlation with *in situ* pCO_2 (R = 0.89; N = 8; Figure 3.3a). Calculated pCO_2 using pH and corrected CENA DIC yielded a similarly robust correlation between the calculated and measured pCO_2 (R = 0.85, N = 24; Figure 2.3b). Throughout the rest of the paper and figures, we report pCO_2 and ALK calculated for all the stations and time points from *in situ* pH and corrected CENA DIC using CO2SYS (Pierrot et al., 2006; K1 & K2 from Millero 1979).

2.3. Inorganic nutrients

Chemical analysis on inorganic nutrient species followed the standard procedures described in APHA (2005). Briefly, NO_2^- was diazotized and coupled with *N*-(l-naphthyl)ethylene-diammonium dichloride and measured using flow-injection technique on a FIAstar 5000A analyzer made by FOSS Tecator. Then, all NO_3^- in the sample was reduced to NO_2^- with a copperized cadmium column before the total NO_x was measured colorimetrically with a FIAstar 5000A analyzer. NO_3^- was calculated as the difference between NO_x and NO_2^-. NH_4^+ was analyzed using a flow-injection system with a gas-diffusion membrane. Total DIN was the sum of NO_3^-, NO_2^-, and NH_4^+. Phosphate (PO_4^{3-}) was measured spectrophotometrically following the formation of phosphomolybdic acid using a Foss FIAstar 5000A Analyzer. Si was analyzed with a Horiba Jobin Yvon Ultima 2 ICP-OES (inductively coupled plasma optical emission spectrometry). All nutrient concentrations were initially determined in mg L^{-1}. We report μmol L^{-1} in this paper after unit conversions using the molecular weight of each measured compound.

2.4. Hydrography

Daily discharges at Óbidos and the three lower tributaries were obtained from the Brazilian National Water Agency (ANA, https://www.snirh.gov.br/hidroweb/apresentacao; Ward et al., 2015) from Jan-2009 to Aug-2012 (Table 2.2; Figure 2.4) and averaged for each

month. The sum of these discharges was assumed to comprise 100% of the combined Amazon discharge at the mouth through N. Macapá, S. Macapá, and Belém (Table 2.2).

Cross-channel discharge was also determined at N. Macapá, S. Macapá, and Belém using an Acoustic Doppler Current Profiler (ADCP; Ward et al., 2015) during four expeditions (May-2011, Jul-2012, Sep-2011, and Dec-2010; Table 2.2). Once summed, these ADCP measurements provided an independent measurement of the total river discharge at the mouth, and the proportions discharged through each outer gateway over time (Table 2.2).

ADCP data correlated well with monthly total ANA discharge for the same months (R = 0.95; Figure 2.5) but a linear regression through the data had both a non-zero y-intercept and a slope significantly different from 1. The ADCP measurements were notably higher than ANA measurements during September. Since we needed a full annual cycle of discharge for the three gateways, we used this regression as a standard curve to correct ANA discharge for the months during which ADCP data were unavailable (i.e., Jan–Apr, Jun, Aug, Oct–Nov). The corrected monthly ANA discharge data (for 8 months) were combined with ADCP discharge data (for 4 months) to estimate seasonal and annual transport of the river. These monthly discharge data were then combined with concentrations (measured, Table 2.3, or interpolated, Table 2.4) to estimate total contributions to the ocean.

2.5. Monthly Transport

To provide a single number to represent the monthly outflow at the river mouth, each of the measured concentrations of DIC, ALK, DIN, PO_4^{3-}, and Si at N. Macapá, S. Macapá, and Belém were weighted by the relative discharges at the three outer gateways and then summed. This weighting was done for each of the 4 expedition months (May-2011, Jul-2012, Sep-2011, and Dec-2010; Table 2.5; note that Belém was not sampled during Sep-2010 and Apr-2012, so a combined number is not available for those times). Monthly transport was calculated by multiplying concentrations at each gateway by the corresponding discharge for

these 4 months. Annual transport was estimated as the sum of all the monthly transport estimates. The variance in individual concentrations and discharge were propagated through the calculations (Bevington & Robinson, 2003) and are reported as a variance on the final transport.

3. Results and Discussion

3.1. Hydrography

At the three outer gateways (N. Macapá, S. Macapá, and Belém), monthly discharge (Table 2.2; Figure 2.4) followed a clear seasonal cycle, declining continuously from the flooded boreal summer (May) to the dry season (December), and then increasing again in the boreal spring (Ward et al. 2015). Here we use the following terminology: “low water” = Oct–Dec; “rising water” = Jan–Mar; “high water” = Apr–Jun; “falling water” = Jul–Sep (Ward et al., 2015). A greater drop in discharge between high (May) and low (December) water was seen at N. Macapá compared to S. Macapa (68% versus 57%). Seasonally, the Macapá channels contributed 81–88% to the total discharge when combined. The proportion of total discharge remained roughly the same for S. Macapá throughout the seasons, while N. Macapá contributed a smaller proportion during low discharge in December, compensated by a 7% increase at Belém. Discharge at Óbidos and inner tributaries (i.e., Tapajós, Xingu, and Tocantins) followed a similar seasonal trend (Table 2.2), with inner tributary discharges dropping measurably from May to December.

3.2. River water properties

Variations in water properties across channels and with depth at each gateway were generally much smaller than differences between gateways (Figure 2.4, 2.6). Thus, for each sampling period, the data values reported below are the average (±1 STD; N = 6) of left, center, and right channel surface and subsurface values across each channel (except for Tapajós where only the center channel was sampled; N=2).

River temperature at the three outer gateways ranged from 28.6–31.3 °C, with cooler waters generally observed during high water, and warmer waters observed during falling and low water (Figure 2.4a-c). Surface temperatures tended to be slightly warmer than subsurface temperatures by 0–0.4 °C. Temperatures at the inner gateways (Tapajós and Óbidos; Figure 2.6a-b) were generally more variable (ranging from 27.9–32.0 °C) than the outer gateways. The greatest vertical gradient was observed at Tapajós during low water (Dec-2010) when the surface was 1.4 °C warmer than subsurface. Surface temperature > 0.5 °C lower than subsurface was only recorded at Tapajós during May-2011 and Jul-2012.

Carbonate system parameters varied ~2 fold at N. Macapá and S. Macapá, and less so at Belém (Figure 2.4d-i). DIC at the three outer gateways ranged from 249–606 μmol L^{-1} and ALK from 189–560 μmol L^{-1}. The highest DIC (> 400 μmol L^{-1}) and ALK (> 350 μmol L^{-1}) values were recorded at N. and S. Macapá. At Belém, DIC and ALK were generally lower and much less variable (DIC: 310–367 μmol L^{-1}; ALK: 278–343 μmol L^{-1}). The lowest DIC and ALK values (both < 150 μmol L^{-1}) were exclusively observed at Tapajós (Figure 2.6g-h).

At all gateways, pH ranged from ~6.5–7.5 (Figure 2.4j-l, 2.6g-h), with more acidic values generally found during high water. Seasonality in pH was relatively weak and differed from gateway to gateway. The highest pH (~7.5) values were observed during low water (Dec-2010) at N. Macapá and S. Macapá, and during falling water (Sep-2011) at Belém. At N. and S. Macapá, pH increased during the transition from high water to falling and low water, in contrast to Belém, Óbidos, and Tapajós, where higher pH values were observed during falling water (Figure 2.4j-l, 2.6g-h).

pCO_2 ranged from 731–4627 μatm at the outer gateways (Figure 2.4m-o) and 428–4867 μatm at the inner gateways (Figure 2.6i-j), generally decreasing from a peak supersaturation value at high water to lower supersaturation during falling and low water. It was lowest (~450 μatm) at Tapajós during falling water (Sep-2010 and Sep-2011) and highest (> 4500 μatm) at

N. Macapá and Óbidos during high water. Most notably, during low water, pCO_2 at the outer gateways was > 2000 µatm lower than at Óbidos.

The concentrations and composition of total DIN were highly variable across gateways and seasons (Figure 2.4p-r, 2.6k-l). DIN concentrations at the three outer gateways ranged between 8.1–26.5 µmol L^{-1} and were dominated by nitrate. At Macapá stations, nitrate contributed 73–97% to the total DIN. The range was substantially lower at Belém (8.1–17 µmol L^{-1}), where 34–66% of the DIN came from ammonium. Nitrite concentrations were relatively small, constituting only 1–10% of the total DIN. The highest DIN reached 40.2 ± 2.6 µmol L^{-1} at Óbidos during low water (Dec-2010), and the lowest DIN of 3.7 ± 1.0 µmol L^{-1} was observed at Tapajós during falling water (Sep-2010).

Phosphate concentrations ranged dramatically from 0.04–0.6 µmol L^{-1} across seasons and gateways (Figure 2.4s-u, 2.6m-n). At the outer gateways, phosphate decreased from a peak at high water to lower concentrations during falling or low water. Highest concentrations (> 0.5 µmol L^{-1}) were mostly observed at N. or S. Macapá stations. At Óbidos and Tapajós, phosphate was primarily < 0.3 µmol L^{-1}, with the exception of Jul-2012, during which the concentrations reached 0.43 ± 0.11 and 0.56 ± 0.06 µmol L^{-1} at Óbidos and Tapajós, respectively.

Dissolved silica concentrations at the Macapá stations ranged between 118–223 µmol L^{-1}, higher than at Belém (28–136 µmol L^{-1}) during all seasons (Figure 2.4v-x). Silica was lowest (< 30 µmol L^{-1}) at Belém during low water, while the highest silica concentrations (> 200 µmol L^{-1}) were observed at Macapá, Óbidos, and Tapajós during falling water (Sep-2011; Table 2.3). No consistent seasonality for silica was observed across gateways.

Monthly variations in material fluxes from the river to the ocean (Table 2.4a) followed discharge closely (Figure 2.7). Thus, the large seasonal changes in discharge dominated any

seasonal variation in material transport. The only exception to this finding was a peak in silica transport in September that did not follow the discharge curve (Figure 2.7).

3.3. Carbon endmembers

The biogeochemistry of the Amazon River mainstem above Óbidos is well characterized in the extensive CAMREX literature (e.g., Devol et al. 1995). One key question we wished to address was how the carbonate system at the mouth differs from the upstream mainstem. Our sampling plan included Óbidos so that we could compare concentrations there to both near-synchronous measurements at the mouth and to historic data sets. Near Manaus (>1000 km upriver from the mouth), a 10-year time series (1983–1993) of river chemistry shows mean concentrations for DIC = 744 ± 126 μmol L^{-1} and ALK = 600 ± 115 μmol L^{-1} (Devol et al., 1995). The data show good linkages between river chemistry and tributary contributions, especially between alkalinity and the Andes contributions. Under *in situ* conditions, pCO_2 is ~4500 μatm. Downstream at Óbidos, roughly halfway between Manaus and the river mouth, DIC historically ranged from 430–645 μmol kg^{-1} (Richey et al., 1990; Table 2.6), a significant DIC reduction with respect to the range observed near Manaus. This loss reflects CO_2 outgassing to the atmosphere in excess of respiration. Near the mouth, a single historic DIC observation of 374 μmol L^{-1} in Nov-1991 (Druffel et al., 2005) suggested additional outgassing between Óbidos and the mouth.

In this study, we found that DIC and ALK at Óbidos were lower than expected, ranging from 308–439 and 226–294 μmol L^{-1}, respectively (Table 2.5). Seasonal variation in the carbonate system at Óbidos was similar to historic reports (Richey et al., 1990), but our concentrations were lower by 100–200 μmol L^{-1} across all seasons (Table 2.6). With this reduction in concentration at Óbidos, we found less of a difference than expected between Óbidos and the near mouth measurements. Our combined (discharge weighted) DIC and

ALK concentrations at the mouth were similar to or higher than our observations at Óbidos, ranging 387–552 and 309–511 μmol L^{-1}, respectively (Table 2.5).

In December 2010, DIC concentrations at the mouth were notably > 200 μmol L^{-1} greater than at Óbidos. These high CO_2 concentrations were likely due to high microbial respiration in December, as reported in Ward et al. (2013). But they also coincided with the observation that dissolved organic carbon (DOC) concentrations at the mouth were > 100 μmol L^{-1} lower than at Óbidos during the same period (Seidel et al., 2016). The decrease of DOC from Óbidos to the Macapá gateways likely reflects microbial respiration enhanced by more reactive organic matter inputs from clear-water tributaries and floodplains close to the mouth (Seidel et al., 2016). Outgassing also occurred during the transit from Óbidos, reflected in the fact that the pCO_2 at the mouth was quite low in Dec-2010 (~1000 μatm) compared to the 4000 μatm at Óbidos. The higher DIC at both N. and S. Macapá can be explained by excess respiration, but the higher pH (7.5) and alkalinity (~500 μmol L^{-1}) at both outer gateways in December seems inconsistent with respiration and outgassing alone. Inputs from the lower tributaries (as represented by Tapajós) have relatively higher pH (Figure 2.6), but they were still quite low in alkalinity. Explanations for the high pH and alkalinity at the mouth in December require additional investigation.

For carbonate system river endmembers, some previous studies used DIC = 744 μmol kg^{-1} (Körtzinger, 2003) and ALK = 600 μmol kg^{-1} (Ternon et al., 2000 reported in Devol et al. 1995). More recent reports gave significantly lower estimates, with DIC = 309 or 369 μmol kg^{-1} (Cooley & Yager, 2006; Cooley et al., 2007). In this study, we increase the annually-averaged river DIC & ALK endmembers to DIC = 457 ± 60 and ALK = 370 ± 82 μmol L^{-1} at the mouth (Table 2.4a). A key implication of this change is the calculation of a greater atmospheric carbon sink in the offshore plume. For example, during May 2010, net community production determined using these new endmembers is 25–50% greater than

initially calculated for mesohaline stations (Yeung et al. 2012) and a number of low-salinity stations flip from being net heterotrophic to being net autotrophic. Estimates of NCP at high-salinity stations were less impacted by these changes.

3.4. Inorganic nutrients

Nutrient concentrations at the river mouth determined by this study can also be compared to historical data (Edmond, 1981; DeMaster & Pope, 1996; Table 3.7). Our total inorganic nutrient concentrations were generally in agreement with historic data (Table 2.7) although there were some key exceptions. Most dramatically, ammonium concentrations were up to 10-fold higher and nitrite was 5–20 times higher than DeMaster & Pope (1996) across all seasons. As a result, total DIN concentrations were elevated and exceeded those reported in DeMaster & Pope (1996) in most seasons. This increase in DIN as well as ammonium and nitrite may reflect increasing human inputs to the watershed between 1980–2010.

Dissolved phosphate concentrations in this study were lower than historic reports across all seasons, by as much as a factor of two. Since phosphate is particle-reactive, this reduction of dissolved P at the mouth could reflect a reduction in the total P at the mouth due to more sediment-trapping dams upstream. Alternatively, a higher particle load, perhaps from greater soil erosion, might adsorb more of the dissolved P near the mouth. Inventories of total P near the mouth would help determine the mechanism.

Silica concentrations at the mouth varied between 129–193 μmol L^{-1}, and were more seasonally variable and somewhat higher than those reported by DeMaster & Pope (1996), who measured silica between 140–150 μmol L^{-1} (Table 2.7). Edmond (1981) also reported significantly lower observations of 100–120 μmol Si L^{-1} during high water in 1981. A regression of silica versus salinity from the outer plume (Yeung et al. 2012) suggested a much lower endmember (~89 μmol L^{-1}), likely not accounting for significant diatom production in the inner plume.

3.5. Transport

Despite seasonal variability in material concentrations (Table 2.4a), variations in monthly discharge dominate seasonal delivery of riverine DIC, ALK, and inorganic nutrients to the ocean (Figure 2.7). Thus, any climate-driven variability or change in watershed hydrology and river discharge will have a large impact on the biogeochemistry of the WTNA. During our study, the annual DIN transport of 140 ± 10 Gmol N yr^{-1} (Table 2.4b) would have supported ~0.9 ± 0.01 Tmol C yr^{-1} of new production offshore (assuming a C:N ratio of 6.6), significantly higher (> 30%) than previous estimates of riverine-supported (0.6 Tmol C yr^{-1}; Subramaniam et al., 2008). Nitrogen fixation provides additional bioavailable N, increasing NCP to ~ 2.3 Tmol C yr^{-1}, if adequate phosphate is available. The delivery of 2.7 ± 0.2 Gmol yr^{-1} of dissolved phosphate, however, would only support 0.3 ± 0.02 Tmol C yr^{-1} (assuming C:P = 106) requiring an additional phosphate supply to support production in the plume (Weber et al. 2017). As humans continue to impact the Amazon basin (Covey et al., 2021), it will be critical that both natural and anthropogenic drivers of carbon sequestration and export are examined along this important river-ocean continuum.

4. Summary

Full carbonate system endmembers of the Amazon River were estimated for the first time, providing a key improvement to the measurements historically used to represent the Amazon's contribution to the ocean. An annual average DIC endmember of 457 ± 60 μmol L^{-1} and ALK endmember of 370 ± 82 μmol L^{-1} were determined for the river mouth. With these river endmembers, previous calculations of carbon sequestration by the plume become underestimates since they were based on biological DIC drawdown from higher initial concentrations.

Our total DIN measurements were elevated from historical records in most seasons, primarily because ammonium and nitrite concentrations were ~10-fold higher, suggesting

greater human perturbations to the river chemistry since 1980s. Our observed phosphate concentrations were lower than historical reports. Net community production estimates for the plume calculated from riverine DIN or DIP are significantly below those based on DIC drawdown in the plume (Cooley et al. 2007; Subramaniam et al. 2008; Mu et al. 2021), confirming that other sources of bio-available N and P (e.g., N_2 fixation, particulate P desorption; Weber et al. 2017) are needed to support carbon sequestration in the plume.

Monthly and annual transport of carbon and nutrient species are significant, but primarily regulated by discharge, despite seasonal variations in concentrations. Our sampling of the lower reaches revealed a river-ocean continuum highly sensitive to changes in watershed hydrology, but also showing clear indications of human impact.

Acknowledgements

Financial support was provided by the Gordon and Betty Moore Foundation Marine Microbial Initiative for the River-Ocean Continuum of the Amazon project (Lead PI: PLY), NSF, and FAPESP Grant #08/58089-9. Sampling in Macapá was assisted by students J. E. Melo Diniz, K. dos Santos, E. Santos, B. Zelinsky, C. Smith, B. Satinsky and C. Fortunato. Sampling in Óbidos was assisted by J. Mauro, T. Beldini and R. da Silva. LM thanks the Department of Marine Sciences at the University of Georgia for financial support through a Teaching Assistantship and a Departmental Fellowship.

Monthly ANA discharge data of the Amazon River at Óbidos and from major tributaries were retrieved from the Brazilian National Water Agency at https://www.snirh.gov.br/hidroweb/apresentacao, cited in Ward et al. (2015). ADCP discharge at outer Amazon River gateways was obtained from Ward et al. (2015). Concentrations and transport of river carbonate & inorganic nutrient species will be deposited in BCO-DMO and publicly available.

References

Abril, G., Martinez, J. M., Artigas, L. F., Moreira-Turcq, P., Benedetti, M. F., Vidal, L., et al. (2014). Amazon River carbon dioxide outgassing fuelled by wetlands. *Nature*, *505*(7483), 395-398. https://doi.org/10.1038/nature12797

APHA. (2005). Standard Methods for the Examination of Water and Wastewater. 21st Edition, American Public Health Association/American Water Works Association/Water Environment Federation, Washington DC.

Araujo, B. F., Hintelmann, H., Dimock, B., de Lima Sobrinho, R., Bernardes, M. C., de Almeida, M. G., et al. (2018). Mercury speciation and Hg stable isotope ratios in sediments from Amazon floodplain lakes—Brazil. *Limnology and Oceanography*, *63*(3), 1134-1145. https://doi.org/10.1002/lno.10758

Bevington, P. R., & Robinson, D. K. (2003). *Data reduction and error analysis*. McGraw-Hill: New York.

Call, M., Santos, I. R., Dittmar, T., de Rezende, C. E., Asp, N. E., & Maher, D. T. (2019). High pore-water derived CO2 and CH4 emissions from a macro-tidal mangrove creek in the Amazon region. *Geochimica et Cosmochimica Acta*, *247*, 106-120. https://doi.org/10.1016/j.gca.2018.12.029

Capone, D. G., Burns, J. A., Montoya, J. P., Subramaniam, A., Mahaffey, C., Gunderson, T., et al. (2005). Nitrogen fixation by *Trichodesmium* spp.: An important source of new nitrogen to the tropical and subtropical North Atlantic Ocean. *Global Biogeochemical Cycles*, *19*(2). https://doi.org/10.1029/2004GB002331

Carpenter, E. J., Montoya, J. P., Burns, J., Mulholland, M. R., Subramaniam, A., & Capone, D. G. (1999). Extensive bloom of a N2-fixing diatom/cyanobacterial association in the

tropical Atlantic Ocean. *Marine Ecology Progress Series*, *185*, 273-283. https://doi.org/10.3354/meps185273

Carpenter, E. J., Subramaniam, A., & Capone, D. G. (2004). Biomass and primary productivity of the cyanobacterium *Trichodesmium* spp. in the tropical N Atlantic Ocean. *Deep Sea Research Part I: Oceanographic Research Papers*, *51*(2), 173-203. https://doi.org/10.1016/j.dsr.2003.10.006

Cole, J. J., Caraco, N. F., Kling, G. W., & Kratz, T. K. (1994). Carbon dioxide supersaturation in the surface waters of lakes. *Science*, *265*(5178), 1568-1570. https://doi.org/10.1126/science.265.5178.1568

Cooley, S. R., & Yager, P. L. (2006). Physical and biological contributions to the western tropical North Atlantic Ocean carbon sink formed by the Amazon River plume. *Journal of Geophysical Research: Oceans*, *111*(C8). https://doi.org/10.1029/2005JC002954

Cooley, S. R., Coles, V. J., Subramaniam, A., & Yager, P. L. (2007). Seasonal variations in the Amazon plume-related atmospheric carbon sink. *Global Biogeochemical Cycles*, *21*(3). https://doi.org/10.1029/2006GB002831

Covey, K., Soper, F., Pangala, S., Bernardino, A., Pagliaro, Z., Basso, L., et al. (2021). Carbon and Beyond: The Biogeochemistry of Climate in a Rapidly Changing Amazon. *Frontiers in Forests and Global Change*, *4*, p11. https://doi.org/10.3389/ffgc.2021.618401

Del Vecchio, R., & Subramaniam, A. (2004). Influence of the Amazon River on the surface optical properties of the western tropical North Atlantic Ocean. *Journal of Geophysical Research: Oceans*, *109*(C11). https://doi.org/10.1029/2004JC002503

DeMaster, D. J., & Pope, R. H. (1996). Nutrient dynamics in Amazon shelf waters: results from AMASSEDS. *Continental Shelf Research*, *16*(3), 263-289. https://doi.org/10.1016/0278-4343(95)00008-O

DeMaster, D. J., & Aller, R. C. (2001). Biogeochemical processes on the Amazon shelf: changes in dissolved and particulate fluxes during river/ocean mixing. In M. E. McClain, R. Victoria, J. E. Richey (Eds.), *The Biogeochemistry of the Amazon Basin* (pp. 328-357). Oxford University Press. https://doi.org/10.1093/oso/9780195114317.003.0020

Devol, A. H., Forsberg, B. R., Richey, J. E., & Pimentel, T. P. (1995). Seasonal variation in chemical distributions in the Amazon (Solimões) River: a multiyear time series. *Global Biogeochemical Cycles*, *9*(3), 307-328. https://doi.org/10.1029/95GB01145

Dickson, A. G., Afghan, J. D., & Anderson, G. C. (2003). Reference materials for oceanic CO2 analysis: a method for the certification of total alkalinity. *Marine Chemistry*, *80*(2-3), 185-197. https://doi.org/10.1016/S0304-4203(02)00133-0

Dickson, A.G., Sabine, C. L. & Christian, J. R. Eds. (2007). Guide to Best Practices for Ocean CO2 Measurements. PICES Special Publication 3, 191 pp.

Druffel, E. R. M., Bauer, J. E., & Griffin, S. (2005). Input of particulate organic and dissolved inorganic carbon from the Amazon to the Atlantic Ocean. *Geochemistry, Geophysics, Geosystems*, *6*(3). https://doi.org/10.1029/2004GC000842

Edmond, J. M., Boyle, E. A., Grant, B., & Stallard, R. F. (1981). The chemical mass balance in the Amazon plume I: The nutrients. *Deep Sea Research Part A: Oceanographic Research Papers*, *28*(11), 1339-1374. https://doi.org/10.1016/0198-0149(81)90038-8

Eppley, R. W., & Peterson, B. J. (1979). Particulate organic matter flux and planktonic new production in the deep ocean. *Nature*, *282*(5740), 677-680. https://doi.org/10.1038/282677a0

Gaillardet, J., Dupre, B., Allegre, C. J., & Négrel, P. (1997). Chemical and physical denudation in the Amazon River Basin. *Chemical geology*, *142*(3-4), 141-173. https://doi.org/10.1016/S0009-2541(97)00074-0

Gibbs, R. J. (1972). Water chemistry of the Amazon River. *Geochimica et Cosmochimica Acta*, *36*(9), 1061-1066. https://doi.org/10.1016/0016-7037(72)90021-X

Hu, C., Montgomery, E. T., Schmitt, R. W., & Muller-Karger, F. E. (2004). The dispersal of the Amazon and Orinoco River water in the tropical Atlantic and Caribbean Sea: Observation from space and S-PALACE floats. *Deep Sea Research Part II: Topical Studies in Oceanography*, *51*(10-11), 1151-1171. https://doi.org/10.1016/j.dsr2.2004.04.001

Johnson, K. M., Wills, K. D., Butler, D. B., Johnson, W. K., & Wong, C. S. (1993). Coulometric total carbon dioxide analysis for marine studies: maximizing the performance of an automated gas extraction system and coulometric detector. *Marine chemistry*, *44*(2-4), 167-187. https://doi.org/10.1016/0304-4203(93)90201-X

Körtzinger, A. (2003). A significant CO_2 sink in the tropical Atlantic Ocean associated with the Amazon River plume. *Geophysical Research Letters*, *30*(24). https://doi.org/10.1029/2003GL018841

Lentz, S. J., & Limeburner, R. (1995). The Amazon River Plume during AMASSEDS: Spatial characteristics and salinity variability. *Journal of Geophysical Research: Oceans*, *100*(C2), 2355-2375. https://doi.org/10.1029/94JC01411

Longhurst, A. (1993). Seasonal cooling and blooming in tropical oceans. *Deep Sea Research Part I: Oceanographic Research Papers*, *40*(11-12), 2145-2165. https://doi.org/10.1016/0967-0637(93)90095-K

Longhurst, A., Sathyendranath, S., Platt, T., & Caverhill, C. (1995). An estimate of global primary production in the ocean from satellite radiometer data. *Journal of plankton Research*, *17*(6), 1245-1271. https://doi.org/10.1093/plankt/17.6.1245

Mikaloff Fletcher, S. E., Gruber, N., Jacobson, A. R., Gloor, M., Doney, S. C., Dutkiewicz, S., et al. (2007). Inverse estimates of the oceanic sources and sinks of natural CO2 and the implied oceanic carbon transport. *Global Biogeochemical Cycles*, *21*(1). https://doi.org/10.1029/2006GB002751

Mu, L., Gomes, H. R., Burns, S. M., Goes, J. I., Coles, V. J., Rezende, C. E., et al. (2021). Temporal variability of air–sea CO2 flux in the western tropical North Atlantic influenced by the Amazon River plume. *Global Biogeochemical Cycles*., *35*(6), e2020GB006798. https://doi.org/10.1029/2020GB006798

Muller-Karger, F. E., McClain, C. R., Fisher, T. R., Esaias, W. E., & Varela, R. (1989). Pigment distribution in the Caribbean Sea: Observations from space. *Progress in Oceanography*, *23*(1), 23-64. https://doi.org/10.1016/0079-6611(89)90024-4

Muller-Karger, F. E., Richardson, P. L., & McGillicuddy, D. (1995). On the offshore dispersal of the Amazon's Plume in the North Atlantic: Comments on the paper by A. Longhurst,

"Seasonal cooling and blooming in tropical oceans". *Deep Sea Research Part I: Oceanographic Research Papers*, *42*(11-12), 2127-2137. https://doi.org/10.1016/0967-0637(95)00085-2

Neu, V., Ward, N. D., Krusche, A. V. and Neill, C. (2016). Dissolved organic and inorganic carbon flow paths in an Amazonian transitional forest. *Frontiers in Marine Science*, *3*, 114. https://doi.org/10.3389/fmars.2016.00114

Pierrot, D., Lewis, E., & Wallace, D. W. R. (2006). MS Excel program developed for CO2 system calculations. In *ORNL/CDIAC-105a. Carbon Dioxide Information Analysis Center, Oak Ridge National Laboratory, US Department of Energy, Oak Ridge, Tennessee* (Vol. 3). https://doi.org/10.3334/CDIAC/otg.CO2SYS_XLS_CDIAC105a

Richey, J. E., Hedges, J. I., Devol, A. H., Quay, P. D., Victoria, R., Martinelli, L., & Forsberg, B. R. (1990). Biogeochemistry of carbon in the Amazon River. *Limnology and oceanography*, *35*(2), 352-371. https://doi.org/10.4319/lo.1990.35.2.0352

Richey, J. E., Victoria, R. L., Salati, E., & Forsberg, B. R. (1991). The biogeochemistry of a major river system: The Amazon case study. In E. T. Degens, S. Kempe, J. E. Richey (Eds.), *Biogeochemistry of Major World Rivers, Scope 42* (pp. 57–74).

Richey, J. E., Melack, J. M., Aufdenkampe, A. K., Ballester, V. M., & Hess, L. L. (2002). Outgassing from Amazonian rivers and wetlands as a large tropical source of atmospheric CO2. *Nature*, *416*(6881), 617-620. https://doi.org/10.1038/416617a

Salisbury, J., Vandemark, D., Campbell, J., Hunt, C., Wisser, D., Reul, N., & Chapron, B. (2011). Spatial and temporal coherence between Amazon River discharge, salinity, and light absorption by colored organic carbon in western tropical Atlantic surface

waters. *Journal of Geophysical Research: Oceans*, *116*(C7), C00H02. https://doi.org/10.1029/2011JC006989

Sawakuchi, H. O., Neu, V., Ward, N. D., Barros, M. D. L. C., Valerio, A. M., Gagne-Maynard, et al. (2017). Carbon dioxide emissions along the lower Amazon River. *Frontiers in Marine Science*, *4*, 76. https://doi.org/10.3389/fmars.2017.00076

Stallard, R. F., & Edmond, J. M. (1983). Geochemistry of the Amazon: 2. The influence of geology and weathering environment on the dissolved load. *Journal of Geophysical Research: Oceans*, *88*(C14), 9671-9688. https://doi.org/10.1029/JC088iC14p09671

Subramaniam, A., Yager, P. L., Carpenter, E. J., Mahaffey, C., Björkman, K., Cooley, S., et al. (2008). Amazon River enhances diazotrophy and carbon sequestration in the tropical North Atlantic Ocean. *Proceedings of the National Academy of Sciences*, *105*(30), 10460-10465. https://doi.org/10.1073/pnas.0710279105

Takahashi, T., Sutherland, S. C., Wanninkhof, R., Sweeney, C., Feely, R. A., Chipman, D. W., et al. (2009). Climatological mean and decadal change in surface ocean pCO2, and net sea–air CO2 flux over the global oceans. *Deep Sea Research Part II: Topical Studies in Oceanography*, *56*(8-10), 554-577. https://doi.org/10.1016/j.dsr2.2008.12.009

Takahashi, T., Sutherland, S. C., & Kozyr, A. (2017). Global Ocean Surface Water Partial Pressure of CO2 Database: Measurements Performed During 1957-2019 (LDEO Database Version 2019) (NCEI Accession 0160492). Version 9.9. NOAA National Centers for Environmental Information. Dataset. https://doi.org/10.3334/cdiac/otg.ndp088(v2015)

Ternon, J. F., Oudot, C., Dessier, A., & Diverres, D. (2000). A seasonal tropical sink for atmospheric CO_2 in the Atlantic Ocean: The role of the Amazon River discharge. *Marine Chemistry*, *68*(3), 183–201. https://doi.org/10.1016/S0304-4203(99)00077-8

Valerio, A. M., Kampel, M., Ward, N. D., Sawakuchi, H. O., Cunha, A. C. and Richey, J. E. (2021). CO2 partial pressure and fluxes in the Amazon River plume using in situ and remote sensing data. *Continental Shelf Research*, *215*, p.104348. https://doi.org/10.1016/j.csr.2021.104348

Ward, N. D., Keil, R. G., Medeiros, P. M., Brito, D. C., Cunha, A. C., Dittmar, T., et al. (2013). Degradation of terrestrially derived macromolecules in the Amazon River. *Nature Geoscience*, *6*(7), 530-533. https://doi.org/10.1038/ngeo1817

Ward, N. D., Krusche, A. V., Sawakuchi, H. O., Brito, D. C., Cunha, A. C., Moura, J. M. S., et al. (2015). The compositional evolution of dissolved and particulate organic matter along the lower Amazon River—Óbidos to the ocean. *Marine Chemistry*, *177*, 244-256. https://doi.org/10.1016/j.marchem.2015.06.013

Ward, N. D., Sawakuchi, H. O., Neu, V., Less, D. F., Valerio, A. M., Cunha, A. C., et al. (2018). Velocity-amplified microbial respiration rates in the lower Amazon River. *Limnology and Oceanography Letters*, *3*(3), 265-274. https://doi.org/10.1002/lol2.10062

Weber, S. C., Carpenter, E. J., Coles, V. J., Yager, P. L., Goes, J. I., & Montoya, J. P. (2017). Amazon River influence on nitrogen fixation and export production in the western tropical North Atlantic. *Limnology and Oceanography*, *62*(2), 618-631. https://doi.org/10.1002/lno.10448

Williams, P. M. (1968). Organic and inorganic constituents of the Amazon River. *Nature*, *218*(5145), 937-938. https://doi.org/10.1038/218937a0

Yeung, L. Y., Berelson, W. M., Young, E. D., Prokopenko, M. G., Rollins, N., Coles, V. J., et al. (2012). Impact of diatom-diazotroph associations on carbon export in the Amazon River plume. *Geophysical Research Letters*, *39*(18). https://doi.org/10.1029/2012GL053356

Table 2.1

Expeditions at major gateways along the lower Amazon River.

Category	Gateway	Sep-2010 §	Dec-2010	May-2011	Sep-2011	Apr-2012 §	Jul-2012
Outer Gateways	N. Macapá	√	√	√	√	√	√
	S. Macapá	√	√	√	√	√	√
	Belém		√	√	√		√
Inner Gateways	Óbidos	√	√	√	√		√
	Tapajós	√	√	√	√		√

§ Measurements were not conducted at Belém during Sep-2010 and Apr-2012, and therefore, carbonate & nutrient concentrations at the river mouth and annual transport of chemical species were only calculated for Dec-2010, May-2011, Sep-2011, and Jul-2012.

Table 2.2

River discharge through the study boundaries (from Ward et al. 2015).

	May-2011	**Jul-2012**	**Sep-2011**	**Dec-2010**
ANA discharge ($m^3 s^{-1}$)				
Óbidos	250000	246000	160000	85000
Tapajós River (tributary)	38400	7500	300	200
Other major tributaries §	46000	8500	5500	4600
ANA total discharge	334400	262000	165800	89800
ADCP discharge ($m^3 s^{-1}$)				
N. Macapá	104000 (35%)	94000 (38%)	61000 (30%)	33000 (27%)
S. Macapá	148000 (50%)	121000 (49%)	105000 (51%)	64000 (52%)
Belém	46000 (15%)	31000 (13%)	39000 (19%)	27000 (22%)
ADCP total discharge	298000	246000	205000	124000

§ The sum of discharge from the Tocantins River and the Xingu River.

Table 2.3

Seasonal concentrations of carbonate and nutrient properties averaged across channels & depths at Óbidos and Tapajós.

Gateway	Month	NO_2^- µmol L^{-1}	NO_3^- µmol L^{-1}	NH_4^+ µmol L^{-1}	NO_2^- % §	NO_3^- % §	NH_4^+ % §	DIN µmol L^{-1}	PO_4^{3-} µmol L^{-1}	Si µmol L^{-1}
Óbidos	Sep-10	0.7 ± 0.2	16.1 ± 1.8	3.5 ± 1.6	3%	79%	17%	20.2 ± 2.4	0.30 ± 0.04	139 ± 1
	Dec-10	1.7 ± 0.1	33.5 ± 1.4	5.1 ± 2.2	4%	83%	13%	40.2 ± 2.6	0.27 ± 0.03	157 ± 1
	May-11	4.7 ± 0.3	15.7 ± 1.9	2.0 ± 0.0	21%	70%	9%	22.4 ± 1.9	0.25 ± 0.03	257 ± 37
	Sep-11	2.3 ± 0.1	22.4 ± 2.2	1.5 ± 0.6	8%	80%	5%	27.8 ± 4.0	0.27 ± 0.06	222 ± 5
	Jul-12	0.6 ± 0.0	18.1 ± 2.8	1.6 ± 0.0	3%	89%	8%	20.3 ± 2.8	0.43 ± 0.11	112 ± 15
Tapajós	Sep-10	0.3 ± 0.2	1.2 ± 1.0	2.2 ± 0.2	8%	33%	59%	3.7 ± 1.0	0.04 ± 0.00	157 ± 0
	Dec-10	1.5 ± 0.3	4.7 ± 0.9	6.1 ± 1.9	12%	39%	49%	12.3 ± 2.2	0.22 ± 0.02	144 ± 2
	May-11	3.7 ± 0.5	11.1 ± 0.4	6.2 ± 0.0	18%	53%	29%	20.9 ± 0.6	0.24 ± 0.07	74 ± 5
	Sep-11	2.1 ± 0.1	6.2 ± 0.8	10.8 ± 1.4	11%	33%	57%	19.1 ± 1.6	0.18 ± 0.01	236 ± 1
	Jul-12	0.6 ± 0.1	5.9 ± 0.9	3.0 ± 0.3	6%	62%	32%	9.4 ± 1.0	0.56 ± 0.06	131 ± 2

§ The percentages in total DIN of each inorganic nitrogen species are reported.

Table 2.4

(**a**) Monthly concentrations (µmol L^{-1}) and transport (Gmol) of carbonate & inorganic nutrient species at the Amazon River mouth with corrected monthly ANA discharge (m^3 s^{-1}).

Month	Year §	DIC		ALK		DIN		PO_4^{3-}		Si		Discharge
		µmol L^{-1}	Gmol	µmol L^{-1}	Gmol	µmol L^{-1}	Gmol	µmol L^{-1}	Gmol	µmol L^{-1}	Gmol	10^{11} m^3
Jan.	**09-12**	533	260	477	233	21.1	10.3	0.4	0.2	134	65	5.0
Feb.	**09-12**	514	308	443	266	21.1	12.6	0.4	0.3	139	83	5.6
Mar.	**09-12**	495	344	409	284	21.1	14.6	0.5	0.3	144	100	7.2
Apr.	**09-12**	476	367	375	289	21.1	16.2	0.5	0.4	149	115	7.7
May.	**2011**	457	353	341	263	21.1	16.3	0.5	0.4	155	119	8.0
Jun.	**09-12**	444	324	325	237	21.8	15.9	0.4	0.3	152	111	7.3
Jul.	**2012**	431	275	309	197	22.5	14.3	0.3	0.2	150	96	6.6
Aug.	**09-12**	409	239	314	183	18.5	10.8	0.3	0.2	172	100	6.0
Sep.	**2011**	387	206	320	170	14.5	7.7	0.3	0.2	193	103	5.3
Oct.	**09-11**	442	167	384	145	16.7	6.3	0.3	0.1	172	65	3.9
Nov.	**09-11**	497	182	447	164	18.9	6.9	0.3	0.1	150	55	3.7
Dec.	**2010**	552	177	511	164	21.1	6.8	0.4	0.1	129	41	3.3

§ Years from which monthly ADCP or corrected ANA discharge was obtained.

(**b**) Annual Amazon transport of DIC, ALK, DIN, PO_4^{3-}, and Si (Gmol) with seasonal variations.

	Annual transport (Gmol)
DIC	3200 ± 270
ALK	2590 ± 220
DIN	140 ± 10
PO_4^{3-}	2.7 ± 0.2
Si	1050 ± 90

Table 2.5

Seasonal concentrations of carbonate and inorganic nutrient properties (µmol L^{-1}) at Óbidos and the river mouth. Concentrations at the mouth are the sum of the discharge-weighted monthly concentrations at the three outer gateways.

Month	Gateway	DIC µmol L^{-1}	ALK µmol L^{-1}	DIN µmol L^{-1}	PO_4^{3-} µmol L^{-1}	Si µmol L^{-1}
Dec-10	Óbidos	333 ± 93	226 ± 96	40.2 ± 2.6	0.3 ± 0.03	157 ± 1
	Mouth	552 ± 6	511 ± 2	21.1 ± 0.4	0.4 ± 0.02	129 ± 3
May-11	Óbidos	439 ± 13	294 ± 10	22.4 ± 1.9	0.2 ± 0.03	257 ± 37
	Mouth	457 ± 11	341 ± 9	21.1 ± 1.6	0.5 ± 0.03	155 ± 1
Jul-12	Óbidos	423 ± 19	274 ± 13	20.3 ± 2.8	0.4 ± 0.11	112 ± 15
	Mouth	431 ± 9	309 ± 8	22.5 ± 2.0	0.3 ± 0.05	150 ± 4
Sep-11	Óbidos	385 ± 10	284 ± 8	27.8 ± 4.0	0.3 ± 0.06	222 ± 5
	Mouth	387 ± 16	320 ± 12	14.5 ± 1.3	0.3 ± 0.03	193 ± 4
Sep-10	Óbidos	308 ± 40	237 ± 32	20.2 ± 2.4	0.3 ± 0.04	139 ± 1

Table 2.6

Seasonal DIC concentrations (µmol L^{-1}) determined for Óbidos compared with Richey et al. (1990).

Study	Discharge stage	DIC (µmol L^{-1})	Month
This study	High water	439±13	May-11
	Falling water	423±19	Jul-12
		385±10	Sep-12
	Low water	333±93	Dec-10
Richey et al. (1990) §	"High water"	~645	Aug-83
	"Falling water"	~605	Nov-83
		~570	Dec-84
		~445	Jan-83
	"Low water"	~430	Mar-84
	"Rising water"	~620	Apr-83
		~570	Jul-84

§ The periods associated with the stages of river discharge are different in Richey et al. (1990) from this study. Instead of specific months, we refer to the same discharge stages when comparing DIC concentrations between the two studies.

Table 2.7

Seasonal inorganic nutrient concentrations (μmol L^{-1}) at the Amazon River mouth compared with DeMaster & Pope (1996) and Edmond (1981).

Period	This study	D&P (96)	Edmond (81)	This study	D&P (96)	This study	D&P (96)	This study	D&P (96)
	High Water			Falling Water		Low Water		Rising Water	
Month	May-11	May-90	May-81	Sep-11	Aug-89	Dec-10	Nov-91	Apr-12 §	Mar-90
NO_3^-	15.9 ± 1.3	13	7-10	11.3 ± 2.4	12	18.1 ± 1.3	18	14 ± 2.8 §	23
NO_2^-	1.3 ± 0.1	0.2	7-12	1.7 ± 0.1	0.1	0.5 ± 0.04	0.1	1.0 ± 0.1 §	0.2
NH_4^+	3.9 ± 1.5	0.4	N/A	1.5 ± 0.5	0.4	2.6 ± 0.4	0.5	3.0 ± 0.6 §	0.4
DIN	21.1 ± 2.0	13.6	>14	14.5 ± 2.5	12.5	21.1 ± 1.4	18.6	18 ± 2.9 §	23.6
PO_4^{3-}	0.5 ± 0.04	0.6	0.4-0.8	0.3 ± 0.1	0.7	0.4 ± 0.1	0.8	0.4 ± 0.1 §	0.7
Si	155 ± 1	141	100-120	193 ± 7	144	129 ± 10	141	156 ± 14 §	149

§ Concentrations of April are estimated using values measured at N. Macapá and S. Macapá during Apr-12 and values measured at Belém during May-11 as no data were available at Belém during April-12. For a lack of discharge data, the relative proportions of April discharge of N. Macapá, S. Macapá, and Belém were assumed to be 35%, 50%, and 15%, respectively, same with May-11.

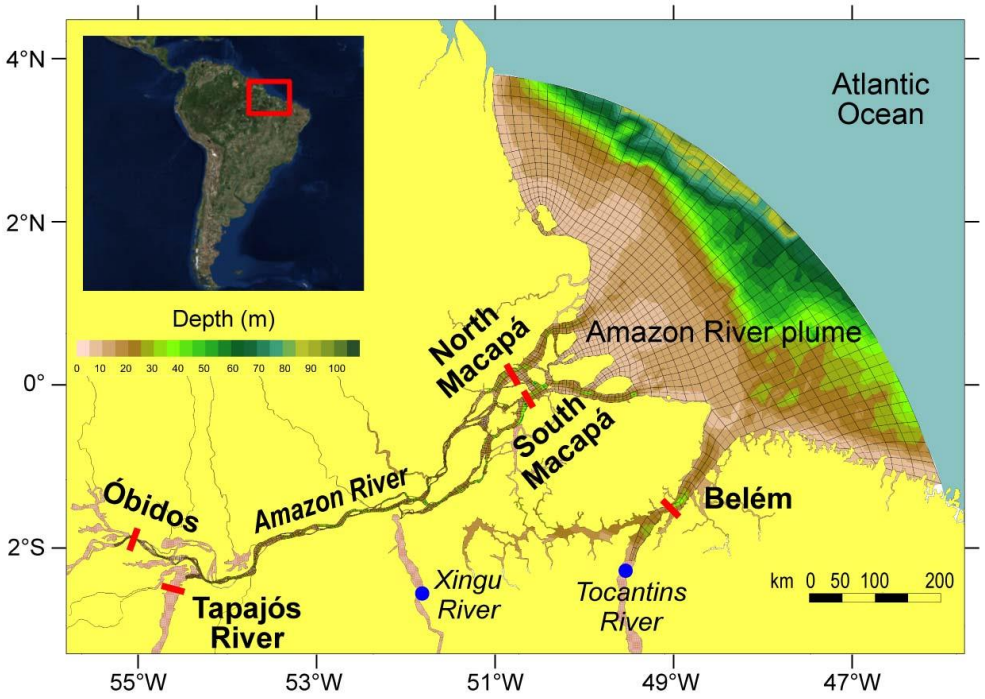

Figure 2.1. Geochemical surveys at two inner gateways (Óbidos and Tapajós) and three outer gateways (North Macapá, South Macapá, and Belém) along the lower Amazon River during 2010–2012 (modified from Ward et al. 2015).

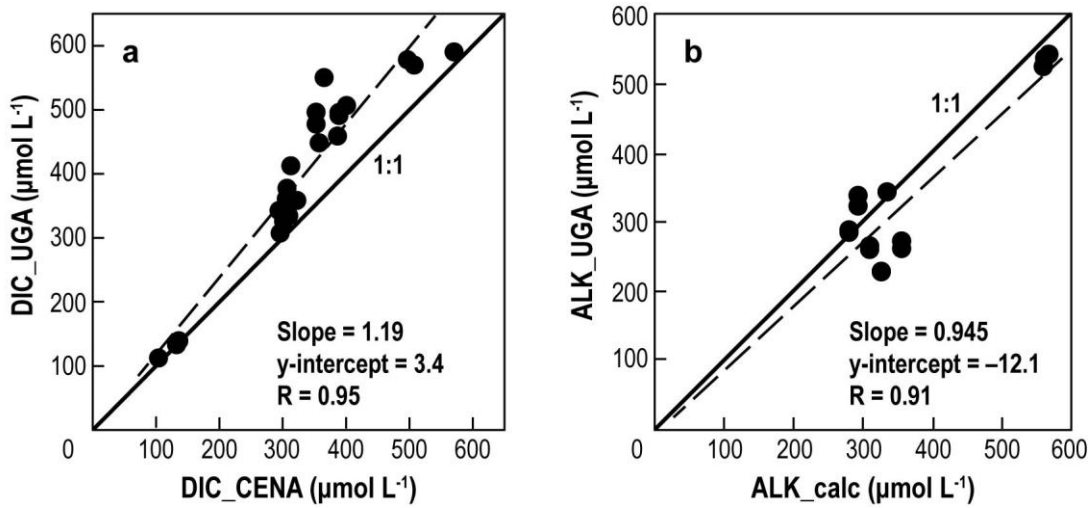

Figure 2.2. (**a**) CENA DIC compared with DIC measured at UGA (N=24; slope = 1.2 ± 0.1; y-intercept = 3.4 ± 29.9, R^2 = 0.90). (**b**) ALK calculated by pH and corrected CENA DIC compared with UGA ALK (N=14; slope = 0.95 ± 0.13; y-intercept = -12.1 ± 48.7, R^2 = 0.82).

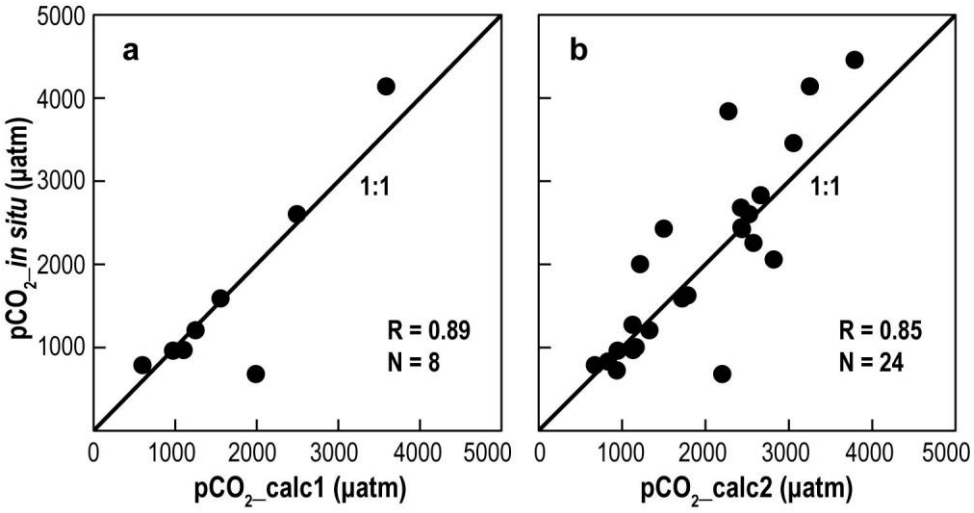

Figure 2.3. Correlation between measured *in situ* pCO_2 and: (**a**) pCO_2 calculated by pH and UGA DIC (N = 8, R = 0.89), and (**b**) pCO_2 calculated by pH and corrected CENA DIC (N = 24, R = 0.85). Solid line is the 1:1 line. One notable outlier in (**a**) is from Belém (center channel, surface) during Jul-2012.

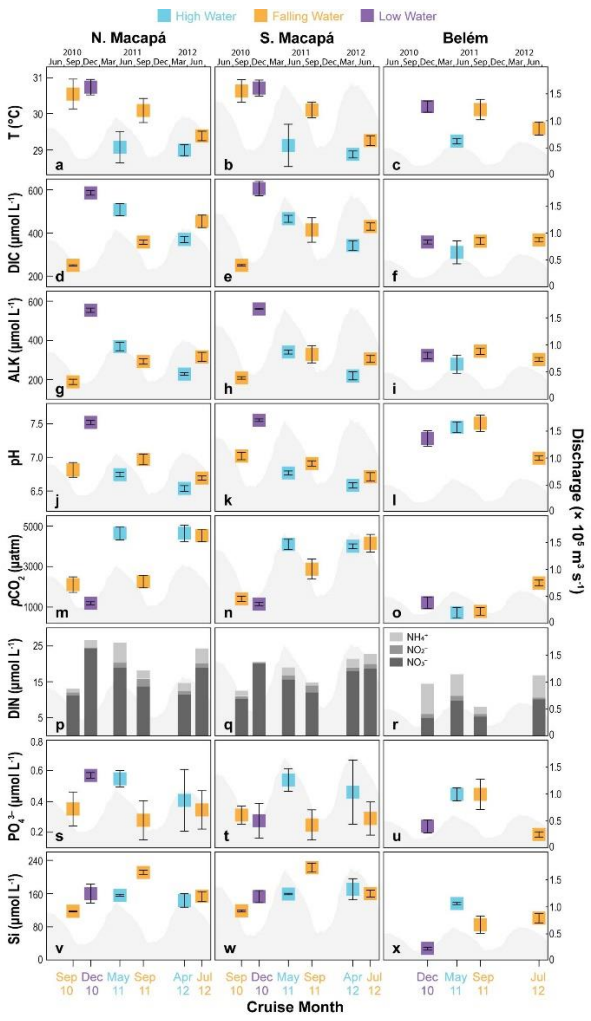

Figure 2.4. Temperature, carbonate and inorganic nutrient parameters averaged at each outer Amazon gateway (N. Macapá, S. Macapá, and Belém): (**a-c**) Temperature, °C; (**d-f**) Corrected CENA DIC, µmol L^{-1}; (**g-i**) CENA ALK calculated by pH and corrected CENA DIC, µmol L^{-1}; (**j-l**) pH; (**m-o**) pCO_2 calculated from pH and corrected CENA DIC, µatm; (**p-r**) Total DIN (nitrate + nitrite + ammonium), µmol L^{-1}; (**s-u**) Phosphate, µmol L^{-1}; (**v-x**) Silica, µmol L^{-1}. Cruise months are categorized by seasonal discharge: high water (April–June), falling water (July–September), and low water (October–December). Error bars show the standard deviation of the measurements across channels and with depth of a gateway. Monthly ANA discharge (m^3 s^{-1}) is shown as shaded area.

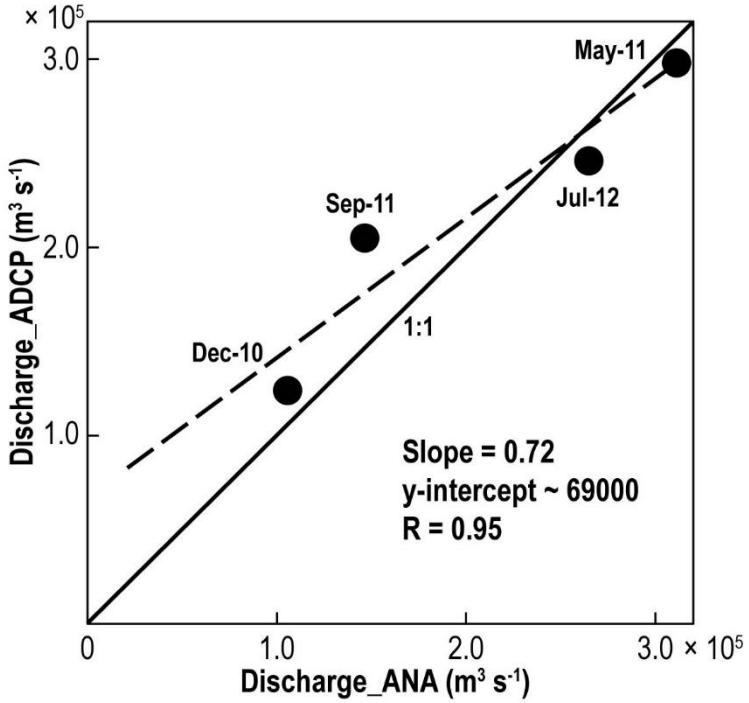

Figure 2.5. Monthly ANA discharge (m^3/s) correlated with ADCP discharge (m^3/s; Ward et al. 2015) of the four expedition months.

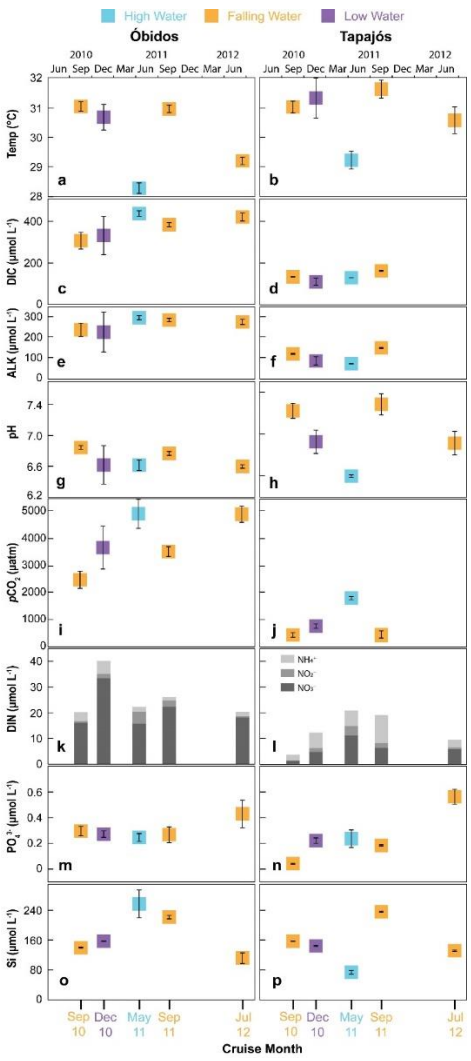

Figure 2.6. Temperature and carbonate parameters averaged at Óbidos and Tapajós: (**a**-**b**) Temperature, °C; (**c**-**d**) Corrected CENA DIC, µmol L^{-1}; (**e**-**f**) ALK calculated by pH and corrected CENA DIC, µmol L^{-1}; (**g**-**h**) pH; (**i**-**j**) pCO_2 calculated from pH and corrected CENA DIC, µatm; (**k**-**l**) Total DIN (nitrate + nitrite + ammonium), µmol L^{-1}; (**m**-**n**) Phosphate, µmol L^{-1}; (**o**-**p**) Silica, µmol L^{-1}. For measurements at Óbidos, the error bars show the standard deviation of the measurements across three channels (left, center, right) with surface and subsurface. At Tapajós, measurements were made at a single channel, and the error bars reflect difference between surface & subsurface waters.

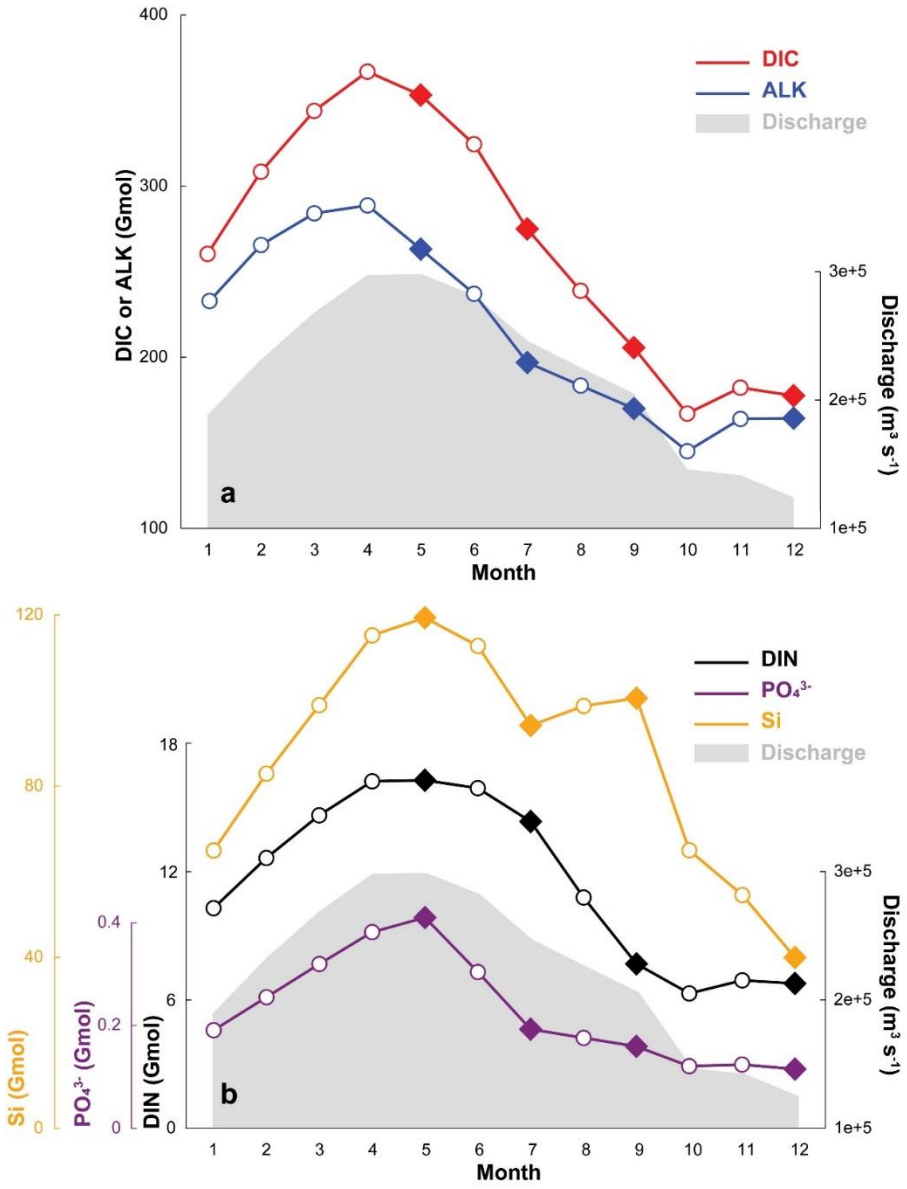

Figure 2.7. Monthly transport of inorganic carbonate and nutrient species at the Amazon River mouth: (**a**) DIC and ALK (Gmol); (**b**) DIN, PO_4^{3-}, and Si (Gmol). Monthly total discharge (m^3 s^{-1}) at the mouth is shown as shaded area. Data points marked with ♦ are calculated monthly transport from measured concentrations, and ○ indicates monthly transport interpolated between two nearest months with calculated transport based on measured concentrations.

CHAPTER 3

TEMPORAL VARIABILITY OF AIR–SEA CO_2 FLUX IN THE WESTERN TROPICAL NORTH ATLANTIC INFLUENCED BY THE AMAZON RIVER PLUME[2]

[2]An edited version of this paper was published by AGU. Copyright (2021) American Geophysical Union

Mu, L., Gomes, H. R., Burns, S. M., Goes, J. I., Coles, V. J., Rezende, C. E., Thompson, F. L., Moura R. L., Page, B., and Yager, P. L. (2021). Temporal variability of air–sea CO2 flux in the western tropical North Atlantic influenced by the Amazon River plume. *Global Biogeochemical Cycles*., *35*(6), e2020GB006798. https://doi.org/10.1029/2020GB006798

Abstract

The partial pressure of carbon dioxide (pCO_2) was surveyed across the Amazon River plume and the surrounding western tropical North Atlantic Ocean (15–0°N, 43–60°W) during three oceanic expeditions (May–June 2010, September–October 2011, and July 2012). Survey timing was chosen according to previously-described temporal variability in plume behavior due to changing river discharge and winds. *In-situ* sea surface pCO_2 and air–sea CO_2 flux exhibited robust linear relationships with sea surface salinity (SSS; 15<SSS<35), although the relationships differed among the surveys. Regional distributions of pCO_2 and CO_2 flux were estimated using SSS maps from high-resolution ocean color satellite (MODIS-Aqua) derived diffuse attenuation coefficient at 490 nm (K_d490) during the periods of study. Results confirmed that the plume is a net CO_2 sink with distinctive temporal variability: the strongest drawdown occurred during the spring flood (-2.39 ± 1.29 mmol m^{-2} d^{-1} in June 2010) while moderate drawdown with relatively greater spatial variability was observed during the transitional stages of declining river discharge (-0.42 ± 0.76 mmol m^{-2} d^{-1} in September–October 2011). The region turns into a weak source in July 2012 (0.26 ± 0.62 mmol m^{-2} d^{-1}) when strong CO_2 uptake in the mid-plume was overwhelmed by weak CO_2 outgassing over a larger area in the outer plume. Outgassing near the mouth of the river was observed in July 2012. Our observations draw attention to the importance of assessing the variable impacts of biological activity, export, and air–sea gas exchange before estimating regional CO_2 fluxes from salinity distributions alone.

1. Introduction

The large but variable outflow of the Amazon River creates an extensive plume area of undersaturated carbon dioxide (CO_2) and atmospheric CO_2 uptake by the western tropical North Atlantic (WTNA; Ternon et al., 2000; Körtzinger, 2003; Cooley et al., 2007; Lefèvre et al., 2010; Ibánhez et al., 2015; Lefèvre et al., 2017), nearly offsetting regional outgassing (Subramaniam et al., 2008), and resulting in an atmospheric CO_2 flux of global importance. Away from the plume, the tropical Atlantic (18°N–18°S) is the world's second largest regional oceanic source for atmospheric CO_2 after the tropical Pacific, with a sea-to-air CO_2 flux of ~100 Tg C yr^{-1} (Takahashi et al., 2009; Landschützer et al., 2014). This steady source of CO_2 to the atmosphere (Lefèvre et al., 2010; Takahashi et al., 2009) is predominantly driven by upwelling of CO_2-rich waters combined with net community production insufficient to counteract CO_2 supersaturation enhanced by warming (Andrié et al., 1986) during westward transport in the South Equatorial Current (SEC). Inadequate sampling in the WTNA coastal waters (Takahashi et al., 2009) has, however, left vast areas near the South American continental shelf unaccounted for in many global CO_2 flux analyses.

On the continental shelves of Brazil and French Guiana, riverine nutrients fuel intense blooms of phytoplankton once turbidity declines (Edmond et al., 1981; Demaster & Pope, 1996; Goes et al., 2014), drawing CO_2 down, and creating undersaturated conditions (Ternon et al., 2000; Cooley & Yager, 2006). The offshore Amazon River plume (ARP; Coles et al., 2013) sustains a large area of primary production by nitrogen-fixing diatom-diazotroph assemblages (DDA) and other phytoplankton (Goes et al., 2014), creating a major pathway of carbon sequestration in this region (Subramaniam et al., 2008; Yeung et al., 2012, Chong et

al., 2014). In contrast, the Amazon River mainstem is a major source of CO_2 to the atmosphere due to the decomposition of large amounts of terrestrial organic matter from wetlands and floodplains (Richey et al., 2002; Raymond et al., 2013; Ward et al., 2013; Abril et al., 2014). High riverine pCO_2 is dramatically reduced, however, when river water mixes with oceanic waters with a high buffering capacity and lower pCO_2 (Cai et al., 2013). The location and lagrangian timescale associated with the transition from CO_2-supersaturated river water to CO_2-undersaturated plume water is a key topic of interest for coastal carbon cycle studies involving large river plumes (Huang et al., 2013; Li et al., 2018).

Quantifying air–sea carbon flux for the entire ARP can be challenging due to the complex nature of plume dynamics. The propagation pathways of the ARP are modulated by discharge rates of the Amazon River, winds, ocean circulation patterns (Coles et al., 2013), as well as climatological conditions, such as the precipitation anomalies caused by seasonal shift of the Intertropical Convergence Zone (ITCZ; Lefèvre et al., 2010; Ibánhez et al., 2016) and other major climatic events (e.g. El Niño; Lefèvre et al., 2013). Remote sensing of the plume has provided some temporal and spatial information (Molleri et al., 2010; Salisbury et al., 2011). Plume waters can be tracked with satellite-derived diffuse attenuation coefficient at 490 nm (K_d490), because it is a good indicator of particulate and dissolved seawater constituents including riverine colored dissolved organic matter (CDOM), suspended materials as well as phytoplankton pigments. Thus K_d490 has a strong linear relationship with sea surface salinity (SSS) and has been used to track the spatial and temporal variability of river plumes (Del Vecchio & Subramaniam, 2004; Fournier et al., 2012). K_d490-generated SSS fields have been applied to ascertain the size of the plume within a specifically defined

salinity range (e.g., Cooley et al., 2007). Estimating a regional carbon flux from satellite-based plume distributions thus depends on obtaining a predictable relationship with these remotely-sensed variables.

Here, we present *in-situ p*CO_2 data collected from the surface of the ARP during the ANACONDAS (Amazon Influence on the Atlantic: Carbon Export from the Nitrogen Fixation by Diatom Assemblages) Project of 2010–2012, which aimed to understand the role of offshore blooms of symbiotic DDA in the drawdown of CO_2. We combine these observations with high-resolution ocean color data to obtain quasi-synoptic estimates of the seasonal variability of the air–sea CO_2 flux in the WTNA influenced by the Amazon outflow. Comparisons are made between our new findings and previously published work in order to shed light on the carbon dynamics in the ARP-influenced WTNA region.

2. Methods

2.1. Measurements at sea

The data used in this study come from three oceanic research expeditions to the WTNA during 2010–2012 onboard *RV Knorr* (May 23–June 23, 2010), *RV Melville* (September 03–October 07, 2011), and *RV Atlantis* (July 13–28, 2012) as part of the ANACONDAS Project (*https://www.bco-dmo.org/project/2097*; ship tracks shown in Figure 3.1). All three expeditions originated from Bridgetown, Barbados, crossed the plume multiple times, and sampled the French Guiana Exclusive Economic Zone (EEZ). The 2010 and 2011 expeditions included crew changes in Cayenne, French Guiana. Only the 2012 expedition entered the Brazil EEZ and sampled near the Amazon River mouth. Although we sampled three time periods in three different years (May–June 2010, July 2012, September–October

2011), we report each expedition as a representative month (June, July, and September, respectively), fully recognizing that some interannual variability also occurs. Monthly discharge of the Amazon River at Óbidos, for periods of these cruises relative to climatology (Figure 3.2), was obtained from the Hydro-geochemistry of the Amazonian Basin database (HYBAM; *https://hybam.obs-mip.fr*). Tributaries downstream of Óbidos added 4–34% additional discharge to the mouth during our study periods, with up to an additional 85,000 $m^3 s^{-1}$ contribution during May (Ward et al., 2015).

Surface ocean properties were measured continuously using automated underway analyzers plumbed into the ship's uncontaminated seawater line (Cooley et al., 2007). An in-line Seabird thermosalinograph monitored underway sea surface temperature (SST) and salinity (SSS), and a fluorometer recorded chlorophyll *a* fluorescence (FLR) near the intake, 5–7 meters below the sea surface. Down the line, an underway pCO_2 analyzer was installed using a 10-L showerhead-type seawater equilibrator (Bates et al., 1998; Sweeney et al., 2000; Takahashi et al., 1997) and an infrared CO_2 detector (LI-6262, Li-Cor, Lincoln, Nebraska; Cooley et al., 2007). The volumetric concentration of CO_2 ($xCO_{2(sw)}$, in ppm) was automatically calibrated at least hourly against six CO_2-N_2 gas mixtures containing 0–510 ppm CO_2 (Certified by the National Oceanographic and Atmospheric Administration Climate Monitoring and Diagnostics Laboratory, NOAA CMDL, Boulder, Colorado, USA). Sea surface pCO_2 was calculated from $xCO_{2(sw)}$ and corrected to *in-situ* SST (see Weiss & Price, 1980, and Takahashi et al., 1993, for details). The gas stream between the equilibrator and the detector was dried, but this filter sometimes failed, leaving gaps in the data along the cruise track where water vapor overwhelmed infrared detection of CO_2. These system failures were

apparent and easily removed manually. Instrument accuracy was ±1 μatm and the response (e-folding; Cooley et al., 2007) time was 6, 2, 10 mins for cruises during June 2010, July 2012, and September 2011, respectively.

To examine variations in observed pCO_2 independent of SST, *in-situ* pCO_2 was normalized to pCO_2 at a constant temperature of 29 °C, $pCO_{2(29)}$, using the CO_2 thermodynamic coefficient of 0.0423 $°C^{-1}$ according to Takahashi et al. (1993):

$$pCO_{2(29)} = \textit{in-situ}\ pCO_2 \times e^{0.0423\times(29-SST)}.$$

The monthly averaged atmospheric $xCO_{2(atm)}$ for June 2010, September 2011, and July 2012 was obtained from the nearest atmospheric CO_2 monitoring station of the NOAA Global Monitoring Division at Ragged Point, Barbados (13.17°N, 59.43°W; *https://www.esrl.noaa.gov/gmd/dv/site/?stacode=RPB*). $xCO_{2(atm)}$ was calculated from atmospheric pCO_2 ($pCO_{2(atm)}$) at each underway data point according to the method described in Weiss and Price (1980):

$$pCO_{2(atm)} = (P - P_v) \times xCO_{2(atm)},$$

where the atmospheric pressure at sea surface (P) was continuously monitored over each cruise period from an underway barometer, and the pressure of the water vapor (P_v) was calculated using *in-situ* SST and SSS.

All underway measurements (SST, SSS, fluorescence) were binned into 6, 2, and 10-min averages in accordance with pCO_2 measurements for June 2010, September 2011, and July 2012, respectively. Surface fluorescence (FLR) from each cruise was converted to chlorophyll *a* concentration (Chl *a*) using a linear regression of FLR against discrete Chl *a* measurements of surface water samples collected with Niskin bottles during each cruise. True

wind speed was measured shipboard by meteorological instruments on each vessel. Wind speed for 10 m above sea surface (u_{10}) was corrected from instrument heights according to Thomas et al. (2005) and was averaged for each cruise.

To calculate the expected value of pCO_2 as a function of salinity given physical mixing only, a river-ocean mixing line was generated for conservative carbonate system constituents: total alkalinity (ALK) and dissolved inorganic carbon (DIC), using measured river and ocean endmembers (river SSS = 0, ALK = 386 μmol kg^{-1}, DIC = 422 μmol kg^{-1}; ocean SSS = 36, ALK = 2369 μmol kg^{-1}, DIC = 2025 μmol kg^{-1}). Uncertainties of ± 5 μmol kg^{-1} for both ALK and DIC endmembers were used to develop the upper and lower boundary conditions of this mixing line. $pCO_{2(29)}$ values from the mixing model were calculated with CO2SYS (Lewis and Wallace, 1998; Pierrot et al., 2006), using the predicted DIC and ALK for each integer salinity value within the range of 0<SSS<36 at SST = 29 °C. Since the resulting pCO_2 is not conservative, data were smoothed to reveal a mixing curve. The difference between the measured $pCO_{2(29)}$ and that predicted from the mixing curve at a given SSS was determined to be the $pCO_{2(29)}$ *residual* (μatm), which was then compared to the underway sea surface estimates of algal biomass (Chl *a*).

2.2. Satellite measurements

Using K_d490 from the MODIS sensor as a proxy, we reconstructed salinity fields for the region (ocean data within the range of 15–0°N, 43–60°W) for each cruise period. Each data set consisted of ~1.0×10^5 oceanic pixels (pixel resolution of 0.04° latitude × 0.04° longitude or 4 × 4 km^2). For each pixel, we computed an 8-day-averaged K_d490 which was then used to obtain a mean K_d490 for the duration of each expedition. For 2010, 2012, and 2011 cruises,

this mean K_d490 was an average of 5, 3, and 6 sets of 8-day K_d490 images, respectively. K_d490 data was not available under heavy clouds or high turbidity, resulting in 14, 22 and 3% of the area having no data in May–June 2010, July 2012, and September–October 2011, respectively. Data regions affected by the Orinoco River plume (0–150 km off the coastline between 55–60°W) were removed from this analysis.

The K_d490 was converted to SSS based on a combination of two published sets of K_d490 vs SSS data that covered different but overlapping salinity ranges (Del Vecchio & Subramaniam, 2004; Fournier et al., 2012). The aCDOM from *Fournier et al.* (2012) was converted to K_d490 according to the aCDOM–K_d490 relationship in Del Vecchio and Subramaniam (2004). A 3rd order polynomial regression was applied on the combined data set (Figure 3.3):

For $0.037\ m^{-1} < K_d490 < 1.006\ m^{-1}$,

$$SSS = -4.83(\pm4.41) \times K_d490^3 + 14.12(\pm8.58) \times K_d490^2 - 30.26(\pm4.61) \times K_d490 + 36.10(\pm0.54),\ r = -0.98.$$

The upper and lower boundaries for K_d490 were determined so that the salinity was confined within 15<SSS<35. An SSS value was derived using the equation above for each MODIS K_d490 pixel. The total area of the plume for each cruise period was then estimated by summing up the areas of all pixels of 15<SSS<35. Regressions and associated errors were derived using the standard linear regression method.

2.3. Regional flux estimation

The three ANACONDAS expeditions crisscrossed the surface of the WTNA waters with differing levels of influence from the ARP. To extrapolate the distribution of pCO_2 to the full

WTNA, we defined a salinity range for the plume (15<SSS<35) and removed oceanic data points outside of this range which were minimally impacted by the plume waters. We also set aside pCO_2 data collected from the highly turbid waters near the port of Cayenne, and the Amazon River mouth (SSS<15).

The wind speed at 10 m above sea level (u_{10}) was also obtained from the European Center for Medium-Range Weather Forecasts reanalysis data set (ERA-interim; *https://apps.ecmwf.int/datasets/data/interim-full-moda/levtype=sfc/*), and compared with cruise-averaged wind speed (Figure 3.4). Monthly averaged wind fields were developed for the ARP region (15°N–0°N, 43–60°W) with 0.25 × 0.25° pixels and used in the flux calculation. The monthly averaged reanalysis SST data set was also retrieved from ERA-interim for each cruise month. Monthly wind speed and SST fields (0.25° resolution) were interpolated onto each K_d490 pixel (0.04° resolution) and used in calculating the air–sea CO_2 flux. The gas transfer velocity (k) for each pixel was expressed as:

$$k = 0.27 \times u_{10}^2 \times (Sc/660)^{-0.5},$$

where Sc is the Schmidt number, a function of SST (Sweeney et al., 2007).

For samples 15<SSS<35, we compared underway SSS with sea surface pCO_2 for each time point, and generated a linear regression equation for each expedition (Table 2.1A) that could be used to predict air–sea CO_2 flux from SSS, propagating errors as the standard deviation of the mean according to Bevington and Robinson (2003). Air–sea CO_2 flux (mmol C m^{-2} d^{-1}) for every K_d490 pixel was then determined by:

$$F = k \times K_0 \times \Delta pCO_2,$$

where K_0 is the solubility of CO_2 in the seawater, which is a function of SST and SSS (Weiss, 1974); ΔpCO_2 (μatm) is the pCO_2 difference at sea surface between sea water and monthly-averaged atmospheric levels for each cruise. The mean flux for the entire plume was estimated by summing up all the pixel-by-pixel fluxes from each cruise month, which was then divided by the total area of the plume for that month. Errors in the mean flux for the plume were propagated following Bevington and Robinson (2003).

We did not collect underway data within the Barbados EEZ, and the French Guiana EEZ data collection were excluded from this analysis because they were collected from very shallow and turbid nearshore waters (likely stirred up by the ship) during crew changes near the port of Cayenne in 2010 and 2011. Near-mouth plume data from the Brazil's EEZ in 2012 were also obtained in shallow (<50 m deep) and turbid water, and were analyzed separately, i.e., excluded from the regional pCO_2 and CO_2 flux calculations.

3. Results

3.1. Surface properties of the ARP and surrounding regions

Observed SSS ranged between 16.2 and 35.3 in June (Figure 3.5A), with a large area of 25<SSS<32 in the northwest, following the northward propagation of the ARP in spring (Coles et al., 2013). More saline, oceanic water (S>35) was observed to the east. The outer French Guiana continental shelf (6–8°N, 51–53°W) featured some of the freshest waters (16<SSS<25), indicating the core of the ARP. Near the port of Cayenne (depth <50 m), however, SSS increased to ~35, suggesting the intrusion of oceanic waters.

In July, SSS = 0 was continuously observed for 24 h near Macapá (depth ~10 m; Figure 3.5B; all SSS ≤ 15 is shown as deep blue). The southern edge of the plume was indicated by a

distinct shift to oceanic salinity (35<SSS<36.5; 46–48°W) just south of the Equator, where circulation is dominated by oceanic waters of the North Brazil Current (NBC; Lefèvre et al., 2017). In contrast to June, the northwestern region in July generally showed SSS>35, likely because of the eastward retroflection of the NBC. Low SSS (15<SSS<25) was seen on the French Guiana shelf in July, consistent with observations in June.

During September, the plume was a narrow band of 25<SSS<30 winding northward but then retroflecting east, with outer plume and oceanic water (SSS>30) observed as the ship criss-crossed the plume core (Figure 3.5C). Similar to observations in June and July, plume waters (25<SSS<35) were observed in September over the French Guiana shelf, and oceanic waters (SSS>35) dominated near Cayenne, but SSS < 24 was not observed.

In-situ SST ranged between 27 and 31 °C during all three expeditions (Figure 3.5D–F). Plume waters were typically warmer than the surrounding Atlantic Ocean, consistent with solar heating of the freshwater barrier layer (Pailler et al., 1999; Ffield, 2007). Regional SST exhibited notable variability, with warmer surface waters observed in June compared to July and September (interquartile range (25–75%) of SST: 29.3–30.0 °C, 28.5–29.0 °C, and 28.8–29.6 °C, respectively).

Surface water Chl *a* concentration exhibited strong spatial contrasts between plume- and ocean-dominated regions (Figure 3.5G–I), generally following the distribution patterns of SSS. While Chl *a* in more oceanic waters (SSS>35) was typically lower (< 1 mg m^{-3}), Chl *a* was highest in the low-salinity zone on the French Guiana shelf during all three cruises (peaks of 9.7 mg m^{-3} in June, 18.7 mg m^{-3} in July, and 9.3 mg m^{-3} in September) confirming a consistent and intense phytoplankton bloom in this region due to the ARP (Smith &

Demaster, 1996; Goes et al., 2014). High Chl *a* was also observed in the mesohaline, northwestern part of the plume (10–15°N, 54–60°W) in June (1–5 mg m^{-3}) derived from a rich population of DDA (Goes et al., 2014; Stenegren et al., 2017), as well as near the eastern edge of the ARP (5–8°N, 45–48°W) in September (1–3 mg m^{-3}). Blooms of the inner plume in June and July were comprised of a rich bloom of diatoms, dinoflagellates and cryptophytes fueled by riverine DIN and SiO_3 (Goes at al., 2014; Gomes et al., 2018). In more oceanic waters (SSS>35), Chl *a* was typically < 1 mg m^{-3} because pico-phytoplankton such as *Prochlorococcus* prevailed (*Gomes et al.*, 2018). Near the river mouth in July, Chl *a* was higher (1.1–2.8 mg m^{-3}; Figure 2.5H) than the surrounding oceanic waters (< 1 mg m^{-3}), despite the high turbidity of the river outflow, perhaps reflecting algal contributions from clear water tributaries (e.g., Tapajós, Xingu, Tocantins; Ward et al., 2015) entering the lower reach.

High spatial variability in *in-situ* surface pCO_2 between 100–1000 μatm (or ΔpCO_2 roughly between -280 and 620 μatm) was observed over the three expeditions (Figure 3.5J–L), confirming the impact of the ARP on regional carbon cycling (Cooley et al., 2007). *In-situ* pCO_2 > 430 μatm (or ΔpCO_2 > 50 μatm) was only detected along the Brazil shelf and close to the Amazon River mouth in July, with the highest pCO_2 (900–1000 μatm) observed during the 24-h period at SSS = 0 near Macapá (Figure 3.5K; all ΔpCO_2 > 100 μatm is shown as deep red). The lowest *in-situ* pCO_2 between 100–150 μatm (-280 < ΔpCO_2 < -230 μatm) was exclusively observed near the French Guiana shelf in June and September. Undersaturated CO_2 with respect to atmospheric level was also found in the northwest region of the ARP in June (Figure 3.5J), as well as across the eastern plume edge in September (Figure 3.5L),

where ΔpCO_2 typically ranged between -130 and 0 μatm. In more oceanic areas, *in-situ* pCO_2 varied slightly above atmospheric values (~380 μatm) by up to 50 μatm.

Observed *in-situ* pCO_2 was highly correlated with SSS during all three cruise periods within the defined range (15<SSS<35; r = 0.92, 0.97, and 0.79, for June, July, and September respectively; Figure 3.6A, B). Salinity explained > 92% of the variance in pCO_2 in June and July, while the relationship was less robust (r = 0.79) in September. The regression statistics varied among cruises, especially in September, where both the slope and y-intercept were significantly steeper or lower, respectively, than from the other seasons (Table 3.1A). Higher pCO_2 values near atmospheric levels were consistently associated with higher salinities (33–35), whereas the lower pCO_2 values (100–200 μatm) were associated with SSS ~16 in June and July, and with SSS ~25 in September. Air–sea pCO_2 equilibrium (i.e. pCO_2 ~380; CO_2 flux = 0) corresponded to SSS between 33.7–34.6 (Figure 3.6D).

The estimated along-track air–sea CO_2 flux exhibited similar spatial patterns (data not shown) as observed *in-situ* pCO_2, as the flux was most sensitive to the ΔpCO_2, while other controls were (or were assumed to be) nearly constant throughout each cruise (Table 3.2). For the defined salinity range (15<SSS<35; excluding the shallow water near the river mouth in July 2012), the greatest CO_2 uptake (influx density = -41.4 mmol m^{-2} d^{-1}) was observed near the French Guiana shelf break in June, and the greatest CO_2 outgassing (efflux density = 5.4 mmol m^{-2} d^{-1}) was found on the outer edges of the plume in September.

3.2. Satellite-derived SSS field and regional CO_2 flux

Regional distributions of K_d490 and derived SSS varied seasonally (Figure 3.7A–C) with the plume area indicated by SSS between 15–35 which roughly corresponded to K_d490

between 0.05–1.0 m^{-1}. In all three seasons, the freshest plume waters (SSS<25) were observed at the outer continental shelf and along the Brazil and French Guiana coasts between 0.5–5°N, following the northwestward extension of the ARP. Due to the high river discharge in June, low-SSS plume waters reached as far north as 15°N where SSS increased (but was still below 35) as the plume mixed with oceanic water. As a consequence, there was a greater percentage of the plume area with 25<SSS<33 (Figure 3.6C). During seasons of declining river discharge and escalating retroflection of the NBC in September, the ARP signal north of 10°N weakened as the plume curled eastward between 6–10°N toward ~45°W (Figure 3.7B, C). As a result, the offshore plume was observed northeast of the French Guiana shelf (6–10°N, 47–52°W) in July before substantially diminishing in September. The percentage of plume area exhibiting 25<SSS<33 in July was reduced compared to June (Figure 3.6C) and then reduced even further in September.

Spatial distributions of the derived regional CO_2 flux (Figure 3.8A–C) followed SSS fields, with strong atmospheric carbon sinks located near the Brazil and French Guiana shelves. These sinks extended to the northwestern region in June, and to the east in July due to NBC retroflection, while moderate sinks and weak sources were seen in surrounding oceanic waters with SSS ~35. This suggested that the ARP (15<SSS<35) was almost entirely an atmospheric CO_2 sink during all three seasons, with possible CO_2 outgassing only within a narrow salinity band close to 35. The higher salinity range (34–35) of the near-zero CO_2 fluxes (Figure 3.6D) corresponded to the same salinity range that was a larger fraction of the plume area in July and September (Figure 3.6C) compared to June. The area of the outgassing outer plume is ~3 times larger than the mid-plume sink during July 2012.

Regionally, the ARP constituted a major atmospheric CO_2 sink (Table 3.3) in June, averaging a flux density of -2.39 ± 1.29 mmol m^{-2} d^{-1} and a plume size of 7.8 × 10^5 km^2. The influx density declined in September (-0.42 ± 0.76 mmol m^{-2} d^{-1}, 8.3 × 10^5 km^2), and became a weak source in July (0.26 ± 0.62 mmol m^{-2} d^{-1}, 6.9 × 10^5 km^2). Because the propagated uncertainty was relatively large, the flux could not be statistically distinguished from zero during July and September, although this aspect may be as much a result of spatial heterogeneity as measurement uncertainty.

3.3. Processes affecting the CO_2 undersaturation in the plume

Removing the influence of temperature variation on *in-situ* pCO_2 further illustrates the importance of salinity (Table 3.1). The correlation coefficient for $pCO_{2(29)}$ versus SSS (Table 3.1B) was similar to *in-situ* pCO_2 versus SSS (Table 2.1A) for June and July, but improved for September, indicating that temperature might have greater impact on pCO_2 in the Fall. The data distribution (Figure 3.9A), as well as the slopes and y-intercepts of the regressions (Table 3.1B), varied significantly among different seasons. In June, the lowest $pCO_{2(29)}$ values (100–200 μatm) were associated with fresher waters of 15<SSS<22, whereas the same SSS range corresponded to $pCO_{2(29)}$ levels ~50 μatm higher in July. In contrast, the lowest $pCO_{2(29)}$ ranged from 120–250 μatm in September, but they were associated with an even higher SSS of 25–30.

Although the relationships between pCO_2 and SSS were robust, they did not follow the physical mixing curve predicted from observed river and ocean endmembers (Figure 3.9A). Notably, 82% and 96% of the combined data sets for salinity ranges of 15<SSS<35 and 15<SSS<31, respectively, fell below the river-ocean mixing curve by as much as 150 μatm.

This result confirms that the CO_2 drawdown from biological net community production plays a critical role in removing CO_2 from the surface, especially in lower SSS areas (SSS<30). In contrast, a few data at intermediate and higher salinities (SSS>25) were up to ~50 μatm above the mixing curve (Figure 3.9A), indicating that community respiration could sometimes overwhelm productivity.

The impact of biological activity, indicated by the $pCO_{2(29)}$ residual, showed a seasonally-variable relationship with algal biomass, estimated as sea surface Chl *a*, for the defined salinity range (15<SSS<35; Figure 3.10A–C). In general, a greater negative $pCO_{2(29)}$ residual corresponded with higher Chl *a* concentrations up to ~10 mg m^{-3}, while a smaller $pCO_{2(29)}$ residual was associated with lower Chl *a* concentrations < 0.1 mg m^{-3}, although these relationships varied with season, and were not always linear. In June and July, the $pCO_{2(29)}$ residual correlated significantly with logarithm-transformed Chl *a* (r = -0.68 and -0.52, respectively). In September, only 16% of the variance in $pCO_{2(29)\_res}$ was explained by Chl *a*, although the $pCO_{2(29)}$ residual did indicate biological uptake of CO_2 (-150 μatm) at higher Chl *a* values associated with the lowest salinity plume waters observed that month (SSS ~25).

3.4. CO_2 outgassing on the Brazil shelf

The subset of underway observations south of 4.7°N in July 2012 (Year Days 203–209) suggested strong CO_2 outgassing on the Brazil shelf, especially at the Amazon River mouth (Figure 3.11). Unlike the strong positive correlation between SSS and pCO_2 for the salinity range (15<SSS<35) elsewhere in the plume (Figure 3.6), *in-situ* pCO_2 on the Brazil shelf did not correlate with SSS (Figure 3.11A). Observed pCO_2 deviated positively from the SSS–

pCO_2 regression for the rest of the cruise (Figure 3.11A, black line) between Days 203–209 (Figure 3.11A, B), with the highest pCO_2 deviation observed near Macapá. *In-situ* pCO_2 varied dramatically between 218–976 μatm (interquartile range (25%–75%) of pCO_2: 395–490 μatm). A rapid shift from undersaturation to supersaturation state of CO_2 was seen early on Day 203 (4.1°N, Figure 3.11C), when pCO_2 reached ~600 μatm at SSS ~30 (Figure 3.11A) during several hours of transit. While the supersaturated CO_2 across the shallow shelf was mostly just above 400 μatm, the highest pCO_2 values (720–976 μatm; over a 24-h tidal cycle) were observed at the northern part of the river mouth near Macapá on Day 204–205 at SSS ~0, where the water was highly turbid. Near Belém (Day ~206), observed pCO_2 correlated positively with salinity between 20<SSS<36, but the relationship was different from the regression derived for the rest of the cruise (black line, Figure 3.11A), perhaps because of the distinct outflow there, more influenced by lower reach tributaries (Ward et al., 2015). The area between 4.4–4.7°N near the 50 m isobath was criss-crossed twice (cruise days 202.8–203.1 and 208.4–208.6, respectively) with very different SSS (Figure 3.5B) and pCO_2 (Figure 3.11C), indicating prominent temporal variations of surface properties. With CO_2 supersaturation observed in this region, the air–sea CO_2 flux density averaged 23.7 ± 22.0 mmol m^{-2} d^{-1}, with the strongest efflux of up to 70 mmol m^{-2} d^{-1} at the river mouth near Macapá. This part of the Brazil shelf covers approximately 9×10^4 km^2, and thus the total efflux from this region could contribute as much as 0.6 ± 0.5 Tg C $month^{-1}$ in July.

4. Discussion

Our work corroborates previous reports (Ternon et al., 2000; Körtzinger, 2003; Cooley et al., 2007; Lefèvre et al., 2010; Ibánhez et al., 2015; Lefèvre et al., 2017) that the outflow of

the Amazon river becomes a sink of atmospheric CO_2 when the plume water mixes with the ocean and significantly alters the air–sea CO_2 equilibrium in the WTNA. This work further explores the robustness of using satellite remotely sensed data for quantifying and tracking CO_2 flux over synoptic scales, which is essential for understanding how anthropogenic changes will alter the Amazon and consequently its contribution as a CO_2 sink.

4.1. Origin of the strong carbon sink in the ARP

The development of a CO_2 undersaturation state across mid-salinity range in the ARP is initially shaped by the conservative mixing between the river and ocean endmembers (Figure 3.9). Along the mixing curve, pCO_2 drops drastically with increasing SSS at low salinity (Figure 3.9B) because of the higher buffering capacity of seawater, staying below the atmospheric level at mid-salinity range before rising towards the air–sea CO_2 equilibrium at high salinities (Figure 3.9A, B). The quasi-linearity of the CO_2 system at mid- to high-salinity dictates the distribution of the observed pCO_2, while negative deviation from the mixing curve can largely be attributed to biological CO_2 uptake by autotrophs.

The biogeography of phytoplankton communities in this region (Goes et al., 2014; Gomes et al., 2018) is shaped by the initial N:P ratio of the river. Coastal diatoms dominated upstream on the French Guiana coast, benefiting from high concentrations of riverine silica and nitrate. This area is where the highest uptake of CO_2 was observed in our study. Further northwest (10–15°N), in the mesohaline region, the CO_2 uptake can be attributed to a large population of symbiotic DDA that are capable of growing actively in the absence of DIN, because their nitrogen requirements are met by the N_2 fixing ability of their endosymbiont *Richelia intracellularis* (Foster et al., 2011; Weber et al., 2017). Associated with the DDA

was a large population of nanoplankton, such as cryptophytes, prasinophytes and haptophytes, likely supported by the DIN from the decaying DDA blooms (Gomes et al., 2018).

While strong CO_2 undersaturation was observed in the plume for all three expeditions, each survey revealed a distinct relationship between *in-situ* pCO_2 and salinity (Figure 3.6A, B and Table 3.1A). The slopes of June 2010 (13.9 ± 0.2) and July 2012 (13.0 ± 0.1) resembled each other, but were significantly lower than that of September 2011 (16.9 ± 0.5), primarily due to the low pCO_2 at mid-salinity range (25<SSS<30). These relationships are in general agreement with the SSS–pCO_2 (fCO_2) correlations from previous studies across multiple years and seasons (Ternon et al., 2000; Körtzinger, 2003; Ibánhez et al., 2015; Figure 3.6B). The slopes from these studies are within the range found in this study, and changes in the intercepts likely reflect the annual enhancement of oceanic pCO_2 with increasing atmospheric burden. The correlation is mostly > 0.9, suggesting that the salinity dependence of oceanic pCO_2 in the ARP has remained very consistent from 1995–2010. On the other hand, unique SSS–pCO_2 relationships during certain months that clearly differ from other months (e.g., September 2011 of this study) may highlight the importance of accessing CO_2 dynamics for separate periods, rather than for an entire year with one relationship, in order to more precisely estimate temporal variations in the CO_2 flux.

In addition, regression plots of $pCO_{2(29)}$ residual vs Chl *a* (Figure 3.10) within the ARP (15<SSS<35) showed the strongest correlation in June when the riverine discharge was at its highest (Figure 3.2). In contrast, the weakest relationship was observed in September when the discharge was lowest, winds were weaker, and outer plume waters have spent the greatest

amount of time away (>100 days) from the river mouth. According to model drifter experiments, the oldest plume waters spread to the northeast, near 40°W, and then are transported back the northwest during retroflection in September (Coles et al., 2013). These northeastern plume waters likely had the longest time to equilibrate with the atmosphere, causing greater deviation from the SSS–pCO_2 regression. This result implies that variability in the distribution of salinity within the plume (Figure 3.6C; a function of both discharge and wind) plays a crucial part in shaping the air–sea CO_2 equilibrium in the WTNA.

4.2. CO_2 supersaturation near the river mouth

While the mid- and outer ARP was established as a major atmospheric carbon sink, CO_2 in the inner plume near the Macapá river mouth was supersaturated and showed greater variability (Figure 3.11). CDOM concentration, measured by Advanced Laser Fluorometer (ALF; Goes et al., 2014), strongly correlated to pCO_2 near the French Guiana–Brazil border ($r = 0.98$; data not shown), confirming that waters near the mouth were indeed net heterotrophic, consistent with Medeiros et al. (2015) and Ward et al. (2013). The net heterotrophy in the shallow waters could be linked to the high carbon remineralization rates in the region's vast mobile mudbelt (Aller and Blair, 2006), leading to the return of organic carbon to the DIC pool, and generating elevated pCO_2 relative to what would be expected based solely on conservative mixing between the river and ocean.

Our ocean pCO_2 data offshore from Belém (1°N–0.5°S, 46–48°W) also agreed with results from Carvalho et al. (2017), which showed that oceanic waters south of the river mouth are oligotrophic and a weak atmospheric CO_2 source. Mixing of the inner plume waters with this clear tropical seawater reduces light attenuation associated with riverine

sediment and CDOM enough for autotrophs to utilize inorganic nutrient pools and lower pCO_2.

4.3. Air–sea CO_2 flux in the ARP-influenced waters

As observed previously, the ARP expanded northward during boreal spring at its highest flow, began to retroflect with the NBC in summer, and gradually diminished in size in fall, due to the eastward NBC retroflection (Cooley et al., 2007; Salisbury et al., 2011; Coles et al., 2013). Such seasonal variation in the plume salinity distribution and size is reflected in the monthly averaged area calculated from K_d490/SSS fields (Table 3.3). Notably, the plume size in July 2012 was smaller than in September, despite the fact that the discharge in July was greater than September by more than 50% (Figure 3.2). It is during summer and fall that changing winds have a greater impact on plume distribution than discharge (Molleri et al., 2010). A fewer number of valid K_d490 pixels in July than in September (~20% fewer; Figure 3.7B, C) because of the shorter cruise period (16 days), may also have favored an underestimation of the July plume area.

Although the size of the ARP in June was about the same as that in July and September, it was a more potent CO_2 sink primarily because of its much greater influx density (Table 3.3), as reflected by the steeper slope in the SSS vs CO_2 flux regression for June (Figure 3.6D). Such slope difference among seasons is partially due to the fact that the wind speed was ~10-35% higher in June (Table 3.2), which resulted in the gas transfer velocity, and consequently, a CO_2 influx > 80% greater than in September.

The observed frequency distribution of K_d490-derived salinity bands showed that high SSS pixels dominated the region in July and September (Figure 3.6C). Thus, the late summer

and fall ARP was dominated by weak exchange at close to the air–sea equilibrium level. This sensitivity of the regional CO_2 flux to conditions in the 34–35 salinity band is consistent with previous studies (Körtzinger, 2003; Lefèvre et al., 2010, 2017; Ibánhez et al., 2015) and suggests a critical region for future efforts to examine more precisely the air–sea exchange in the plume region. Our findings suggest that a large overestimate of the sink can be made when assuming an even spatial distribution across the river-ocean salinity gradient.

Several studies have provided estimates of the CO_2 exchange in the ARP from extrapolations based on a relatively stable relationship between the pCO_2 and salinity (Ternon et al., 2000; Körtzinger, 2003; Cooley et al., 2007; Lefèvre et al., 2010; Ibánhez et al., 2015; Lefèvre et al., 2017; Figure 2.6B and Table 2.3). Körtzinger (2003) combined a pCO_2 versus SSS relationship (15<SSS<34.9) from a single November cruise with the monthly climatological SSS means of the World Ocean Atlas to compute annual air–sea CO_2 flux, resulting in -14 Tg C yr^{-1} for a plume area of 2.4×10^6 km^2 (defined as SSS<34.9) and corresponding to an average air-sea CO_2 flux density of -1.37 mol m^{-2} d^{-1}. That annual flux could be an overestimation because the plume area in November (low discharge season) is almost 3 times larger than the area during peak discharge of this study (Table 3.3). Cooley et al. (2007) estimated monthly CO_2 fluxes based on multiple cruises from different seasons and different years, and reported an annual sink of -15 ± 6 Tg C yr^{-1}. Lefèvre et al. (2010) estimated a CO_2 flux of -0.35 mol m^{-2} yr^{-1} and a smaller plume surface area of 1.1×10^6 km^2 (SSS<34.9), giving an integrated CO_2 flux of -5 Tg C yr^{-1} for the ARP. Because of the strong seasonality of plume CO_2 dynamics, monthly averaged carbon flux can vary greatly, ranging from a large to a moderate carbon sink. Our estimation of the monthly flux density was on

par with Ibánhez et al. (2015), but significantly different from Cooley et al. (2007), especially for July and September. One explanation for this discrepancy could be due to the different plume areas considered by each study. Cooley et al. (2007) obtained an area for the ARP from a 10-year-averaged climatology. That average plume area was ~30–60% larger than the one we observed, and may represent an overestimation of the magnitude of the CO_2 sink. Unfortunately, we could not estimate the full annual air–sea CO_2 flux in the ARP due to a lack of observations. More *in-situ* measurements and sampling are required in the future, especially during climate extremes, considering the global significance of the CO_2 flux dynamics associated with the ARP and the escalating deforestation and climate impacts affecting the Amazon's hydrological cycle (Nobre et al., 2016). More exploration of the seasonal dynamics of plume salinity distribution also seems warranted.

4.4. Variability in the ARP

Sea surface pCO_2 dynamics in the ARP are affected by both biological and physical processes that vary seasonally and interannually to influence its regional status as a CO_2 sink/source. Increases in biological carbon drawdown enhance ΔpCO_2 initially created by physical river-ocean mixing, while changes in physical processes, such as discharge and wind speed/direction, affect gas transfer mechanics by changing piston velocity, solubility, and the amount of time surface water spends equilibrating with the atmosphere.

Since early CZCS satellite observations of the plume (Muller-Karger et al., 1989, 1995; Longhurst, 1993; Longhurst et al., 1995), oceanographers have recognized seasonal changes in the shape of the plume, driven by regional variation in surface currents and wind (Coles et al., 2013). Our expeditions were designed to capture the spring flood to the Caribbean and the

retroflection in the late summer. Thus, our expeditions were meant to sample the two most important plume seasons. A July expedition was added to sample the mouth of the river. Subsequently, Salisbury et al. (2011) have demonstrated how the shape of the plume varies seasonally. They grouped months into four time periods (November–January, February–April, May–July, August–October). Our data represent two of these key seasonal time periods. Notably, the spring/early summer data correspond to peak discharge and the northern position of the ITCZ, whereas our late summer and fall data correspond to declining discharge and a southerly shift in the ITCZ.

Although our analysis initially assumed no interannual variability, there certainly is interannual variability in this region. In our estimation for this Chapter, we first suspect that June 2010 may represent a smaller and non-typical June plume impacted by ENSO (Lewis et al., 2011; Marengo et al., 2011). Cooley et al. (2007) also reported some ENSO impact. However, exploration in the interannual variability in this region (Addendum) revealed that the size of the plume in June-2010 was actually greater than any other years between 2003–2020, and the CO_2 uptake was also the highest. No clear sign of ENSO in the monthly discharge was observed for June-2010 (Figure 3.2). We do not know what factors caused the largest June plume during a supposedly ENSO-affected year. In any case, differences between our estimated fluxes and those of other studies, may therefore be due not to methodology, but seasonal and interannual variability, or perhaps a long-term trend (e.g., Durack and Wijffels, 2010) in the distribution of SSS in this region.

5. Conclusions

Although the tropical North Atlantic Ocean is generally considered a net source of CO_2 to the atmosphere by global air–sea CO_2 flux climatologies, our results show that vast areas influenced by the outflow of Amazon River plume are a net sink of atmospheric CO_2. The pCO_2 at the plume surface correlates strongly to salinity within 15<SSS<35, and a robust linear relationship was determined during June, July and September. The plume is a major sink of CO_2 in June during the high-flow period of the Amazon River enhanced by higher wind speed, primarily because nutrients delivered by the river create ecological niches for several different phytoplankton communities across the river-ocean continuum. A moderate sink with greater variability is observed during the transitional stage of declining river discharge with relatively lower wind speed in September. The strong sink in some areas of the plume during July was almost completely offset by outgassing in the outer reaches of the plume (SSS ~35). Supersaturated pCO_2 in shallow waters (depth <50 m) near the Amazon River mouth was estimated to outgas as much as 0.6 ± 0.5 Tg C $month^{-1}$ in July. Further sampling would improve this estimate as well as our understanding of the processes driving variability in this region, including the balance of net community production and the degradation/reactivity of organic matter transported by the world's largest river.

Acknowledgements

This study was supported by the National Science Foundation (ANACONDAS, OCE-0934095 and OCE-1133277), and the Gordon & Betty Moore Foundation (ROCA, GBMF-MMI-2293 and 2928). We thank the captains and crew of the RV Knorr, RV Melville, RV Atlantis for their support of the scientific goals of the ANACONDAS project, and the Brazil

government for the permission to sample in the Brazil EEZ in 2012. We acknowledge the two anonymous reviewers and editors for their valuable comments that helped to improve this manuscript considerably. LM thanks the Department of Marine Sciences at the University of Georgia for financial support through a Teaching Assistantship and a Departmental Fellowship. LM thanks Dr. Renato Castelao and Caitlin Amos from the UGA Department of Marine Sciences for help with data analysis. Ocean color data were retrieved from NASA's OceanColor Web: https://oceancolor.gsfc.nasa.gov/l3/. Underway data during the three cruises are publicly available at https://www.bco-dmo.org/dataset/849870.

References

Abril, G., Martinez, J. M., Artigas, L. F., Moreira-Turcq, P., Benedetti, M. F., Vidal, L., et al. (2014). Amazon River carbon dioxide outgassing fuelled by wetlands. *Nature*, *505*(7483), 395–398. https://doi.org/10.1038/nature12797

Aller, R. C., & Blair, N. E. (2006). Carbon remineralization in the Amazon–Guianas tropical mobile mudbelt: A sedimentary incinerator. *Continental Shelf Research*, *26*(17–18), 2241–2259. https://doi.org/10.1016/j.csr.2006.07.016

Andrié, C., Oudot, C., Genthon, C., & Merlivat, L. (1986). CO_2 fluxes in the tropical Atlantic during FOCAL cruises. *Journal of Geophysical Research: Oceans*, *91*(C10), 11741-11755. https://doi.org/10.1029/JC091iC10p11741

Bates, N. R., Takahashi, T., Chipman, D. W., & Knap, A. H. (1998). Variability of pCO2 on diel to seasonal timescales in the Sargasso Sea near Bermuda. *Journal of Geophysical Research: Oceans*, *103*(C8), 15567–15585. https://doi.org/10.1029/98JC00247

Bevington, P. R., & Robinson, D. K. (2003). Data reduction and error analysis. *McGraw-Hill: New York*.

Cai, W. J., Chen, C. A., & Borges, A. (2013). Carbon dioxide dynamics and fluxes in coastal waters influenced by river plumes. In T. S. Bianchi, A. A. Allison, W. J. Cai (Eds.), *Biogeochemical dynamics at major river-coastal interfaces: linkages with global change* (pp. 155–173). New York, NY: Cambridge University Press.

Carvalho, A. C. O., Marins, R. V., Dias, F. J. S., Rezende, C. E., Lefèvre, N., Cavalcante, M. S., & Eschrique, S. A. (2017). Air-sea CO2 fluxes for the Brazilian northeast continental

shelf in a climatic transition region. *Journal of Marine Systems*, *173*, 70–80. https://doi.org/10.1016/j.jmarsys.2017.04.009

Chong, L. S., Berelson, W. M., McManus, J., Hammond, D. E., Rollins, N. E., & Yager, P. L. (2014). Carbon and biogenic silica export influenced by the Amazon River Plume: Patterns of remineralization in deep-sea sediments. *Deep Sea Research Part I: Oceanographic Research Papers*, *85*, 124–137. https://doi.org/10.1016/j.dsr.2013.12.007

Coles, V. J., Brooks, M. T., Hopkins, J., Stukel, M. R., Yager, P. L., & Hood, R. R. (2013). The pathways and properties of the Amazon River Plume in the tropical North Atlantic Ocean. *Journal of Geophysical Research: Oceans*, *118*(12), 6894–6913. https://doi.org/10.1002/2013JC008981

Cooley, S. R., & Yager, P. L. (2006). Physical and biological contributions to the western tropical North Atlantic Ocean carbon sink formed by the Amazon River plume. *Journal of Geophysical Research: Oceans*, *111*(C8). https://doi.org/10.1029/2005JC002954

Cooley, S. R., Coles, V. J., Subramaniam, A., & Yager, P. L. (2007). Seasonal variations in the Amazon plume-related atmospheric carbon sink. *Global Biogeochemical Cycles*, *21*(3). https://doi.org/10.1029/2006GB002831

Del Vecchio, R., & Subramaniam, A. (2004). Influence of the Amazon River on the surface optical properties of the western tropical North Atlantic Ocean. *Journal of Geophysical Research: Oceans*, *109*(C11). https://doi.org/10.1029/2004JC002503

Demaster, D. J., & Pope, R. H. (1996). Nutrient dynamics in Amazon shelf waters: results from AMASSEDS. *Continental Shelf Research*, *16*(3), 263–289. https://doi.org/10.1016/0278-4343(95)00008-O

Durack, P. J., & Wijffels, S.E. (2010). Fifty-year trends in global ocean salinities and their relationship to broad-scale warming. *Journal of Climate*, 23(16), 4342–4362. https://doi.org/10.1175/2010JCLI3377.1

Edmond, J. M., Boyle, E. A., Grant, B., & Stallard, R. F. (1981). The chemical mass balance in the Amazon plume I: The nutrients. *Deep Sea Research Part A: Oceanographic Research Papers*, *28*(11), 1339–1374. https://doi.org/10.1016/0198-0149(81)90038-8

Ffield, A. (2007). Amazon and Orinoco River plumes and NBC rings: bystanders or participants in hurricane events? *Journal of climate*, *20*(2), 316–333. https://doi.org/10.1175/JCLI3985.1

Foster, R. A., Kuypers, M. M., Vagner, T., Paerl, R. W., Musat, N., & Zehr, J. P. (2011). Nitrogen fixation and transfer in open ocean diatom–cyanobacterial symbioses. *The ISME journal*, *5*(9), 1484–1493. https://doi.org/10.1038/ismej.2011.26

Fournier, S., Reul, N., Chapron, B., & Tenerelli, J. (2012). Spatio-Temporal Coherence between Spaceborne Measurements of Salinity and Light Absorption in the Amazon Plume Region. *ESA Special Publication*, *703*(10).

Goes, J. I., Gomes, H. R., Chekalyuk, A. M., Carpenter, E. J., Montoya, J. P., Coles, V. J., et al. (2014). Influence of the Amazon River discharge on the biogeography of phytoplankton communities in the western tropical North Atlantic. *Progress in Oceanography*, *120*, 29–40. https://doi.org/10.1016/j.pocean.2013.07.010

Gomes, H. D. R., Xu, Q., Ishizaka, J., Carpenter, E. J., Yager, P. L., & Goes, J. I. (2018). The influence of riverine nutrients in niche partitioning of phytoplankton communities–a contrast between the Amazon River Plume and the ChangJiang (Yangtze) River diluted water of the East China Sea. *Frontiers in Marine Science*, *5*, 343. https://doi.org/10.3389/fmars.2018.00343

Huang, W. J., Cai, W. J., Castelao, R. M., Wang, Y., & Lohrenz, S. E. (2013). Effects of a wind-driven cross-shelf large river plume on biological production and CO2 uptake on the Gulf of Mexico during spring. *Limnology and oceanography*, *58*(5), 1727-1735. https://doi.org/10.4319/lo.2013.58.5.1727

Ibánhez, J. S. P., Diverrès, D., Araujo, M., & Lefèvre, N. (2015). Seasonal and interannual variability of sea-air CO_2 fluxes in the tropical Atlantic affected by the Amazon River plume. *Global Biogeochemical Cycles*, *29*(10), 1640–1655. https://doi.org/10.1002/2015GB005110

Ibánhez, J. S. P., Araujo, M., & Lefèvre, N. (2016). The overlooked tropical oceanic CO_2 sink. *Geophysical Research Letters*, *43*(8), 3804–3812. https://doi.org/10.1002/2016GL068020

Körtzinger, A. (2003). A significant CO_2 sink in the tropical Atlantic Ocean associated with the Amazon River plume. *Geophysical Research Letters*, *30*(24). https://doi.org/10.1029/2003GL018841

Landschützer, P., Gruber, N., Bakker, D. C. E., & Schuster, U. (2014). Recent variability of the global ocean carbon sink. *Global Biogeochemical Cycles*, *28*(9), 927–949. https://doi.org/10.1002/2014GB004853

Lefèvre, N., Diverrès, D., Gallois, F. (2010). Origin of CO_2 undersaturation in the western tropical Atlantic. *Tellus B: Chemical and Physical Meteorology*, *62*(5), 595–607. https://doi.org/10.1111/j.1600-0889.2010.00475.x

Lefèvre, N., Caniaux, G., Janicot, S., & Gueye, A. K. (2013). Increased CO2 outgassing in February-May 2010 in the tropical Atlantic following the 2009 Pacific El Niño. *Journal of Geophysical Research: Oceans*, *118*(4), 1645–1657. https://doi.org/10.1002/jgrc.20107

Lefèvre, N., Flores Montes, M., Gaspar, F. L., Rocha, C., Jiang, S., De Araújo, M. C., & Ibánhez, J. (2017). Net Heterotrophy in the Amazon Continental Shelf Changes Rapidly to a Sink of CO_2 in the Outer Amazon Plume. *Frontiers in Marine Science*, *4*, 278. https://doi.org/10.3389/fmars.2017.00278

Lewis E. R., Wallace D. W. R. (1998). Program developed for CO2 system calculations (No. cdiac: CDIAC-105). Environmental System Science Data Infrastructure for a Virtual Ecosystem. https://doi.org/10.15485/1464255

Lewis, S. L., Brando, P. M., Phillips, O. L., van der Heijden, G. M., & Nepstad, D. (2011). The 2010 Amazon drought. *Science*, *331*(6017), 554. https://doi.org/10.1126/science.1200807

Li, D., Chen, J., Ni, X., Wang, K., Zeng, D., Wang, et al. (2018). Effects of biological production and vertical mixing on sea surface pCO2 variations in the Changjiang River plume during early autumn: A buoy-based time series study. *Journal of Geophysical Research: Oceans*, *123*(9), 6156-6173. https://doi.org/10.1029/2017JC013740

Longhurst, A. (1993). Seasonal cooling and blooming in tropical oceans. *Deep Sea Research Part I: Oceanographic Research Papers*, *40*(11-12), 2145-2165. https://doi.org/10.1016/0967-0637(93)90095-K

Longhurst, A., Sathyendranath, S., Platt, T., & Caverhill, C. (1995). An estimate of global primary production in the ocean from satellite radiometer data. *Journal of plankton Research*, *17*(6), 1245-1271. https://doi.org/10.1093/plankt/17.6.1245

Marengo, J. A., Tomasella, J., Alves, L. M., Soares, W. R., & Rodriguez, D. A. (2011). The drought of 2010 in the context of historical droughts in the Amazon region. *Geophysical Research Letters*, *38*(12). https://doi.org/10.1029/2011GL047436

Medeiros, P. M., Seidel, M., Ward, N. D., Carpenter, E. J., Gomes, H. R., Niggemann, J., et al. (2015). Fate of the Amazon River dissolved organic matter in the tropical Atlantic Ocean. *Global Biogeochemical Cycles*, *29*(5), 677–690. https://doi.org/10.1002/2015GB005115

Molleri, G. S., Novo, E. M. D. M., & Kampel, M. (2010). Space-time variability of the Amazon River plume based on satellite ocean color. *Continental Shelf Research*, *30*(3–4), 342–352. https://doi.org/10.1016/j.csr.2009.11.015

Muller-Karger, F. E., McClain, C. R., Fisher, T. R., Esaias, W. E., & Varela, R. (1989). Pigment distribution in the Caribbean Sea: Observations from space. *Progress in Oceanography*, *23*(1), 23-64. https://doi.org/10.1016/0079-6611(89)90024-4

Muller-Karger, F. E., Richardson, P. L., & McGillicuddy, D. (1995). On the offshore dispersal of the Amazon's Plume in the North Atlantic: Comments on the paper by A. Longhurst, “Seasonal cooling and blooming in tropical oceans”. *Deep Sea Research Part I:*

Oceanographic Research Papers, *42*(11-12), 2127-2137. https://doi.org/10.1016/0967-0637(95)00085-2

Nobre, C. A., Sampaio, G., Borma, L. S., Castilla-Rubio, J. C., Silva, J. S., & Cardoso, M. (2016). Land-use and climate change risks in the Amazon and the need of a novel sustainable development paradigm. *Proceedings of the National Academy of Sciences*, *113*(39), 10759–10768. https://doi.org/10.1073/pnas.1605516113

Pailler, K., Bourlès, B., & Gouriou, Y. (1999). The barrier layer in the western tropical Atlantic Ocean. *Geophysical Research Letters*, *26*(14), 2069–2072. https://doi.org/10.1029/1999GL900492

Pierrot, D., Lewis, E., & Wallace, D. W. R. (2006). MS Excel program developed for CO2 system calculations. In *ORNL/CDIAC-105a. Carbon Dioxide Information Analysis Center, Oak Ridge National Laboratory, US Department of Energy, Oak Ridge, Tennessee* (Vol. 3). https://doi.org/10.3334/CDIAC/otg.CO2SYS_XLS_CDIAC105a

Raymond, P. A., Hartmann, J., Lauerwald, R., Sobek, S., McDonald, C., Hoover, M., et al. (2013). Global carbon dioxide emissions from inland waters. *Nature*, *503*(7476), 355–359. https://doi.org/10.1038/nature12760

Richey, J. E., Melack, J. M., Aufdenkampe, A. K., Ballester, V. M., & Hess, L. L. (2002). Outgassing from Amazonian rivers and wetlands as a large tropical source of atmospheric CO_2. *Nature*, *416*, 617–620. https://doi.org/10.1038/416617a

Salisbury, J., Vandemark, D., Campbell, J., Hunt, C., Wisser, D., Reul, N., & Chapron, B. (2011). Spatial and temporal coherence between Amazon River discharge, salinity, and light absorption by colored organic carbon in western tropical Atlantic surface waters.

Journal of Geophysical Research: Oceans, *116*(C7). https://doi.org/10.1029/2011JC006989

Smith Jr, W. O., & Demaster, D. J. (1996). Phytoplankton biomass and productivity in the Amazon River plume: correlation with seasonal river discharge. *Continental Shelf Research*, *16*(3), 291–319. https://doi.org/10.1016/0278-4343(95)00007-N

Stenegren, M., Berg, C., Padilla, C. C., David, S. S., Montoya, J. P., Yager, P. L., & Foster, R. A. (2017). Piecewise structural equation model (SEM) disentangles the environmental conditions favoring diatom diazotroph associations (DDAs) in the western tropical north Atlantic (WTNA). *Frontiers in microbiology*, *8*, 810. https://doi.org/10.3389/fmicb.2017.00810

Subramaniam, A., Yager, P. L., Carpenter, E., Mahaffey, C., Björkman, K., Cooley, S., et al. (2008). Amazon River enhances diazotrophy and carbon sequestration in the tropical North Atlantic Ocean. *Proceedings of the National Academy of Sciences of the United States of America*, *105*(30), 10460–10465. https://doi.org/10.1073/pnas.0710279105

Sweeney, C., Hansell, D. A., Carlson, C. A., Codispoti, L. A., Gordon, L. I., Marra, J., et al. (2000). Biogeochemical regimes, net community production and carbon export in the Ross Sea, Antarctica. *Deep Sea Research Part II: Topical Studies in Oceanography*, *47*(15–16), 3369–3394. https://doi.org/10.1016/S0967-0645(00)00072-2

Sweeney, C., Gloor, E., Jacobson, A. R., Key, R. M., McKinley, G., Sarmiento, J. L., & Wanninkhof, R. (2007). Constraining global air-sea gas exchange for CO2 with recent bomb 14C measurements. *Global Biogeochemical Cycles*, *21*(2). https://doi.org/10.1029/2006GB002784

Takahashi, T., Olafsson, J., Goddard, J. G., Chipman, D. W., & Sutherland, S. C. (1993). Seasonal variation of CO_2 and nutrients in the high-latitude surface oceans: A comparative study, *Global Biogeochemical Cycles*, *7*(4), 843–878. https://doi.org/10.1029/93GB02263

Takahashi, T., Feely, R. A., Weiss, R. F., Wanninkhof, R. H., Chipman, D. W., Sutherland, S. C., & Takahashi, T. T. (1997). Global air-sea flux of CO2: An estimate based on measurements of sea–air pCO2 difference. *Proceedings of the National Academy of Sciences*, *94*(16), 8292–8299. https://doi.org/10.1073/pnas.94.16.8292

Takahashi, T., Sutherland, S. C., Wanninkhof, R., Sweeney, C., Feely, R. A., Chipman, D. W., et al. (2009). Climatological mean and decadal change in surface ocean pCO2, and net sea–air CO_2 flux over the global oceans. *Deep Sea Research Part II: Topical Studies in Oceanography*, *56*(8–10), 554–577. https://doi.org/10.1016/j.dsr2.2008.12.009

Ternon, J. F., Oudot, C., Dessier, A., and Diverres, D. (2000). A seasonal tropical sink for atmospheric CO_2 in the Atlantic Ocean: The role of the Amazon River discharge. *Marine Chemistry*, *68*(3), 183–201. https://doi.org/10.1016/S0304-4203(99)00077-8

Thomas, B. R., Kent, E. C., & Swail, V. R. (2005). Methods to homogenize wind speeds from ships and buoys. *International Journal of Climatology*, *25*(7), 979–995. https://doi.org/10.1002/joc.1176

Wanninkhof, R. (1992). Relationship between wind speed and gas exchange over the ocean. *Journal of Geophysical Research: Oceans*, *97*(C5), 7373–7382. https://doi.org/10.1029/92JC00188

Ward, N. D., Keil, R. G., Medeiros, P. M., Brito, D. C., Cunha, A. C., Dittmar, T., et al. (2013). Degradation of terrestrially derived macromolecules in the Amazon River. *Nature Geoscience*, *6*(7), 530–533. https://doi.org/10.1038/ngeo1817

Ward, N. D., Krusche, A.V., Sawakuchi, H. O., Brito, D. C., Cunha, A. C., Sousa Moura, J. M., da Silva, R., Yager. P.L., Keil, R. G., & Richey, J. E. (2015). The compositional evolution of dissolved and particulate organic matter along the lower Amazon River—Óbidos to the ocean. *Marine Chemistry*, *177*, 244–256. http://doi.org/10.1016/j.marchem.2015.06.013

Weber, S. C., Carpenter, E. J., Coles, V. J., Yager, P. L., Goes, J., & Montoya, J. P. (2017). Amazon River influence on nitrogen fixation and export production in the western tropical North Atlantic. *Limnology and Oceanography*, *62*(2), 618–631. https://doi.org/10.1002/lno.10448

Weiss, R. F. (1974). Carbon dioxide in water and seawater: the solubility of a non-ideal gas. *Marine Chemistry*, *2*(3), 203–215. https://doi.org/10.1016/0304-4203(74)90015-2

Weiss, R. F., & Price, B. A. (1980). Nitrous oxide solubility in water and seawater. *Marine Chemistry*, *8*(4), 347–359. https://doi.org/10.1016/0304-4203(80)90024-9

Yeung, L. Y., Berelson, W. M., Young, E. D., Prokopenko, M. G., Rollins, N., Coles, V. J., et al. (2012). Impact of diatom-diazotroph associations on carbon export in the Amazon River plume. *Geophysical Research Letters*, *39*(18). https://doi.org/10.1029/2012GL053356

Table 3.1

Standard linear regressions between *in-situ* sea surface salinity (**SSS**, unitless) and (**A**) *in-situ* sea surface pCO_2 (***p*CO₂**, μatm), and (**B**) temperature-normalized pCO_2 (μatm) at 29 °C (***p*CO₂₍₂₉₎**, μatm) for the three ANACONDAS expeditions in the ARP region. SSS ranges within 15<SSS<35 for both (A) and (B). Parentheses indicate ±95% confidence interval.

(A)	**SSS vs *p*CO₂** (15<SSS<35)	**r**	**N**
Jun. 2010	***p*CO₂** = 13.9 (±0.2) × **SSS** – 96.4 (±6.9)	0.92	2621
Jul. 2012	***p*CO₂** = 13.0 (±0.1) × **SSS** – 55.4 (±3.2)	0.97	4593
Sep. 2011	***p*CO₂** = 16.9 (±0.5) × **SSS** – 208.7 (±15.7)	0.79	2729

(B)	**SSS vs *p*CO₂₍₂₉₎** (15<SSS<35)	**r**	**N**
Jun. 2010	***p*CO₂₍₂₉₎** = 14.1 (±0.2) × **SSS** – 110.7 (±6.4)	0.92	2621
Jul. 2012	***p*CO₂₍₂₉₎** = 13.8 (±0.1) × **SSS** – 75.9 (±3.0)	0.96	4593
Sep. 2011	***p*CO₂₍₂₉₎** = 17.8 (±0.3) × **SSS** – 243.6 (±10.7)	0.84	2729

Table 3.2

Key properties used in calculating the underway air–sea CO_2 flux of the Amazon River plume during each expedition: $xCO_{2(atm)}$ (in ppm) is the monthly averaged molar concentration of the atmosphere, $pCO_{2(atm)}$ (in μatm) is the cruise-averaged partial pressure of CO_2 in the atmosphere calculated with $xCO_{2(atm)}$ and *in-situ* surface temperature & salinity, $U10_{reanalysis}$ (in m s^{-1}) is the monthly averaged reanalysis wind speed at 10 m above sea surface.

	$xCO_{2(atm)}$ (ppm)	$pCO_{2(atm)}$ (μatm)	$U10_{reanalysis}$ (m s^{-1})
Jun. 2010	391.65	381.09	6.0 (± 1.2)
Jul. 2012	393.07	383.53	5.8 (± 1.3)
Sep. 2011	388.02	376.81	5.1 (± 1.1)

Table 3.3

Comparison of CO_2 flux estimates for the ARP between the three ANACONDAS expeditions and past studies. Errors are presented as standard deviation of the mean.

	Air–sea CO_2 Flux		Area	SSS	Period
	mmol m^{-2} d^{-1}	Tg C mo^{-1}	km^2	unitless	
AN2010	-2.39 ± 1.29	-0.68 ± 0.36	7.76×10^5	15–35	June
AN2012	0.26 ± 0.62	0.07 ± 0.15	6.87×10^5	15–35	July
AN2011	-0.42 ± 0.76	-0.13 ± 0.23	8.31×10^5	15–35	September
***Cooley et al.* 2007**	-5.21 ± 5.22	-2.49 ± 2.50	1.33×10^6	28–35	June
	-5.37 ± 5.39	-2.59 ± 2.60	1.34×10^6	28–35	July
	-3.65 ± 3.81	-1.20 ± 1.25	9.06×10^5	28–35	September
***Ibánhez et al.* 2015**	-1.05 ± 0.24	N/A	N/A	None	June
	-0.12 ± 0.08	N/A	N/A	None	July
	-0.36 ± 0.09	N/A	N/A	None	October
***Körtzinger* 2003**	-1.35	-1.17	2.40×10^6	15–34.9	Entire Year
***Lefèvre et al.* 2010**	-0.96 ± 1.20	-0.38 ± 0.48	1.10×10^6	15–34.9	Entire Year

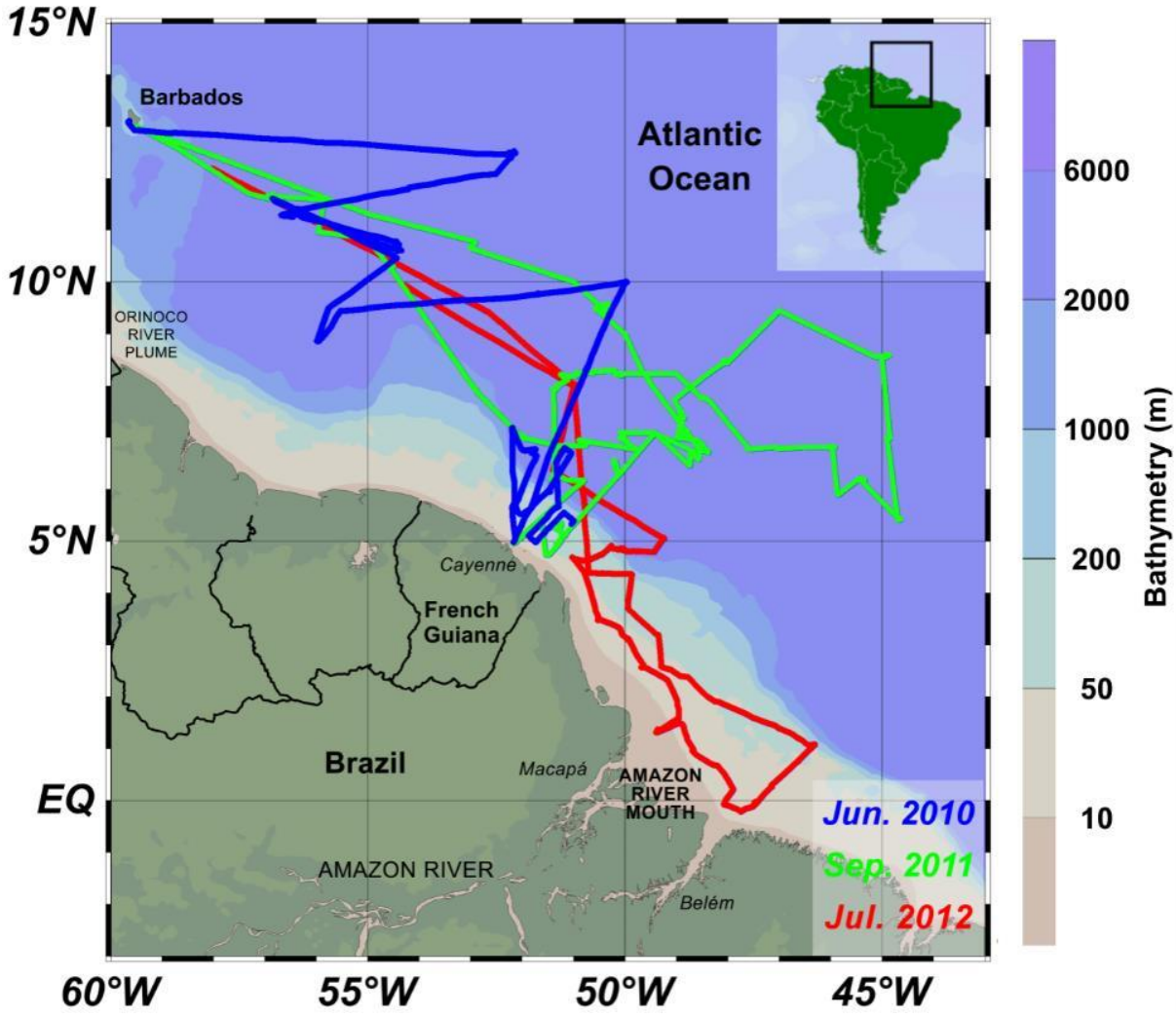

Figure 3.1. Cruise tracks for ANACONDAS research expeditions in May–June 2010 (blue; abbreviated to "June" in the text), September–October 2011 (green; abbreviated to "September" in the text), and July 2012 (red) superimposed on a bathymetry map. Inset at the top right corner displays the study site relative to the South American continent.

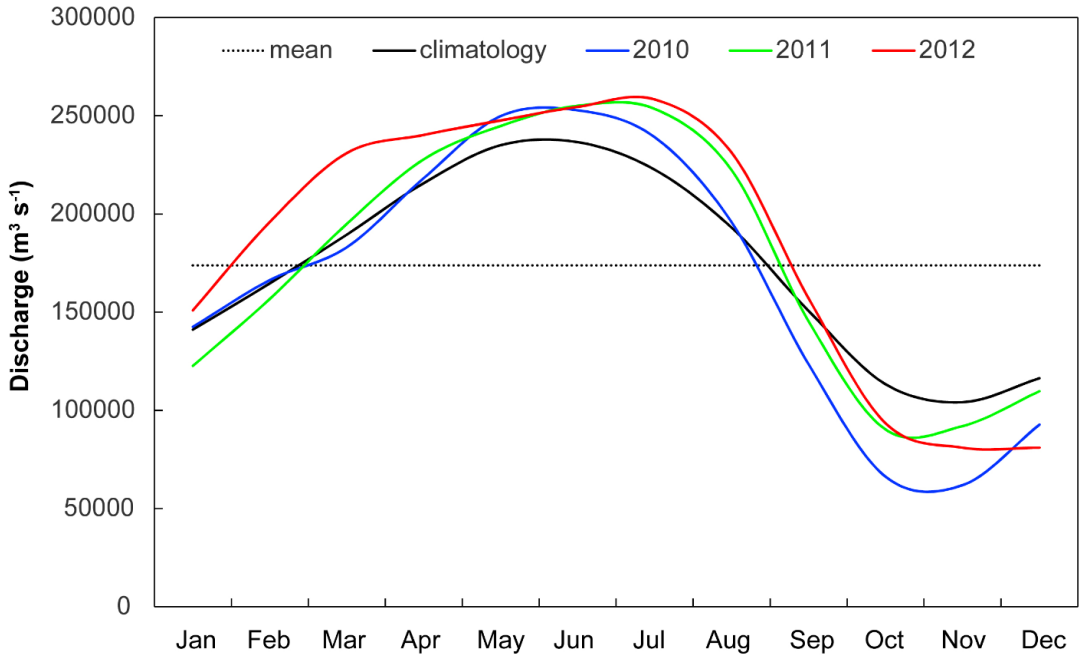

Figure 3.2. Monthly discharge of the Amazon River (m^3 s^{-1}) at the Óbidos gauge station for the years 2010 (blue line), 2011 (green line), 2012 (red line), and averaged over 1968–2012 (black line), in reference to the mean annual discharge 1968–2012 (dotted line). Note that discharge at the mouth is 4–34% greater than the discharge at Óbidos, with a peak contribution from the lower tributaries of up to 85,000 m^3 s^{-1} in May (Ward et al., 2015).

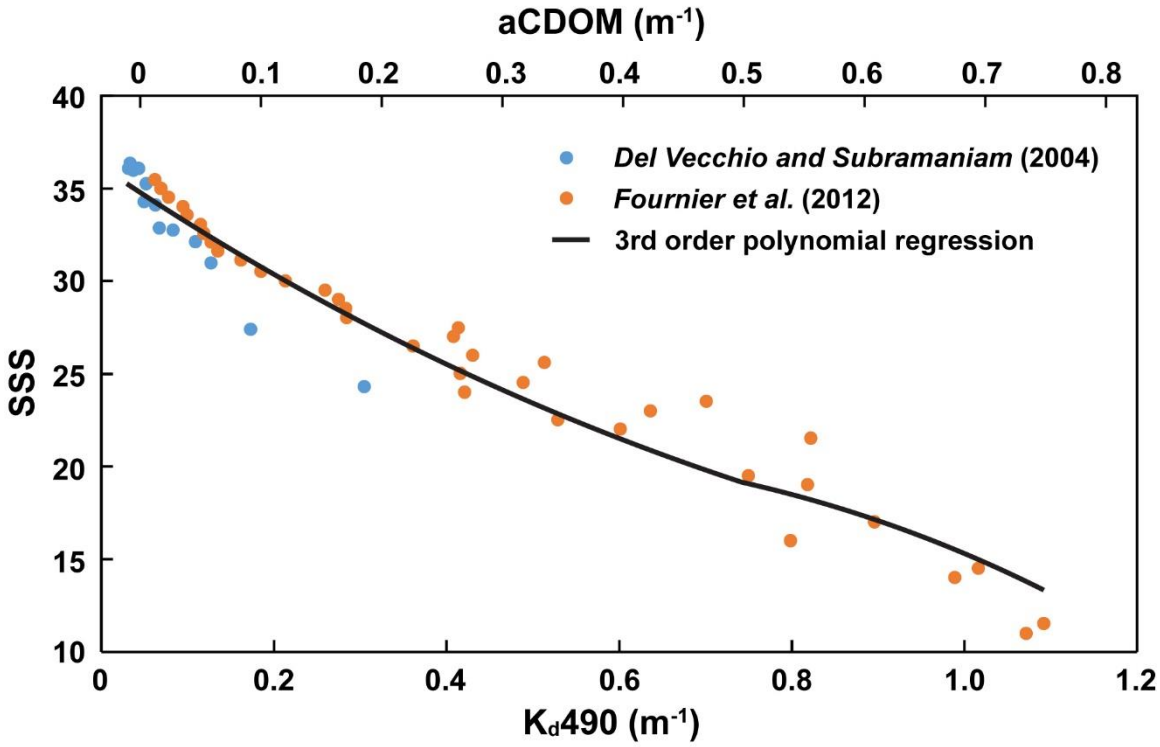

Figure 3.3. Scatterplot of binned K_d490/aCDOM and SSS from Del Vecchio and Subramaniam (2004; N = 13; blue dots) and Fournier et al. (2012; N = 38; orange dots). aCDOM from Fournier et al. (2012) was converted to K_d490 using the equation: aCDOM = 0.704 × K_d490 – 0.026 (r^2 = 0.98), reported in Del Vecchio and Subramaniam (2004). A 3rd order polynomial fit is applied for the combined K_d490–SSS datasets (N = 51, r = -0.98; regression is shown in the Method).

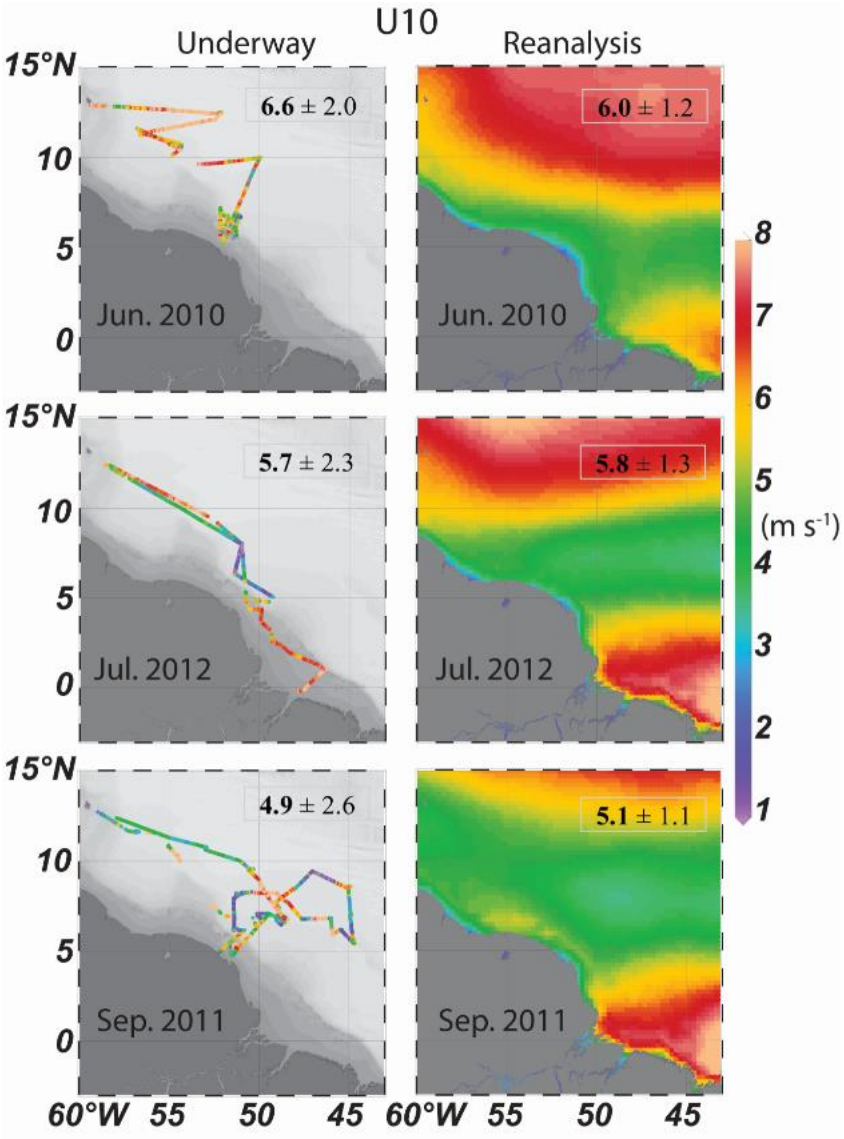

Figure 3.4. Comparison between cruise-averaged wind speeds corrected at 10 m above sea surface (U10, m s^{-1}) and monthly reanalysis U10 for the three months of the cruises.

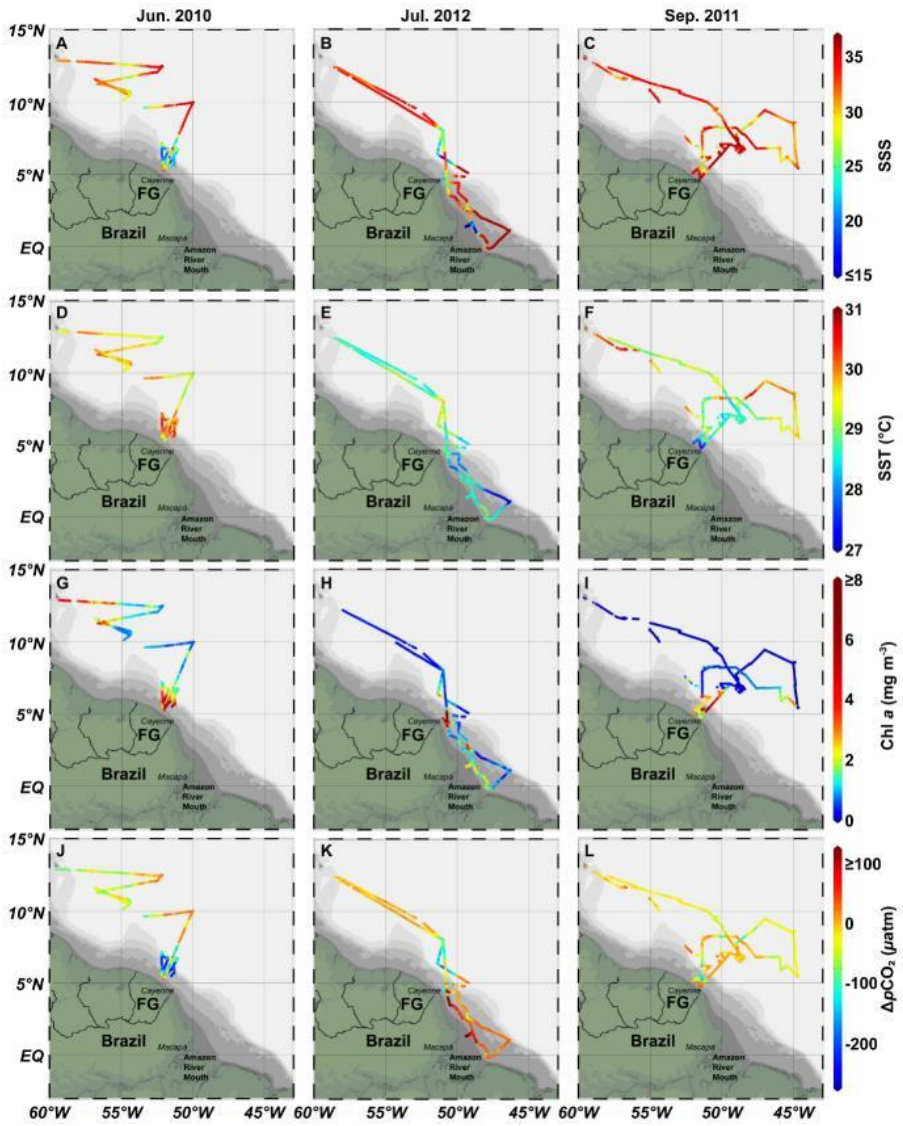

Figure 3.5. Surface water properties in June 2010 (A, D, G, J), July 2012 (B, E, H, K), and September 2011 (C, F, I, L): sea surface temperature (SST, °C; A–C), sea surface salinity (SSS, unitless; D–F), chlorophyll *a* concentration (Chl *a*, mg m^{-3}; G–I), and difference between *in-situ* sea surface & atmospheric partial pressure of CO_2 (ΔpCO_2, μatm; J–L). SSS below 15 in 2012 (B) and ΔpCO_2 above 100 μatm in 2012 (K) are displayed with the same color range as their closest boundary color. Gray shading represents 10, 50, 200, 1000, 2000, and 6000 m isobaths (see Figure 2.1).

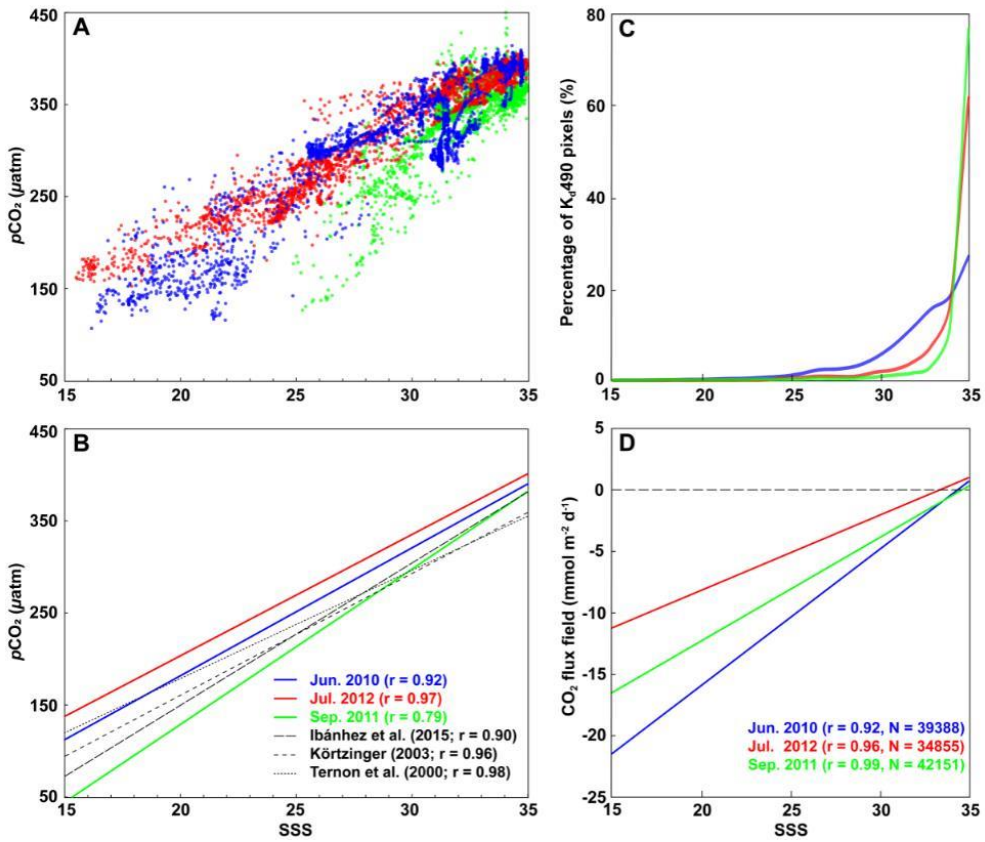

Figure 3.6. (**A**) Scatterplot of underway SSS (unitless) and *in-situ* surface pCO_2 (μatm) for 15<SSS<35 during the three ANACONDAS expeditions (June, blue; July, red; September, green). (**B**) Linear regressions between SSS and *in-situ* surface pCO_2 for the ANACONDAS expeditions (same colors as in A) compared to previously reported relationships. (**C**) Smoothed histogram of salinity distribution during the three cruises, and (**D**) seasonal linear regressions of CO_2 flux (negative sign is ocean uptake) as a function of salinity, reflecting the impact of wind speed.

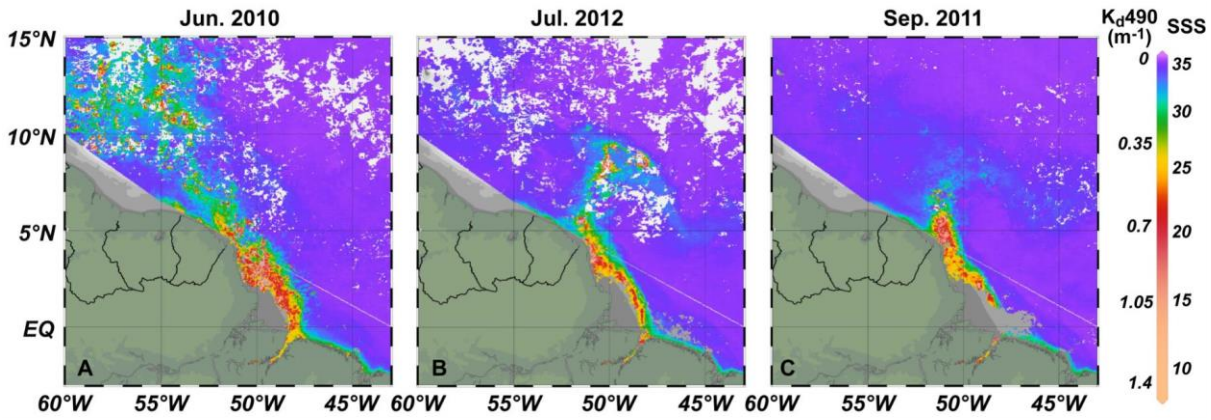

Figure 3.7. Binned diffuse attenuation coefficient at 490 nm (K_d490, m^{-1}) and K_d490-derived SSS fields (unitless) averaged over each expedition period within the ARP (15°N–3°S, 43–60°W) for (**A**) May–June 2010, (**B**) July 2012, and (**C**) September–October 2011. Bin size is 0.04° latitude × 0.04° longitude. Gray areas on the maps indicate K_d490 is unavailable (usually due to clouds or highly turbid nearshore waters).

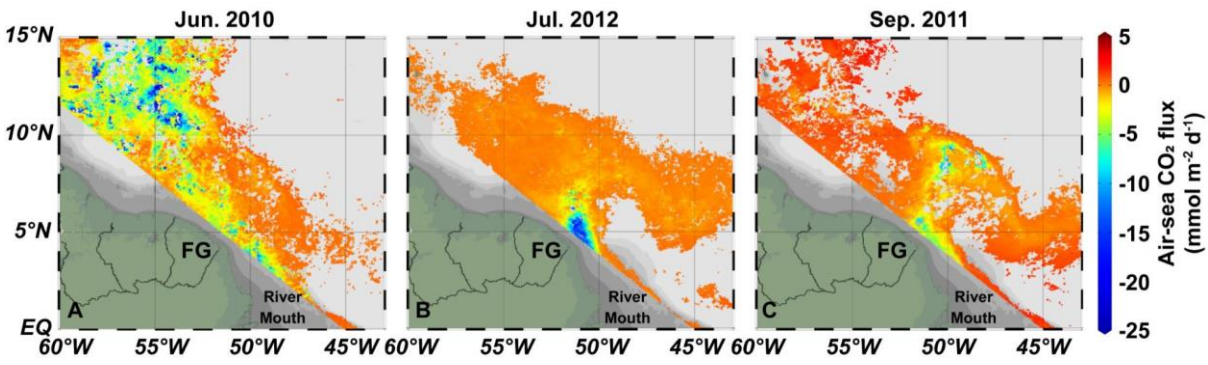

Figure 3.8. Binned air-sea CO_2 flux (mmol m^{-2} d^{-1}) derived from temporally-averaged K_d490 for the ARP (15<SSS<35) for (**A**) May–June 2010, (**B**) July 2012, and (**C**) September–October 2011. Shallow waters near the river mouth are excluded. Positive fluxes indicate CO_2 outgassing from the ocean (i.e. effluxes) and negative fluxes suggest oceanic CO_2 uptake from the atmosphere (i.e. influxes). Gray background represents areas either with no K_d490 data or out of the defined SSS range of the plume.

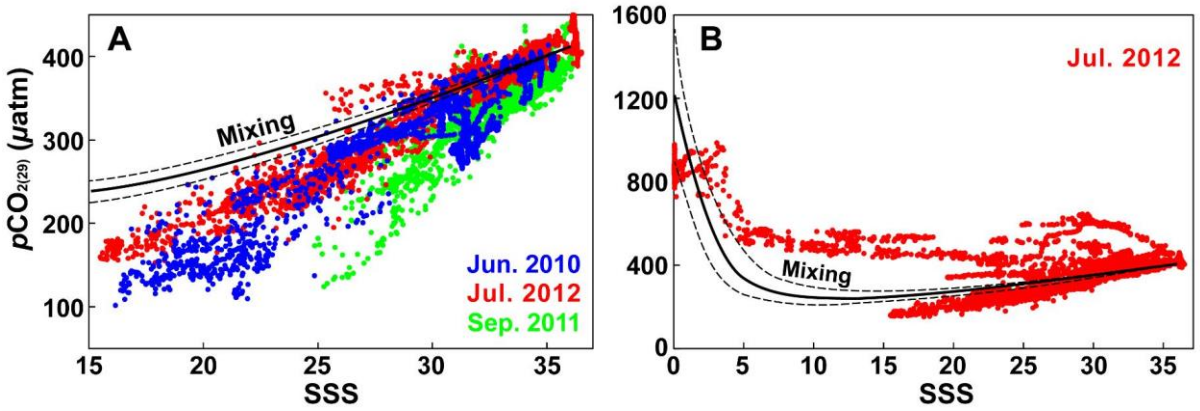

Figure 3.9. (**A**) Scatter diagram between the underway sea surface salinity (SSS; 15–37) and the temperature-normalized *in-situ* seawater pCO_2 (μatm) at 29 °C ($pCO_{2(29)}$) for cruises in June 2010 (blue dots), July 2012 (red dots), and September 2011 (green dots). The mixing curve (black line) indicates the expected pCO_2 from total alkalinity (ALK) and total dissolved inorganic carbon (DIC) resulting from conservative mixing between riverine & oceanic endmembers at 29 °C, with the uncertainty range as dashed lines. (**B**) SSS vs $pCO_{2(29)}$ regression for July 2012 expedition including data near the Amazon River mouth, relative to the mixing curve.

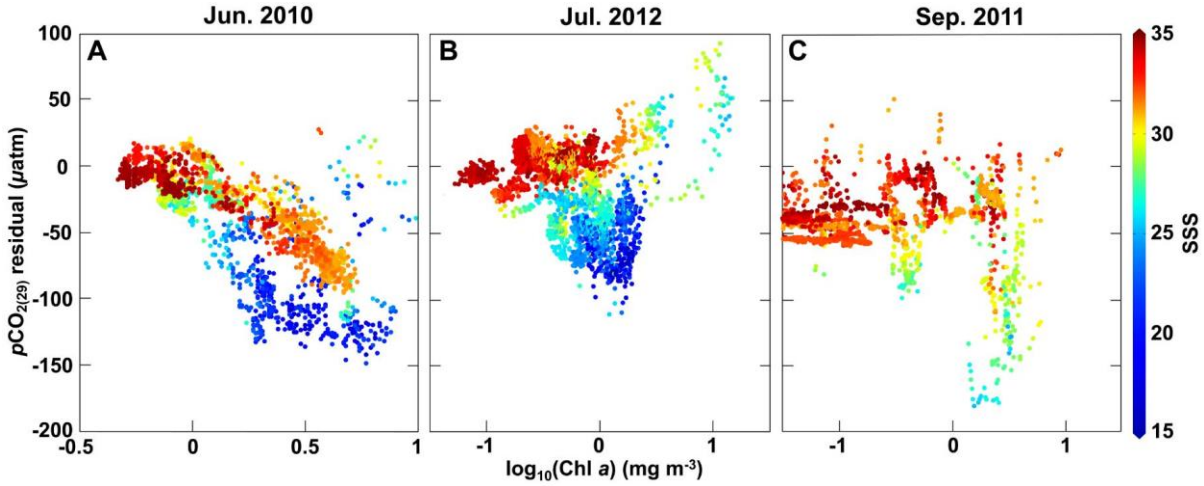

Figure 3.10. Scatter diagrams of *in-situ* chlorophyll *a* concentration (Chl *a*, mg m^{-3}) on base 10 logarithm scale and $pCO_{2(29)}$ residual, with colors representing SSS within the ARP (15<SSS<35) during the cruises in June 2010 (**A**), July 2012 (**B**), and September 2011 (**C**).

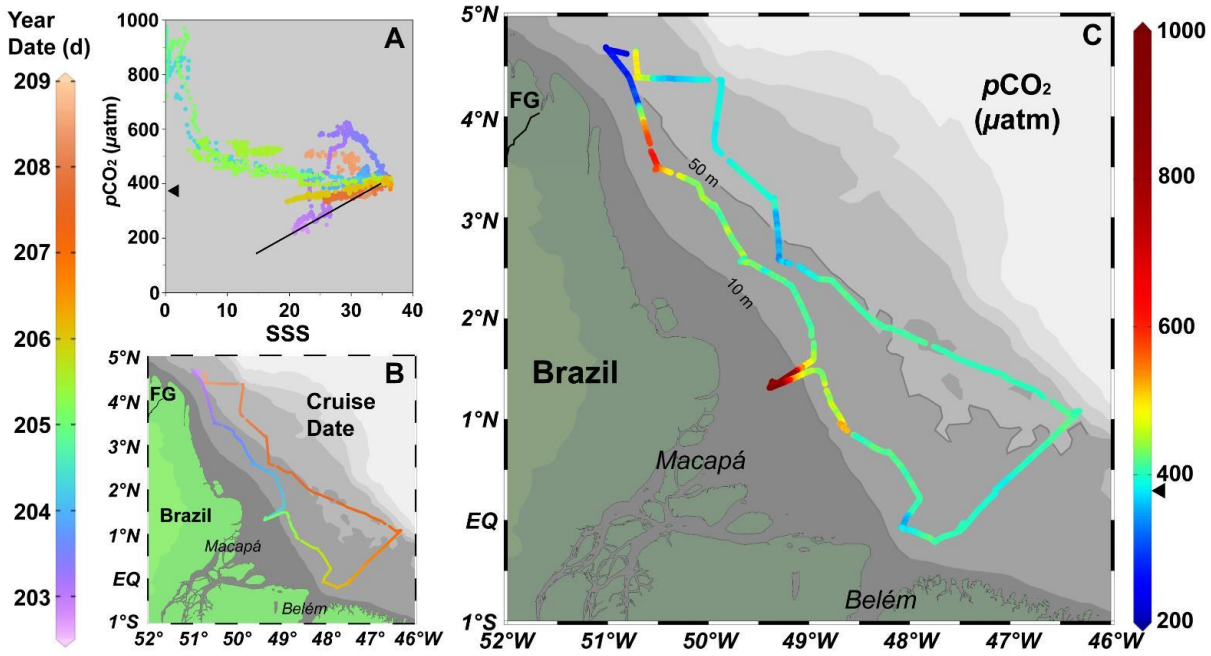

Figure 3.11. Underway observations during the July 2012 cruise from the Brazil shelf only, south of 4.7°N. (**A**) Scatterplot of *in-situ* SSS and pCO_2 (μatm) data colored according to cruise dates (by Year Day, d). Black line represents the linear regression (from Figure 3) between *in-situ* SSS vs pCO_2 for the defined salinity range (15<SSS<35) during July 2012. (**B**) Cruise track colored with the dates (d) as in **A**. (**C**) *In-situ* pCO_2 (μatm) along the cruise track. ◄ in the pCO_2 color bar denotes the approximate value of atmospheric pCO_2 at the time of the cruise.

ADDENDUM to CHAPTER 3

INTERANNUAL VARIABILITY OF CO_2 UPTAKE BY THE AMAZON RIVER PLUME DURING HIGH RIVER DISCHARGE IN JUNE 2003–2020[3]

[3]Linquan Mu, Helga do Rosario Gomes, and Patricia L. Yager. To be submitted to *Global Biogeochemical Cycles*.

Summary

This addendum builds upon the finding from Chapter 3 that the Amazon River plume is a strong sink for atmospheric CO_2 in June-2010. My primary goal was to explore interannual variability and trends in the total area and carbon flux of the offshore plume and ask whether they may reflect the impacts of climate change. Such trends, if they exist, could impact the atmospheric carbon dioxide uptake by the plume, and account for some of the different estimates of the annual sink. Here, I examine the climatology of a single key month of June, following Amazon flood stage for the river plume during 18 years (2003–2020), analyzing the interannual variability of plume size and CO_2 uptake.

Although long-term trends were seen in both the size and variance of the plume, these "signal" trends were not strong enough to rise out of the high variability "noise" of this region. A longer data set may be needed to detect any significant trends. Because monthly delineations are somewhat arbitrary, a more complete study should also include other months during high discharge as well.

Notably, the CO_2 uptake in June 2010 (reported in Chapter 3) was 1.2 Tg C mo^{-1}, significantly higher than the June mean for the climatology (2003–2020). This difference reflects some differences in methodology, which also need to be explored in terms of the sensitivity of the outcome to analytical choices.

1. Introduction

The magnitude of the air–sea CO_2 flux in the ARP is mainly affected by the size of the plume, as well as the salinity distribution at the plume surface (Mu et al., 2021). The plume size depends largely on wind and river discharge (Coles et al. 2013). The large interannual variability of the Amazon River discharge (e.g., Giffard et al., 2019) and the climate-sensitivity of the Amazon River watershed (Marengo et al., 2018) are well established although complicated. We wondered whether a satellite data time-series of the plume might indicate any temporal trends in either total plume size or plume size variability, which might then cause year-to-year differences in atmospheric CO_2 uptake by the plume.

We choose the key month of June to examine. The largest plume area is usually seen during the high-water season (Apr. – Jun.), where the extensive river outflow delivers low-salinity waters farther north along the Brazil shelf, and the winds transport the plume waters northward as far as the Caribbean. The distribution of low SSS is strongly associated with CO_2 undersaturation (Mu et al., 2021), making June an important season for atmospheric CO_2 uptake by the plume.

2. Methods

Methods were identical to those used in Chapter 3 except as indicated below. Level-3 monthly K_d490 was obtained for each June between 2003 and 2020 from NASA Ocean Color database (https://oceancolor.gsfc.nasa.gov/l3/), with spatial resolution of 4 km; this differs from the use of 8-day averages in Chapter 3. A slightly larger coordinate frame (15°N–5°S, 40–60°W; as opposed to 15–0°N, 43–60°W) was used, and shallow shelf and Orinoco plume areas were not removed. As before, the total area of the plume was calculated by summing up all the pixels within the defined K_d490 range for the plume between 0.037–1.006 m^{-1}, corresponding to SSS range of 15–35. K_d490 was not available under heavy clouds or high turbidity, causing 10–40% of the area having no data across the years.

The SSS field was divided into 4 bands: 15–30, 30–33, 33–34, and 34–35; the percentages of SSS pixels were calculated for each salinity band (Table A.1). The CO_2 flux was estimated for each SSS pixel from the SSS–flux relationship for June 2010 (Mu et al., 2021):

$$\text{Flux} = (1.109 \pm 0.1) \times \text{SSS} - (38.088 \pm 1.2);\ (N = 39390,\ R = 0.92).$$

Although the magnitude and spatial distribution of SST, wind speed, and atmospheric pCO_2 likely varied between 2003–2020, we assumed for this preliminary study that they were identical to those observed during June 2010.

3. Results

3.1. K_d490-derived SSS distribution

Regional distributions of K_d490 and derived SSS in June were generally similar across 2003–2020 (Figure A.1), with the plume area indicated by SSS between 15–35, which roughly corresponded to K_d490 between 0.04–1.0 m^{-1}. The freshest plume waters (SSS < 25) were observed at the outer continental shelf and along the Brazil and French Guiana coasts between 0.5–5°N, following the northwestward extension of the ARP. In most of the years, plume waters reached as far north as 15°N where SSS increased (but was still below 35) as the plume mixed with oceanic water. North of 7.5°N, the plume signal appeared to be enhanced in 2010, weakened in most other years, and was the weakest in 2008, although different cloudiness distributions made direct comparisons difficult. Plume salinities were rarely seen east of ~47°W, except for 2006, 2008, and 2020, during which low-salinity waters extended as far east as ~45°W, perhaps indicating an earlier than average summer retroflection (Coles et al. 2013).

The total plume area in June varied ±30% during the 18 years (Figure A.2, Table A.1). Mean area was 954,000 ± 118,000 km^2, with largest plume area of 1,150,000 km^2 in 2010 and smallest plume area of 755,000 km^2 in 2013. Regression of plume size against time

yielded a negative slope (slope = –4296 ± 11537, R^2 = 0.0375) that was not significantly different from 0. No interannual trend in plume area was thus detected within this relatively short time series. A longer data set is needed to test for any definitive trend.

The residual (difference from the mean plume area) was as much as 200,000 km^2 (Figure A.3). Regressed against time, the residual had a positive slope of 1150 ± 5393 (Figure A.4), suggesting an increase in plume size variability over time that was also not statistically significant, however.

The distribution of salinity showed some variation over time. Percentages of the K_d490-derived SSS pixels in the defined salinity bands (i.e., 15–30, 30–33, 33–34, and 34–35) varied by 12–27% (Figure A.5). A majority (51 ± 6%) of the plume area was comprised of waters with highest salinity (34 < SSS < 35), followed by 18 ± 3% at 33 < SSS < 34, and ~15% at mid- (30 < SSS < 33) and low salinity (15 < SSS < 30), respectively (Table A.1). Although there was no significant trend in SSS distribution over time, June 2010 was unusually low (33% versus 51±6%) for the 34 < SSS < 35 range, and was unusually high (30% versus 18±3%) for the mid-salinity range (30 < SSS < 33).

3.2. Interannual trends of air–sea CO_2 fluxes in the plume

Monthly CO_2 uptake in June ranged between 0.5–0.7 Tg C mo^{-1} for all the years except for 2010. The somewhat unique SSS distribution in 2010 had a direct impact on the magnitude of the air–sea CO_2 flux (Figure A.6). The total CO_2 uptake by the plume was 1.2 Tg C mo^{-1} in June 2010, somewhat higher than the mean of 0.7±0.4 Tg C mo^{-1} over 2003–2020. Despite large variations in the total plume area (Figure A.2, also shaded gray on Figure A.6), total CO_2 uptake by the ARP was less variable over time because the influence of the SSS distribution.

3.3. June-2010 plume size and CO_2 flux comparison with Chapter 3

The mean CO_2 uptake of 1.2 Tg C mo^{-1} calculated for June-2010 in this Addendum was more than 0.5 Tg mo^{-1} greater than determined in Chapter 3. Such a discrepancy can be attributed to the differences in the plume size. The total area of the plume in June-2010 was calculated to be 0.78×10^6 km^2 in Chapter 3, but 1.15×10^6 km^2 in this Addendum. The different set of coordinates (15°N–5°S, 40–60°W) used to represent the plume region resulted in an 80–100% greater plume area than calculated in Chapter 3 using 15–0°N, 43–60°W. This comparison also does not account for any differences in the fraction of no-data pixels. Furthermore, data regions affected by the Orinoco River plume (0–150 km off the coastline between 55–60°W) as well as shallow regions at the river mouth with depth < 50 m were masked in the analysis in Chapter 3, whereas these data were not removed from the preliminary calculation in this Addendum, further increasing the difference.

The CO_2 flux density in June-2010 from this Addendum (–2.8 mmol m^{-2} d^{-1}) was ~15% greater than reported in Chapter 3 (–2.4 mmol m^{-2} d^{-1}). Such observation might indicate the salinity distributions were not precisely the same in both estimations. This was perhaps connected to the difference in the period length of the K_d490 data: in this Addendum, monthly averaged K_d490 for June-2010 was used, whereas in Chapter 3, five 8-day-averages between May 25 – July 3, 2010 were combined to represent June-2010. This difference in the type and time period when selecting K_d490 data may have affected the salinity distributions and the resulting magnitude of CO_2 flux in the "June" plume, and therefore requires further investigations.

4. Conclusions

With the large interannual variability found in the Amazon River system, it is not much of a surprise to find that we could not detect a significant temporal trend in either plume size

or its residual withing an 18-year data set. Still, hints of a decrease in plume size and an increase in variability are likely worth examining further with a longer time-series.

Despite large variations in the plume area over time (Figure A.6), total CO_2 uptake by the ARP was less variable over the time span examined because the total flux is partially compensated by the sensitivity to the SSS distribution. CO_2 uptake in June 2010 was significantly higher than average because the smaller area of high salinity waters (with weak CO_2 outgassing), and greater than average mid-salinity waters ($30 < SSS < 33$; with CO_2 uptake). The unusual nature of June 2010 warrants further exploration, and suggests some caution in broadly extrapolating the findings of Chapter 3.

Reference

Coles, V. J., Brooks, M. T., Hopkins, J., Stukel, M. R., Yager, P. L., & Hood, R. R. (2013). The pathways and properties of the Amazon River Plume in the tropical North Atlantic Ocean. *Journal of Geophysical Research: Oceans*, *118*(12), 6894-6913.

Giffard, P., Llovel, W., Jouanno, J., Morvan, G., & Decharme, B. (2019). Contribution of the Amazon river discharge to regional sea level in the tropical Atlantic Ocean. *Water*, *11*(11), 2348.

Marengo, J. A., Souza Jr, C. M., Thonicke, K., Burton, C., Halladay, K., Betts, R. A., et al. (2018). Changes in climate and land use over the Amazon region: current and future variability and trends. *Frontiers in Earth Science*, *6*, 228.

Mu, L., Gomes, H. R., Burns, S. M., Goes, J. I., Coles, V. J., Rezende, C. E., et al. (2021). Temporal variability of air–sea CO2 flux in the western tropical North Atlantic influenced by the Amazon River plume. *Global Biogeochemical Cycles*., *35*(6), e2020GB006798. https://doi.org/10.1029/2020GB006798

Table A.1.

The variations in the size, salinity distribution, and CO_2 uptake of the Amazon River plume calculated from the K_d490 distribution in June during 2003–2020.

Year	Plume area $\times 10^5$ km^2	Residual $\times 10^5$ km^2	% of K_d490-derived SSS pixels				CO_2 uptake rate mmol C m^{-2} d^{-1}	Total CO_2 Uptake Tg C mo^{-1}
			15≤S<30	30≤S<33	33≤S<34	34≤S≤35		
2003	9.1	-8.1E+04	16%	17%	22%	45%	2.1	0.7
2004	8.9	-9.2E+04	15%	14%	15%	57%	1.8	0.6
2005	10.6	7.5E+04	13%	13%	17%	58%	1.5	0.6
2006	10.7	9.3E+04	13%	12%	22%	52%	1.7	0.7
2007	8.5	-1.3E+05	18%	15%	17%	50%	2.1	0.7
2008	10.7	9.9E+04	14%	14%	17%	55%	1.8	0.7
2009	10.0	3.1E+04	16%	16%	19%	49%	2.1	0.7
2010	11.5	1.9E+05	19%	31%	17%	33%	2.8	1.2
2011	10.6	1.0E+05	16%	15%	14%	55%	1.9	0.7
2012	9.7	2.0E+04	16%	11%	21%	53%	2.0	0.7
2013	7.6	-1.9E+05	20%	13%	12%	54%	2.5	0.7
2014	9.2	-2.5E+04	16%	16%	20%	49%	2.1	0.7
2015	7.7	-1.7E+05	19%	16%	15%	50%	2.4	0.7
2016	8.9	-4.6E+04	13%	11%	16%	60%	1.6	0.5
2017	10.8	1.5E+05	14%	15%	17%	54%	1.8	0.7
2018	8.1	-1.2E+05	18%	15%	15%	51%	2.2	0.6
2019	8.8	-4.0E+04	15%	16%	20%	48%	1.9	0.6
2020	10.6	1.4E+05	13%	17%	22%	48%	1.7	0.7

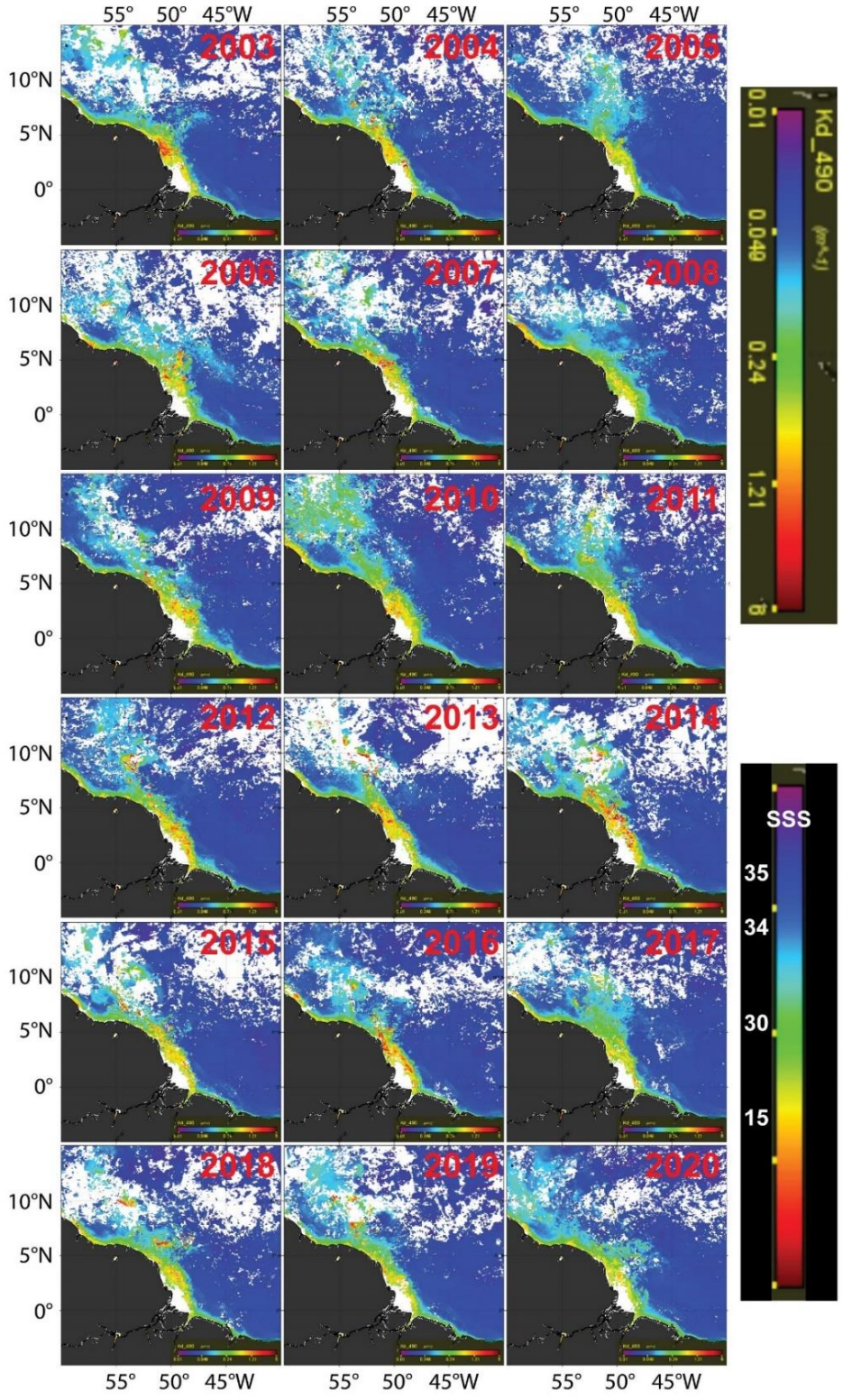

Figure A.1. K_d490 and K_d490-derived SSS field for June during 2003–2020. Gaps are regions with no data entries due to heavy clouds.

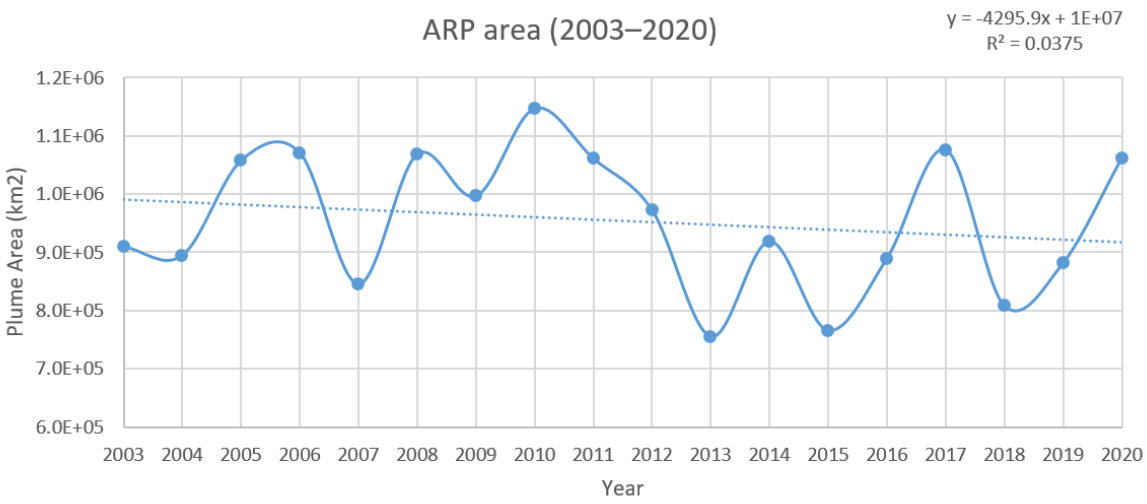

Figure A.2. Time series of the June plume area between 2003–2020. The negative slope (-4296) of the regression line (shown as blue dotted line) has a 95% confidence interval of 11537, and is not significantly different from zero.

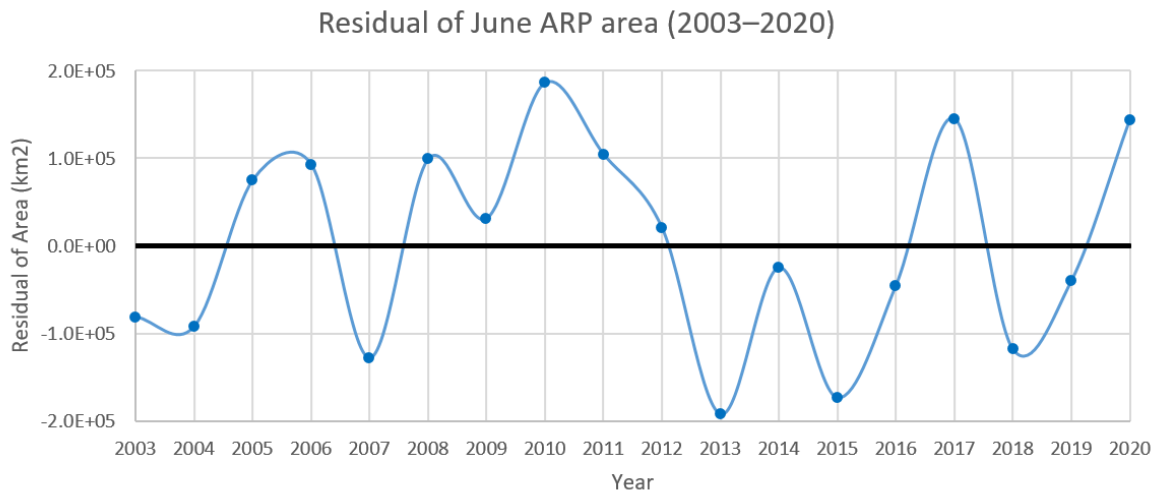

Figure A.3. Annual variations of the plume area in June between 2003–2020, with the mean area set to zero and displayed as the black line.

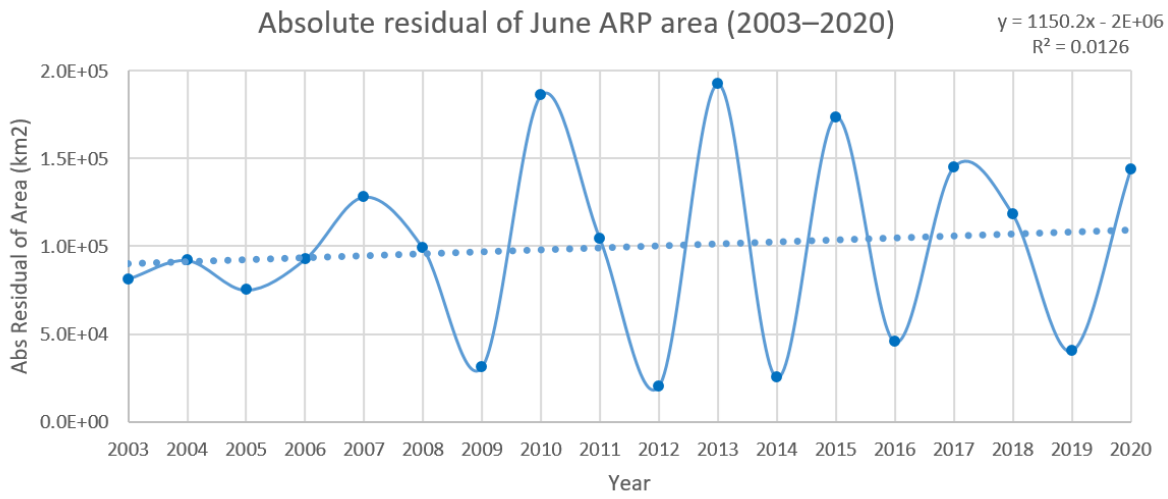

Figure A.4. The residual for the plume area over time between 2003–2020. The slope of the regression line (shown as blue dotted line) was 1150 with a 95% confidence interval of 5393.

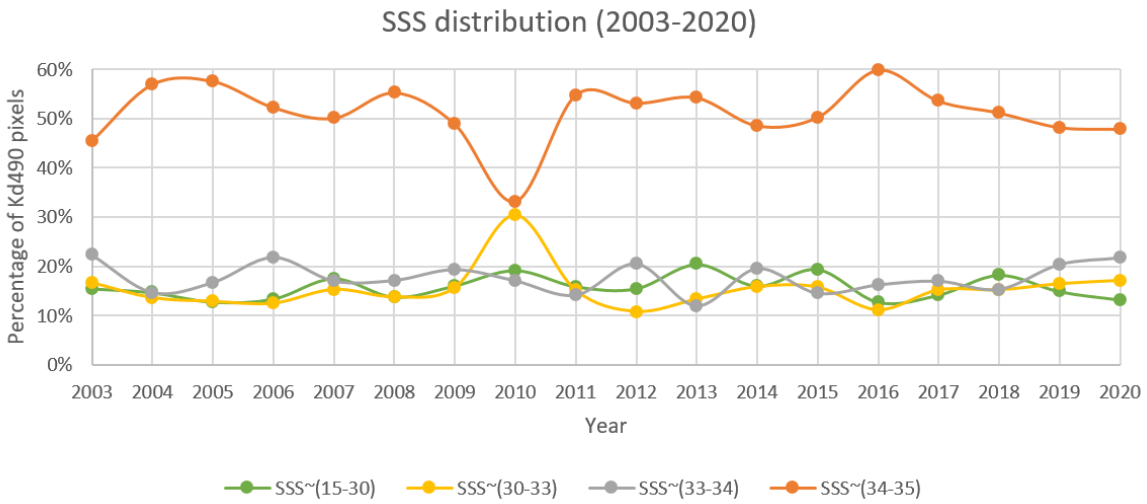

Figure A.5. Time series of SSS distribution presented by the percentages of Kd490 pixels for each salinity band.

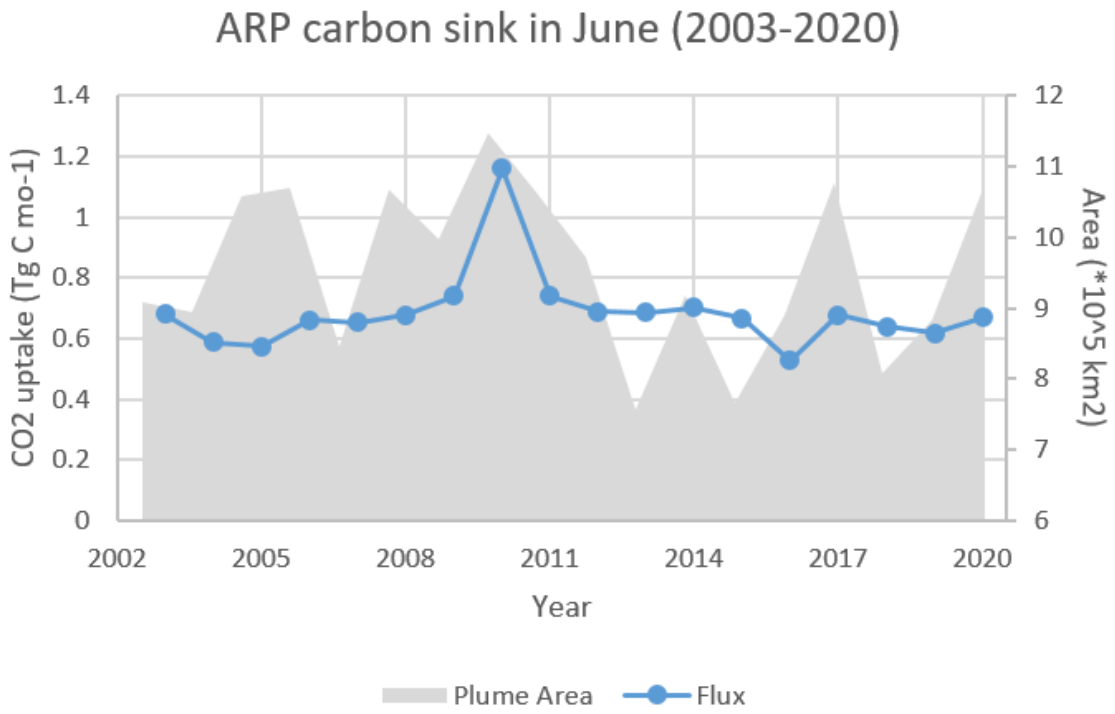

Figure A.6. Interannual variability of the atmospheric CO_2 sink (Tg C mo^{-1}) in the ARP for June, 2003–2020.

CHAPTER 4

CONCLUSIONS

In Chapter 2, the full carbonate system endmembers of the Amazon River were estimated for the first time, providing a key improvement to the values historically used to represent the Amazon's contribution to the ocean. An annual average DIC endmember of 457 ± 60 μmol L^{-1} and ALK endmember of 370 ± 82 μmol L^{-1} were determined for the river mouth. With these river endmembers, our calculations of carbon sequestration by the plume increase since they were based on biological DIC drawdown from lower initial concentrations (Yeung et al. 2012).

Our total DIN measurements at the river mouth were elevated from historical records in most seasons, primarily because ammonium and nitrite concentrations were ~10-fold higher, suggesting greater human perturbations to the river chemistry since 1980s. Our observed phosphate concentrations were lower than historical reports, perhaps related to changes in particulate load due to hydroelectric dams. Net community production estimates for the plume calculated from riverine DIN or DIP are significantly below those based on DIC drawdown in the plume (Cooley et al. 2007; Subramaniam et al. 2008; Mu et al. 2021), confirming that other sources of bio-available N and P (e.g., N_2 fixation, particulate P desorption; Weber et al. 2017) are needed to support carbon sequestration in the plume. Monthly and annual transport of carbon and nutrient species are large, but primarily regulated by discharge, despite some seasonal variations in concentrations. Our sampling

of the lower reaches revealed a river-ocean continuum highly sensitive to changes in watershed hydrology, but also showing clear indications of human impact.

In Chapter 3, we find that although the tropical North Atlantic Ocean is generally considered a net source of CO_2 to the atmosphere by global air–sea CO_2 flux climatologies, our results show that vast areas influenced by the outflow of Amazon River plume are a net sink for atmospheric CO_2. The pCO_2 at the plume surface correlates strongly to salinity within 15<SSS<35, and robust linear relationships were determined during June, July and September. The plume is a major sink of CO_2 in June during the high-flow period of the Amazon River enhanced by higher wind speed, primarily because nutrients delivered by the river create ecological niches for several different phytoplankton communities across the river-ocean continuum. A moderate sink with greater variability is observed during the transitional stage of declining river discharge with relatively lower wind speed in September. The strong sink in some areas of the plume during July was almost completely offset, however, by outgassing in the outer reaches of the plume (SSS ~35). Supersaturated pCO_2 in shallow waters (depth <50 m) near the Amazon River mouth was estimated to outgas as much as 0.6 ± 0.5 Tg C $month^{-1}$ in July. Further sampling would improve this estimate as well as our understanding of the processes driving variability in this region, including the balance of net community production and the degradation/reactivity of organic matter transported by the world's largest river.

Finally, in the Addendum, I examined the climatology in a single key month of June following Amazon flood stage for the river plume during 18 years (2003–2020), analyzing the interannual variability of the plume size and CO_2 uptake by the plume. Our initial

examinations of the interannual variability in the offshore plume yielded a slow decline in the plume size, with an increase in variability over time, although the trends were not strong enough to be statistically significant. Another finding, however, was the surprising result that our June expedition in 2010 occurred during what appeared to be an anomalous year compared to the past two decades. This result suggests that we may need to be careful before extrapolating our results from that year too broadly.